Perspectives on viscoelastic flow instabilities and elastic turbulence

Sujit S. Datta [*]

Department of Chemical and Biological Engineering, Princeton University,
Princeton, New Jersey 08544, USA

Arezoo M. Ardekani

School of Mechanical Engineering, Purdue University, West Lafayette, Indiana 47907, USA

Paulo E. Arratia

Department of Mechanical Engineering and Applied Mechanics, University of Pennsylvania,
Philadelphia, Pennsylvania 19104, USA

Antony N. Beris

Center for Research in Soft Matter and Polymers, Department of Chemical and Biomolecular Engineering,
University of Delaware, Newark, Delaware 19716, USA

Irmgard Bischofberger and Gareth H. McKinley

Department of Mechanical Engineering, Massachusetts Institute of Technology,
Cambridge, Massachusetts 02139, USA

Jens G. Eggers

School of Mathematics, University of Bristol, Fry Building, Woodland Road,
Bristol BS8 1UG, United Kingdom

J. Esteban López-Aguilar

Facultad de Química, Departamento de Ingeniería Química,
Universidad Nacional Autónoma de México (UNAM), Ciudad Universitaria,
Coyoacán, Ciudad de México 04510, Mexico

Suzanne M. Fielding

Department of Physics, Durham University, Science Laboratories, South Road,
Durham DH1 3LE, United Kingdom

Anna Frishman

Department of Physics, Technion Israel Institute of Technology, 32000 Haifa, Israel

Michael D. Graham

Department of Chemical and Biological Engineering, University of Wisconsin–Madison,
Madison, Wisconsin 53706, USA

Jeffrey S. Guasto

Department of Mechanical Engineering, Tufts University, Medford, Massachusetts 02155, USA

---

[*]ssdatta@princeton.edu
[†]hastone@princeton.edu

Simon J. Haward and Amy Q. Shen

Okinawa Institute of Science and Technology, Onna-son, Okinawa 904-0495, Japan

Sarah Hormozi

Robert Frederick Smith School of Chemical and Biomolecular Engineering,
Cornell University, Ithaca, New York 14853, USA

Alexander Morozov

SUPA, School of Physics and Astronomy, The University of Edinburgh, James Clerk Maxwell Building,
Peter Guthrie Tait Road, Edinburgh EH9 3FD, United Kingdom

Robert J. Poole

School of Engineering, University of Liverpool, Liverpool, L69 3GH, United Kingdom

V. Shankar

Department of Chemical Engineering, Indian Institute of Technology, Kanpur 208016, India

Eric S. G. Shaqfeh

Department of Chemical Engineering and Department of Mechanical Engineering,
Stanford University, Stanford, California 94305, USA

Holger Stark

Institute of Theoretical Physics, Technische Universität Berlin, Berlin 10587, Germany

Victor Steinberg

Department of Physics of Complex Systems, Weizmann Institute of Science, Rehovot 76100, Israel
and The Racah Institute of Physics, Hebrew University of Jerusalem, Jerusalem 91904, Israel

Ganesh Subramanian

Engineering Mechanics Unit, Jawaharlal Nehru Centre for Advanced Scientific Research,
Bangalore 560064, India

Howard A. Stone[†]

Department of Mechanical and Aerospace Engineering, Princeton University,
Princeton, New Jersey 08544, USA

Viscoelastic fluids are a common subclass of rheologically complex materials that are
encountered in diverse fields from biology to polymer processing. Often the flows of vis-
coelastic fluids are unstable in situations where ordinary Newtonian fluids are stable, owing
to the nonlinear coupling of the elastic and viscous stresses. Perhaps more surprisingly, the
instabilities produce flows with many of the hallmarks of turbulence—even though the ef-
fective Reynolds numbers may be $O(1)$ or smaller. We provide perspectives on viscoelastic
flow instabilities by integrating the input from speakers at a recent international workshop:
historical remarks, characterization of fluids and flows, discussion of experimental and
simulation tools, and modern questions and puzzles that motivate further studies of this
fascinating subject. The materials here will be useful for researchers and educators alike,
especially as the subject continues to evolve in both fundamental understanding and
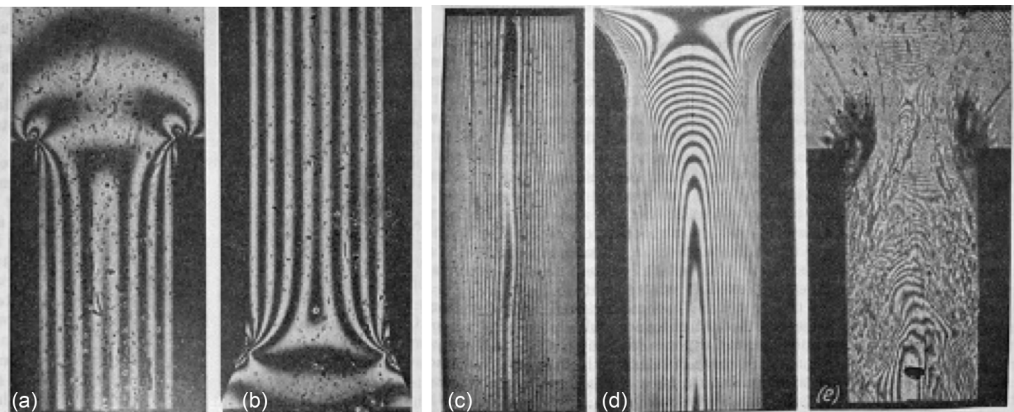applications in engineering and the sciences.

FIG. 1. Flow-induced birefringence of a viscoelastic polymer melt flowing into (a) and exiting (b) a channel die; note that the shapes of the corners are slightly different between the two. The fringe patterns show lines of constant retardance and constant principal stress difference in the flowing melt. As the flow rate into the die increases, the elastic stress differences increase rapidly and fringes become increasingly numerous and closely spaced (c), (d). Beyond a critical imposed pressure drop the flow becomes unsteady and time dependent (e) as reflected in the chaotic fringe pattern, which is an apparent signature of a phenomenon named *elastic turbulence*. Adapted from [1].

I. INTRODUCTION

Authors: S. S. Datta and H. A. Stone

Viscoelastic instabilities often occur during the flow, at sufficiently strong forcing, of polymer solutions and other viscoelastic fluids—driven by the strong coupling between the (viscous) fluid flow and the material's elasticity. A classic example of a molten polymer entering a planar contraction is shown in Fig. 1; beyond a critical flow rate, the flow field is dramatically disrupted, even though inertial effects are negligible. The dynamics of these complex fluids is both fundamentally interesting and technologically important, and continues to be studied by researchers around the world. In some cases, such flow instabilities lead to *elastic turbulence*—a chaotic, strongly fluctuating regime of fluid flow, such as Fig. 1(e), which, amazingly, occurs at low Reynolds number. The statistical features of the flow in this regime have been suggested to be universal, insensitive to the details of the viscoelastic fluid. Although some flow configurations are well studied, perhaps surprisingly there remain poorly understood aspects of the flows, and these questions lead to many open fundamental and applied problems in the dynamics of complex fluids.

S. S. Datta and H. A. Stone organized a virtual workshop of the Princeton Center for Theoretical Sciences in January 2021 to bring together researchers to discuss problems related to viscoelastic flow instabilities, assess successes as well as examples of the lack of predictability in current theory, models and simulations, identify theoretical pathways linking tools of statistical and polymer physics to mean field models of the flows, and highlight applications of these instabilities. The ultimate goal was to bring this community together and clarify, as well as identify, unifying/open questions for future research to address. We had nearly 500 registered participants from institutions in academia and industry from all over the world. This Perspective, which includes contributions from the invited speakers, summarizes some of the research presented and discussions generated at the workshop. Indeed, the participants expressed the viewpoint that the discussions were particularly enlightening as they crystallized poorly understood topics, offered ideas where theory and experimental findings diverged, and highlighted where mechanistic understanding was poor or even lacking.

A. This article: A summary and perspective

The goal of this article is to provide a short record of the main themes of the workshop, including, where possible, some of the spirit of the discussions that occurred between the talks. A wide range of topics are discussed briefly, with the hope that a researcher new to the field, or even an established researcher in one corner of the subject, will find introductory ideas that can launch them into a new research topic if they are so enthused.

This article is organized similar to the structure of the talks in the workshop. Any study of the subject of the flow of complex fluids necessarily touches on important ideas in fluid mechanics, from the geometry of a wide range of (steady) base flows that are possible to the nature of constitutive equations that are needed to close the equations of motion. Even though this closure treats the fluid as a continuum, it must include the fact that the microstructure of the fluid is deformable, which changes the mechanical, i.e., elastic, response. In addition to reversible deformations, various irreversible effects take place in the form of relaxation and viscous dissipation. Experimental observations have been crucial to identifying the rich nature of the dynamics that can occur, and it should not be forgotten that often the experts were surprised when many of the observations were first made. Furthermore, in some cases, elementary models have been helpful in rationalizing observations, at least qualitatively, in the field of complex fluids generally and polymer solutions in particular, e.g., the bead-spring model suggested in 1953 by Rouse [2] and improved three years later by Zimm [3] and then used by de Gennes [4] and Hinch [5] to propose the coil-stretch transition as responsible for some of the most dramatic viscoelastic flow responses.

Hence, by means of introduction to this field, we provide a discussion of these complex fluid dynamics in Sec. II, with emphasis on the dimensionless parameters needed to characterize the flow, and with historical developments in the field highlighted. We introduce viscoelastic flow instabilities and provide a discussion of the different kinds of kinematics that both characterize different flow configurations and indicate their potential as a trigger for flow instability. Also, we highlight how in the case of instabilities in common flows with curved streamlines, Pakdel and McKinley [6] provided an insightful characterization that has proven to be helpful quite broadly. Most of the discussion here and elsewhere is thinking about polymeric fluids (but see Sec. VIII below).

Numerical simulations using macroscopic, necessarily approximate, constitutive equations linking the state of stress to the strain and rate of strain in these viscoelastic materials have proven to be increasingly insightful in unraveling (no pun intended) the dynamics of these flows with deformable microstructure. Hence, Sec. III provides background on constitutive models and numerical tools, including open-source code, for studying viscoelastic fluid flows. This discussion can also serve as an introduction to flow modeling more generally.

The subject of viscoelastic flow instabilities in model (canonical) geometries and the connections to turbulent dynamics is introduced in Sec. IV. The discussion includes a review of the main observations as well as new ideas, related to mechanisms, that have come from two-dimensional (2D) and three-dimensional (3D) numerical simulations. Elastic flow instabilities in more complex geometries, such as the flow between a pair of cylinders, or flow in ordered or disordered porous media, are discussed in Sec. V. Section VI deals with the combined effects of elasticity and inertia in engendering novel instabilities in rectilinear shearing flows. The role of these instabilities *vis-à-vis* transition from the laminar state, and in reducing drag in the fully developed turbulent regime (the maximum drag-reduced regime, in particular), is discussed. Connections between the different turbulent regimes—elastic, inertial, and elastoinertial—are highlighted. Flow instabilities in simplified free-surface flows are discussed in Sec. VII. Some of the flow instabilities that are observed in other nonpolymeric complex fluids are indicated in Sec. VIII and the article closes in Sec. IX with future outlooks across this fascinating subject. We hope the reader enjoys this tour of instabilities in the flow of complex fluids.

II. VISCOELASTIC FLUIDS AND FLOWS

Author: G. H. McKinley, with input from S. S. Datta, R. J. Poole, E. S. G. Shaqfeh, and H. A. Stone

As introduced in undergraduate classes, ordinary small-molecule liquids are *viscous* and Newtonian: the stress is a linear function of the shear rate (also known as the strain rate), with the coefficient of proportionality given by the dynamic shear viscosity. By contrast, ordinary solid materials are *elastic*: the stress is a linear function of the strain, and the coefficient of proportionality is the elastic modulus. Conceptually it is useful to imagine an elastic material as made up of simple springs with a restoring force linear in displacement, e.g., Hooke's law derives from Robert Hooke's observation, in Latin, in the mid-late 1600s that "ut tensio, sic vis" or "as the extension, so the force." The materials we are concerned with have elements of both: they are viscoelastic, so that the state of stress depends on both the strain and the strain rate. Conceptually, such a material has some responses expected of a matrix of damped linear springs, e.g., the generalized Maxwell or Voigt linear viscoelastic models have this character and can be used to characterize such materials in the small-amplitude limit.

Polymer solutions are a common and industrially relevant example of a viscoelastic fluid. Thus, a wide variety of industrial processes such as molding, extrusion, coating, spraying, etc., that involve polymer solutions give rise to the challenge of modeling and controlling viscoelastic flows. These polymer solutions can be dilute or concentrated (and in the latter case they also share many properties with polymer melts), and can be described by a variety of different constitutive relations [7,8]. Other viscoelastic fluids include micellar surfactant solutions, emulsions, liquid crystals, etc.

A. Typical flows and kinematics

As in all areas of fluid dynamics, flows can be driven by the motion of boundaries or by a pressure difference. Thus, the two prototype flows that are characterized most are Taylor-Couette flow, which refers to the wall-driven flow in the annular gap between two concentric cylinders, and pressure-driven (or Poiseuille) flow in a channel or circular pipe. The former has curved streamlines, whereas the latter flow is rectilinear far from the inlet when the flow is fully developed—although streamline curvature can also be introduced when the channel or pipe has a curving centerline (often termed "Dean" flow) or when a boundary-driven flow is forced to recirculate in a closed cavity.

Early in the 20th century, in an experimental and theoretical study of a Newtonian fluid in a concentric cylinder device, G. I. Taylor characterized the instability of this flow experimentally and numerically: above a critical rotation rate (Reynolds number) the flow is unstable when the inner boundary is rotated with the outer boundary fixed, but the opposite case (inner boundary fixed and outer boundary rotating) is always linearly stable [9]. Over the next few decades there were hints that viscoelastic fluids had a qualitatively different response—but the definitive work on the topic, clarifying the existence and onset of *elastic instabilities*, and the fact that they could occur for low-Reynolds-number flows when the inner boundary was fixed and outer boundary rotating would not occur until the late 1980s and early 1990s.

In addition, to understand the motion of fluids that contain a deformable microstructure, it is important to recognize the distinction between *shear-dominated* and *extension-dominated* flows. For steady flows, in the former case, because of the presence of a finite rate of rotation, material points separate algebraically in time, and orientable objects tumble at a rate nominally tied to the vorticity in the flow. By contrast in the latter flow type, because of the absence of vorticity, material points separate exponentially in time. It should not be surprising that exponential stretching can cause large changes in the state of stress within a viscoelastic material.

B. Rheology and rheological parameters

The field of non-Newtonian fluid mechanics, with its unfamiliar notation and specific terminology/jargon, can be initially bewildering to newcomers. This is, in some sense, unavoidable because of the vast range of fluids that fall into the class of what used to be called generically

non-Newtonian fluids and that are now increasingly defined by the catchall phrase *complex fluids*. These materials may range from dilute polymer solutions and melts to dense suspensions with high volume fractions of particles, surfactant solutions that self-assemble into long "wormlike" micellar structures to soft swollen polymer microgels, liquid crystalline dispersions and beyond. The key feature of interest in understanding viscoelastic flow instabilities is the presence of an underlying deformable microstructure in the fluid that can be affected by the flow, and which, in turn, can modify the underlying equations of motion—as a consequence of the generation of additional non-Newtonian contributions to the total stress field that arise from changes in the microstructural configurational distribution. It is the nonlinear feedback between these two features of flow and fluid that give rise to entirely new instabilities not present in Newtonian fluids that are characterized by a linear relationship between stress and deformation rate.

It is not possible in a short perspective article to cover this entire zoology of fluids (for more details the reader is directed to [8]), but it is possible to summarize five of the key phenomena and the corresponding material properties that are displayed by prototypical complex fluids. These involve the following:

(1) Fluid viscoelasticity, as parameterized by a stress relaxation time, commonly denoted λ (but also often defined as τ in the physics literature) and a complex (shear) modulus $G^*(\omega) = G'(\omega) + iG''(\omega)$, where ω is the frequency of the time-varying strain field in small-amplitude oscillatory shear (SAOS). Here the storage modulus G' characterizes the elastic response of the material and the loss modulus G'' characterizes the viscous response of the material. The elastic and viscous stresses resulting from this deformation grow linearly with the strain amplitude and are, respectively, in phase and 90 degrees out of phase with the imposed sinusoidal strain oscillation.

(2) The development in steady simple shear of large normal stresses along the principal axes of the flow characterized by two nonzero *normal stress differences*, commonly denoted by material functions N_1 and N_2.

(3) Shear rate dependence of the viscometric material functions that are measured in steady shearing flow with shear rate $\dot{\gamma}$; e.g., a shear-thinning viscosity, $\eta(\dot{\gamma}) = \tau_{12}/\dot{\gamma}$ and normal stress coefficients $\Psi_1(\dot{\gamma}) = N_1/\dot{\gamma}^2$ and $\Psi_2(\dot{\gamma}) = N_2/\dot{\gamma}^2$.

(4) Time and rate dependence, often corresponding to *strain hardening* and *tension thickening* (e.g., flexible linear polymers in dilute solution) respectively, in the time-dependent extensional viscosity function, $\eta_E^+(\dot{\epsilon}, t)$, where $\dot{\epsilon}$ is the local extension rate in an extensional flow.

(5) The possible appearance of a yield stress τ_y (and a corresponding yield strain γ_y) at sufficiently high concentrations of the microstructural constituents.

Just as in the case of a communicable disease, such as the flu (or COVID-19!), the list of symptoms described above may be present or absent to different extents in a particular fluid, or constitutive model, and care must be taken to understand these limitations. For example, the Oldroyd-B model, which is discussed extensively in the rest of this paper, predicts some of the phenomena in the above list; specifically items no. 1, 2 (but only partially as $N_2 = 0$), and 4, but does not predict rate dependency of the viscometric functions. To compare experimental observations and theoretical predictions, the rheological material response of a given fluid needs to be carefully characterized in several different flow fields, e.g., at minimum, SAOS, as well as a large deformation shearing flow such as steady simple shear flow at large shear rates (i.e., $\dot{\gamma} \gg 1/\lambda$) or large-amplitude oscillatory shear (LAOS) as well as an extensional flow of some kind, so that accurate model parameters can be extracted from experimental data. Highly elastic dilute polymer solutions, or "Boger fluids" [10,11] were formulated to exhibit an approximately constant shear viscosity but significant elasticity. Early fluid formulations used corn syrup as the viscous base solvent and were subject to pronounced bacterial degradation (and even fermentation!) issues; however, these issues were overcome by the formulation of purely synthetic hydrocarbon-based Boger fluids based on high molecular weight polymers such as (polydisperse) polyisobutylene [12] or, later, (monodisperse) polystyrene [13]. The rheological response of these Boger fluids correspond quite closely to the predictions of the Oldroyd-B model so that quantitative comparisons between the predictions of linear stability analysis and careful experimental observations could be

performed without the complications of the interplay between viscoelasticity and shear thinning in the viscosity.

Additional, more-complex rheological phenomena arising from complications such as finite extensibility of the polymer chains or coil overlap in semidilute/concentrated solutions can be incorporated by including additional physics in the microstructural description of the complex fluid. This invariably gives rise to additional (often dimensionless) model parameters, such as the finite extensible, nonlinear elastic (FENE) parameter L that describes the finite extensibility of solvated polymer chains [14] or the Giesekus mobility parameter α [15] describing anisotropic drag on the underlying flow-aligned microstructural elements, detailed further in Sec. III. Incorporating these additional microscopic effects into the constitutive model typically leads to nonlinear responses such as shear thinning in the viscometric material functions [16] as well as a bounded stress growth in steady homogeneous elongational flows, which agree even more closely with experimental data [13,16]. Importantly, this nonlinear response, even in an "ideal" elastic liquid makes the characteristic relaxation time of the fluid, defined typically (in shear) as $\lambda(\dot{\gamma}) \equiv \Psi_1(\dot{\gamma})/2\eta(\dot{\gamma})$, rate dependent. Consequently great care must be taken in calculating the magnitude of the Deborah or Weissenberg number (which are formally defined in Sec. II C below).

A useful estimate of the relative importance of elastic effects in a given flow characterized by a typical shear rate $\dot{\gamma}_c$ can often be obtained by evaluating the *stress ratio* [7] defined by $S_R \equiv N_1(\dot{\gamma}_c)/2\tau(\dot{\gamma}_c)$. In real fluids this ratio can evolve nonmonotonically with shear rate due to the different levels of shear thinning occurring in the first normal stress difference and the shear stress of the fluid; it is of course identically zero for a Newtonian fluid. An extensive review of the current state of the art in the constitutive modeling of polymer melts and solutions is given by Larson and Desai [17]. For more complex materials, such as particle-filled viscoelastic fluids, in which a yield stress also appears, suitable frame-invariant tensorial constitutive models are just beginning to appear [18,19], but very few stability analyses have yet been performed for this class of materials, which can be conveniently described as elastoviscoplastic (EVP) materials. The reader is referred to a recent review that discusses these rheological complexities further [20].

C. Dimensionless parameters for complex fluids

For fluid mechanicians it is natural to aim to quantitatively compare experimental observations and numerical computations of steady flows and flow stability in terms of appropriate dimensionless quantities. However, the number of material parameters or functions required to describe a specific complex fluid can lead to a rapid increase in the dimensionality of the problem as well as some nonuniqueness in the definitions of material parameters.

For a fluid of density ρ and shear viscosity η, in a canonical flow with a typical velocity scale V and length scale ℓ, in addition to a Reynolds number $\mathrm{Re} = \frac{\rho V \ell}{\eta}$ parameterizing the relative importance of inertial stresses $O(\rho V^2)$ to viscous stresses $O(\eta V/\ell)$, it is essential to also quantify the level of non-Newtonian effects in the flow. This is commonly done through a Deborah number, De, or a Weissenberg number, Wi. The preferred usage of each term has evolved over time and formal definitions of these dimensionless parameters are subtly different from each other (see [21] for additional discussion). Nevertheless, they both represent a dimensional relaxation time (which may itself be rate dependent) compared with respect to a characteristic timescale for the flow. In the Deborah number, the characteristic time for the flow is represented directly by an estimate of the time over which the flow changes, whereas in the Weissenberg number, the timescale is parameterized indirectly using an inverse shear rate. Alternatively, a dimensionless stress ratio, $S_R(\dot{\gamma})$, defined in terms of the ratio of the first normal stress difference to the shear stress, can also be used to directly quantify the level of non-Newtonian effects in the flow (as seen using the Oldroyd-B model, described further in Sec. III, in the limit of negligible solvent viscosity).

Careful inspection of any particular research paper is required to ensure that one understands clearly the definition being used; but a simple example can suffice here. In the steady viscometric flow of a viscoelastic fluid in a cone-and-plate rheometer, where Ω is the steady rotation rate of
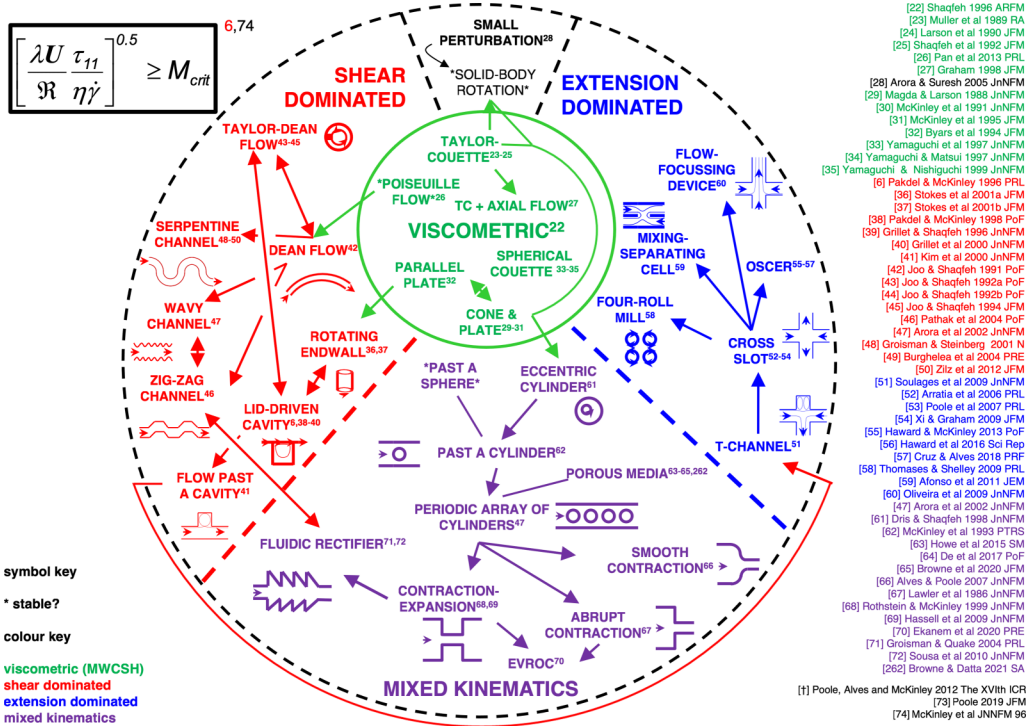
FIG. 2. A map of the different viscoelastic flow instabilities that have been documented to date, with references to selected works exemplifying the different kinematics. Please note that the references shown here ([6,22–74,262]) are numbered with respect to the papers in this Perspective article. Also note that here we have used U to represent the flow velocity scale, instead of V as in the rest of the text.

the conical fixture and $\theta_0 \ll 1$ is the (very small) conical angle of the domain within which the fluid is confined, the conical fixture generates a homogeneous deformation rate $\dot{\gamma}_{\phi\theta} = \Omega/\theta_0$. The Deborah number would be properly defined in terms of a *ratio of timescales* between the stress relaxation timescale and the characteristic flow timescale, $T_{\text{flow}} \approx 1/\Omega$, so that $\text{De} = \lambda\Omega$. However, the magnitude of the normal stress differences and the shear stress developed in the viscometric shearing flow established by the rotating cone (typically) have magnitudes that scale with $\dot{\gamma}^2$ and $\dot{\gamma}$, respectively, so that the dimensionless Weissenberg number parametrizing this stress ratio is properly defined as $\text{Wi} = \lambda\dot{\gamma} = \lambda\Omega/\theta_0$.

These two non-Newtonian dimensionless groups, De and Wi, are of course not completely independent, and their ratio is given simply by a dimensionless geometric factor characterizing the flow; for example, in the cone-and-plate example above $\text{Wi}/\text{De} = 1/\theta_0$. Similar definitions and distinctions apply in all flow domains, from viscometric flows such as a Taylor-Couette geometry—with inner and outer radii R_i and R_o, respectively, where the gap ratio $(R_o - R_i)/R_i$ plays the corresponding role to θ_0—to more complex geometries such as viscoelastic flow past a cylinder or sphere, or through a contraction/expansion. One possible taxonomy, based on kinematic distinctions, of the different viscoelastic flow instabilities that have been documented to date, is suggested in Fig. 2.

Because of this indeterminacy and variability between different approaches and geometries, it is good practice—particularly in stability analyses where one seeks to compare experiments and predictions—to use only one dimensionless group as a dynamical parameter measuring the
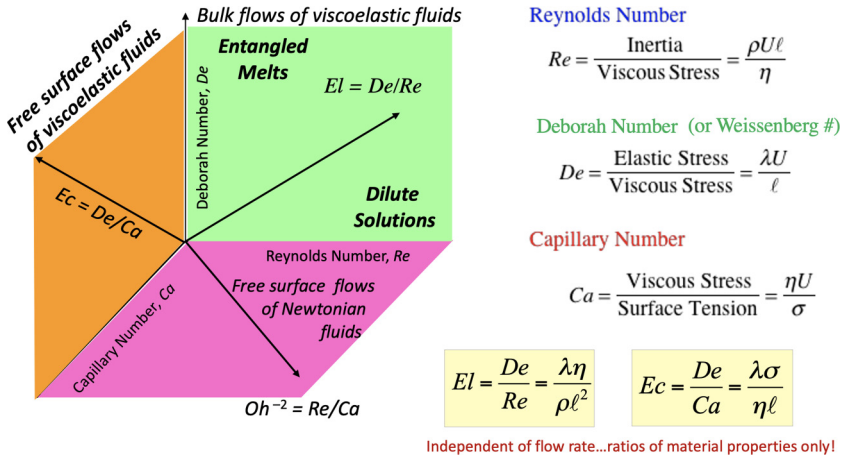
FIG. 3. A three-dimensional representation of the parameter space accessed in processing flows of complex fluids. Taking ratios of each pair of axes results in new dimensionless material parameters that are independent of the kinematics of the flow [75]. Note that here the flow velocity scale is denoted by U, instead of V as in the rest of the text, and we have defined the Deborah number De as a ratio of stresses instead of the ratio of timescales presented in the text.

flow strength and then report dimensionless ratios of material and geometric parameters that are independent of kinematics to fully specify the flow situation being considered. For example, a dimensionless elasticity number El = De/Re = $\lambda \eta / (\rho \ell^2)$ conveniently represents the relative magnitude of viscoelastic and inertial effects in a flow (or the ratio of the timescale of the fluid to the time for vorticity to diffuse across a distance ℓ) and is constant for a particular fluid and geometry. In many computational studies the Deborah number and Reynolds number may be systematically varied independently to explore the dynamical response of a system; unfortunately, for an experimentalist this corresponds to having to perform experiments with a range of different fluids and/or flow geometries, which can be very challenging! Another point to keep in mind is that in numerical simulations, one can "turn off" the influence of inertia, whereas experiments typically have some finite degree of inertia.

This problem of flow characterization is further compounded when a free surface is present due to the additional introduction of a surface or interfacial tension coefficient (which we denote here by σ). We neglect more complex interfacial effects such as surface diffusivity or viscoelasticity, which would result in yet more dimensionless parameters. It is then natural to discuss a capillary number, Ca = $\eta V/\sigma$. In principle, for viscoelastic free surface flows the locus of a particular process, e.g., a fiber-spinning or inkjet printing or spraying/atomization operation, can then be represented in a three-dimensionless space constructed from the Deborah number, Reynolds number, and capillary number as sketched in Fig. 3. Taking ratios of the dimensionless parameters plotted on each axis gives rise, respectively, to the elasticity number El = De/Re and the Ohnesorge number Oh^2 = $\frac{\eta^2}{\rho \sigma \ell}$ = Ca/Re. Additional dimensionless parameters can be defined in specific problems, such as the Weber number We = ReCa, which is commonly encountered in analyses of jet stability. The (as yet unnamed) dimensionless ratio of the elastic stresses and capillary pressure is also of importance in the stability analysis of such problems and can be conveniently parameterized by the ratio of the Deborah number and capillary number, which we suggest should be referred to as an elastocapillary number, Ec = De/Ca = $\lambda \sigma / (\eta \ell)$.

With these ideas and scalings it becomes natural to represent experimental measurements and theoretical analyses of the critical conditions for onset of viscoelastic flow instabilities in terms of stability diagrams such as the one sketched generically in Fig. 4; detailed results for pipe and channel
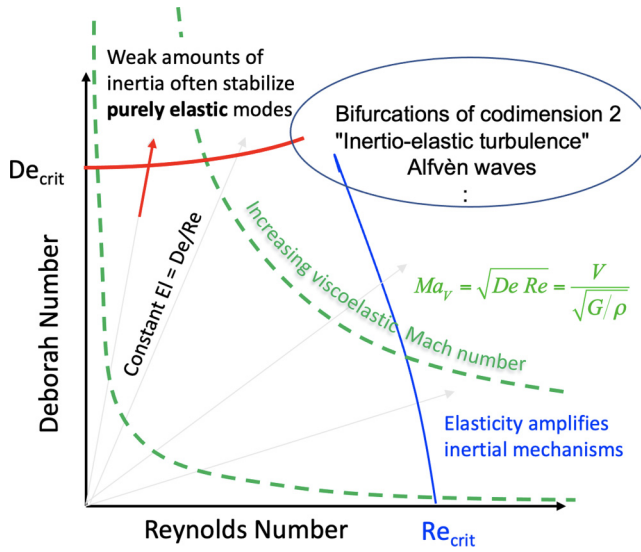
FIG. 4. Sketch of a canonical stability diagram for representing the onset of viscoelastic flow instabilities in a complex fluid. The green curves show lines of constant El, while the red and blue curves show the critical Deborah and Reynolds numbers that represent the boundaries of stability.

flows, respectively, are provided below in Figs. 21 and 22. The characteristic Reynolds number of the flow is plotted on the abscissa and the corresponding Deborah number of the complex fluid, or alternatively the Weissenberg number, is represented on the ordinate. The stability boundaries for each given wave number or perturbation type correspond to bounding curves in this parameter space. A set of exploratory experiments with a given fluid in a fixed geometry correspond to a sequence of points that traverse along a line of constant slope El = De/Re that eventually intersects with a stability boundary marking the critical conditions (Re_{crit}) for onset of an observable instability. All experiments with Newtonian fluids can explore only the abscissa of this plot and a purely inertial instability corresponds to a critical point along this horizontal line. In macroscale flows, weakly elastic fluids, such as dilute aqueous polymer solutions, move along lines of small slope and explore the lower right of this parameter space. Highly elastic materials, such as gels and polymer melts, explore the upper left portions of the plot.

Although every flow geometry and instability mode studied represents a unique stability locus in a stability diagram such as Fig. 4, some general remarks are possible. Elasticity can either strengthen or weaken inertial mechanisms of instability, with the precise results depending on the geometric details of the flow geometry as well as the magnitudes of rheological parameters such as the first and second normal stress differences (see for example the seminal studies by [76,77]). In Fig. 4 we show schematically a case in which weak elastic effects destabilize an inertial mode of instability (as for example in viscoelastic flow in the Taylor-Couette geometry), i.e., the critical Re required for the instability is reduced by increasing elasticity, thus inclining the stability locus, indicated schematically by the blue line, as shown. Conversely, small levels of inertia often stabilize viscoelastic base flows against *purely elastic instabilities*, which correspond to critical loci that intersect the ordinate axis, leading to trajectories as indicated by the red line; nevertheless, we note that Joo and Shaqfeh have shown, for viscoelastic Taylor-Couette flow, that the purely elastic instability is destabilized (for nonzero inertia) when the inner cylinder is rotating, while it is stabilized when the outer cylinder is rotating [44]. The spatiotemporal characteristics of these *purely elastic* and *inertio-elastic* modes often differ very substantially.

At large levels of both flow inertia and fluid elasticity (corresponding to the upper right of this plot) more exotic "beasts" and complex dynamical modes of instability such as "codimension

two" bifurcations exist; see for example the work of Renardy *et al.* [78]. With the definitions introduced in this section it becomes self-evident that because the elasticity number $El = \lambda \eta / (\rho \ell^2)$ depends inversely on the length scale of the geometry, it is possible to experimentally access such regimes using microfluidic devices in which the characteristic length scale is very small. Indeed for microfluidic researchers handling complex microstructured fluids, such as blood, DNA suspensions, or protein solutions, flow instabilities are to be expected in such devices whenever they have smallest dimensions $\ell \ll (\lambda \eta / \rho)^{1/2}$.

Finally, with respect to this representation of parameter space, we note that in inertio-elastic flow fields the speed of viscoelastic shear waves is given by $c_s = (G/\rho)^{1/2}$, where $G \equiv |G^*|$ is the magnitude of the complex shear modulus of the viscoelastic fluid [79]. It is important to note that these viscoelastic shear waves are distinct from the sound modes associated with the bulk modulus of the fluid and instead are associated with the transmission of perturbations through the entropic elasticity of the underlying microstructure in the complex fluid. Since the elastic modulus may be only of order 10^2–10^6 Pa, the resulting viscoelastic shear wave speed may therefore be quite modest. If we neglect the role of the solvent viscosity and identify $G \approx \eta / \lambda$ (in which case η is dominated by the polymer contribution), then in dimensionless form we can construct a viscoelastic Mach number $Ma_V = V/c_s = (Re\, De)^{1/2}$, and lines of constant Mach number correspond to hyperbolae in Fig. 4, as indicated by the green dashed lines. Flows at high viscoelastic Mach number result in a *change of type* in the underlying constitutive equations, from parabolic (similar to a diffusion equation) to hyperbolic (similar to a wave equation), and give rise to many anomalous phenomena in the inertio-elastic flow of complex fluids [80]. Examples include finite upstream propagation of vortices ahead of a blockage such as a cylinder in a channel [81,82] as well as the development of traveling waves of elastic stress that are analogous to the Alfvén waves observed in magnetohydrodynamic flows [83]. We note that this topic was an active topic of discussion at the workshop, with multiple perspectives presented; the perspective put forward by V. Steinberg is presented in Sec. IX.

Analogous stability diagrams may also be constructed for free surface instabilities of complex fluids, for example in terms of the Deborah number and Ohnesorge number [84] or in terms of a capillary and Weber number [85]. For complex problems, in which multiple dimensionless material parameters control the constitutive response of a complex fluid, the stability loci correspond to surfaces in 3D or higher-dimensional diagrams, which can be difficult to represent graphically. However, simpler 2D "slices" of this space are still useful graphically to represent the sensitivity of the stability diagrams to other effects, such as the magnitude of second normal stress differences, changes in the finite extensibility of the dissolved macromolecules, or sensitivity to the effects of viscous heating, for example [86,87].

A particularly common, and indeed almost unavoidable, example of this kind is the role of fluid shear thinning, which becomes increasingly important at progressively higher shear rates (except for the case of carefully formulated highly elastic constant viscosity fluids such as "Boger fluids" [11]). Understanding the central role of shear thinning in viscoelastic flow instabilities is critical because both the fluid relaxation timescale and the viscosity typically decrease in most complex fluids (with the important exception of shear-thickening materials; see, for example, [88]). A convenient way to graphically represent these effects is by defining a (dimensionless) function $\mathcal{S}(\dot{\gamma}) = 1 - (d \ln \tau / d \ln \dot{\gamma})$, which is evaluated from the flow curve measuring the shear stress τ at a steady shear rate $\dot{\gamma}$ [89–91]; thus, $\mathcal{S} = 0$ corresponds to no shear thinning (i.e., the Oldroyd-B limit) and $\mathcal{S} \to 1$ corresponds to the upper limit of a strongly shear-thinning fluid such as an elastoviscoplastic material near its yield stress, or a shear-banding wormlike micellar solution. It is clear from the definition of the elasticity number given above that the slope (given by $El = De/Re$) of a specific fluid's trajectory through the {Re, De} stability diagram becomes progressively shallower under increasingly strong shearing deformations, and this can dramatically constrain the range of parameter space that can be explored.

To briefly illustrate these ideas we show in Fig. 5 the results of a detailed study of the types of viscoelastic flow instabilities observed in the flow of a range of dilute polymer solutions through
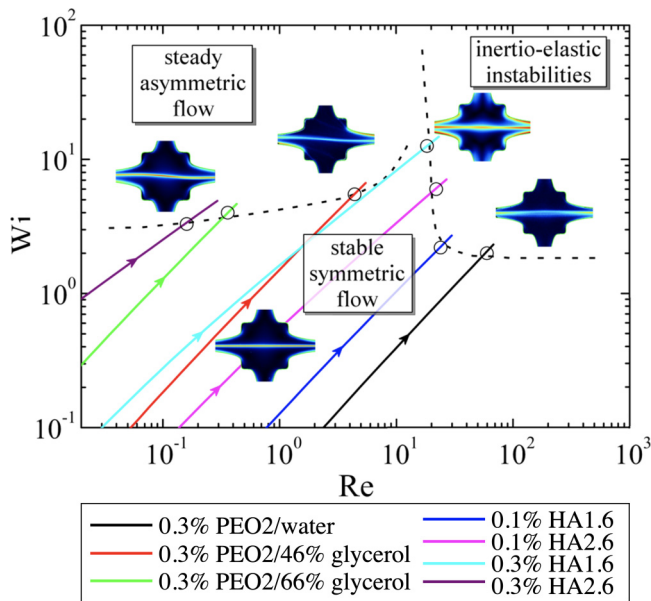
FIG. 5. A stability diagram for viscoelastic flow of dilute solutions of poly(ethylene oxide) (PEO) and hyaluronic acid (HA) through an OSCER (optimized shape cross-slot extensional rheometer) device. The elasticity number of each fluid (shown by the colored lines of constant Wi/Re) is varied by changing the polymer concentration or solvent viscosity. Two distinct modes of instability can be observed at high Weissenberg and Reynolds numbers; the symbols mark the critical conditions for the onset of each mode of instability. Modified from [55].

a microfluidic cross-slot device that has been optimized to generate a strong and homogeneous extensional flow [55]. The trajectories through {Re,Wi} space followed by each fluid as the imposed flow rate is increased are shown by colored lines. These pathlines are almost straight (corresponding to the limit El = Wi/Re = const) but the weakly varying effects of shear thinning in the fluid rheology slowly modulate this [corresponding to evolving values of the function $\mathcal{S}(\dot{\gamma})$]. A fully 3D representation of this kind of stability diagram in {Re, Wi, $\mathcal{S}$} space can also be constructed [90]. However, it is clear even in this 2D projection that two distinct modes of instability are observed: a steady 2D symmetry-breaking purely elastic mode (corresponding to a transcritical bifurcation) at high levels of fluid elasticity, as well as an oscillatory inertio-elastic mode (corresponding to a Hopf bifurcation) that is dominant at higher levels of fluid inertia. In each case, the onset of these viscoelastic instabilities disrupt the homogeneous elongational kinematics that are desired for an extensional rheometric device. Understanding, exploring, and predicting these kinds of instabilities was a major focus of this workshop.

D. Some (pre)history

Although the term *elastic turbulence* has grown into relatively common usage in the 21st century, the origins of the term date back to the very beginnings of research in complex fluids. As early as 1926, Ostwald and Auerbach [92] remarked on the anomalously high pressure drops (and enhanced fluctuations) that were required to pump certain complex microstructured fluids through cylindrical tubes at low flow rates where laminar flow conditions were to be expected. As they noted "it is thus a peculiarity of ammonia oleat and similar sols to exhibit, *in addition to normal turbulence also a structural turbulence*." Some 40 years later Hanswalter Giesekus [93], in his pioneering studies on nonlinear effects of viscoelastic flows through converging nozzles and slits, carefully documented

the apparently turbulent, i.e., strongly time-varying and highly chaotic, flow conditions that could be achieved in nondilute polyacrylamide solutions even at moderate concentrations of 3–4 wt% polymer.

In the years between these two papers the more applied polymer processing literature is full of many documented instances of unstable flow fields arising from the viscoelastic nature of the molten plastics being used in injection molding and other processing operations. The systematic analysis of these empirical observations by Pearson and colleagues, as well as Denn and colleagues, is particularly impactful in this regard; see, for example, the extensive reviews by these authors [94,95]. Much of the work on polymer processing instabilities is nicely captured in the path-breaking book by Vinogradov and Malkin [1] published first in the Soviet Union in 1977 and subsequently in English in 1980. The term *elastic turbulence* appears explicitly in the index of this work multiple times, and beautiful flow visualization images of the stress field (using crossed polarizing optical elements to reveal flow-induced birefringence) in a molten polymer entering a planar contraction (reproduced in Fig. 1) show the dramatic disruption in the flow field that occurs beyond a critical flow rate, even though the relevant Reynolds number is Re $\ll$ 1.

Quantitative study of such flow instabilities and the term "purely elastic instability" first appeared in 1989 through the work of Muller, Larson, and Shaqfeh in a paper on viscoelastic Taylor-Couette flow [23] that was fittingly dedicated to Giesekus on his retirement as editor of *Rheologica Acta*. In particular, in the late 1980s and early 1990s, these researchers at Bell Labs and MIT and later at Stanford focused on discovering and understanding purely elastic instabilities, i.e., those elastic instabilities for which inertial forces play a negligible role, in viscometric flows. These flows were marked by curved streamlines and the associated elastic instabilities prevented rheological measurements in certain parameter regimes. In all instances there existed a separation of scales: a thin gap across which there was shear, characterized for elastic fluids by the shear Weissenberg number, Wi, and a significantly larger radius of curvature, where the ratio of gap to radius of curvature was denoted by ϵ. These flows included Taylor-Couette flow, and torsional shearing flows between parallel plates, and in a cone-and-plate flow [24,30,32]. Measurements in Boger fluids (where the viscosity remains approximately constant and the elasticity number is high) demonstrated that beyond a certain critical Weissenberg number, the flows were unstable, thus bifurcating from axisymmetric shear flows to cellular 3D flows.

The linear stability of a number of canonical shearing flows and the dependence of the spatiotemporal waveforms of the resulting 3D flow fields was studied in the subsequent years and is summarized in a 1996 review by Shaqfeh [22]; see also Steinberg [96]. In particular, the linear stability analysis and resulting eigenvalue problems that were developed to describe the experiments demonstrated that such instabilities could be driven by the nonlinearities associated with the upper-convected Oldroyd derivative acting on the stress and the rate-of-strain tensors. In a small ϵ expansion, these critical conditions generally scaled with $\epsilon \mathrm{Wi}^2$, which is the elastic equivalent of the Taylor number to use the language common to the Taylor-Couette literature, or equivalently, DeWi, where De is a Deborah number based on the time it takes a fluid element to be advected a distance corresponding to the radius of curvature of the flow.

Although the initial Taylor-Couette studies probing the conditions for instability exhibited qualitative agreement between experiments and the first linear stability calculations, and had recognized the physical mechanism underlying the elastic instability, there was quantitative disagreement, which took some time to explore and understand. In particular, the initial linear stability theory assumed that the observed unstable mode was axisymmetric and resulted in a time-dependent response, but reality proved more complex: Beris and colleagues showed numerically that, in fact, the largest growth rate corresponds to a nonaxisymmetric mode [97,98]. Experiments by Groisman and Steinberg [102–104] found good agreement with isothermal theory based on identifying the most unstable nonaxisymmetric mode. Investigating the underlying mechanisms further, Al-Mubaiyedh *et al.* [105] showed theoretically and by numerical simulations that viscous heating can also play a significant role, influencing the nature of the instability and affecting conclusions regarding flow stability based on axisymmetric versus nonaxisymmetric modes. The relative magnitude of non-

isothermal effects in a highly elastic fluid depend on the magnitude of the viscosity and relaxation time, as well as their (typically exponential) sensitivity to temperature, through a *thermoelastic number* [87]. In detail, an *isothermal* analysis of the Oldroyd-B model yields nonaxisymmetric and time-dependent modes, while a *nonisothermal* (energetic) analysis, yields a time-independent (stationary) but axisymmetric instability. While these finer details are inconsistent with the interpretation offered for the original experimental results of Larson, Muller, and Shaqfeh, they are fully consistent with later more detailed experimental work by White and Muller [106–108]; see also [96] and the work by Baumert and Muller [99–101]. This understanding then sheds light on the detailed "polymer-scale" mechanism coupling radial perturbations and polymer stretch in driving instability in the Taylor-Couette geometry, as discussed more below.

This class of elastic instabilities was broadened by other researchers to include the Taylor-Dean (cylindrical Couette flow with an additional pressure-driven flow in the axial and azimuthal directions) and Dean flows (flows in curved channels) [43] as well as lubrication bearing flows [61], which are generally not used for viscometric measurements but contain the same kinematic elements, i.e., shear-dominated flow along curved streamline, as those in the original Taylor-Couette studies. Researchers again demonstrated through experiment and eigenvalue analysis that the instabilities were characterized by a critical value of the product (DeWi). An examination of the mechanisms of all of these instabilities demonstrated at least three separate modes and mechanisms of instability, all of which involved the interaction of the base state (either the kinematics or existing hoop stress field) with a velocity fluctuation to locally enhance hoop stresses and further drive the fluctuation.

All mechanisms leading to unstable conditions scaled, in the small gap limit, with DeWi. Thus, McKinley *et al.* [74] suggested a scaling approach to the critical conditions, now known as the Pakdel-McKinley scaling, namely that if one writes the Weissenberg number more generally as $\text{Wi} = \tau_{11}/(\eta\dot{\gamma})$, where τ_{11} is the primary normal stress component along the streamlines and η the total fluid viscosity, then the dimensionless magnitude defined as $M^2 \equiv \text{DeWi}$ could be developed into a general criterion whose critical value signaled the onset of elastic instabilities in many curvilinear shear flows. In particular, the onset of elastic instability is related to the characteristic curvature of the flow and stress along the streamlines, and corresponds to exceeding a critical value of this parameter given by

$$\frac{\lambda V}{\mathcal{R}} \frac{N_1}{|\tau|} \geqslant M_{\text{crit}}^2, \tag{1}$$

where λ is the relaxation time of the fluid, V is the characteristic streamwise fluid velocity, $\mathcal{R}$ is the characteristic radius of curvature of the streamline, N_1 is the first normal stress difference of the fluid, and τ is the total shear stress in the fluid.

As summarized by Poole in Fig. 2, now a plethora of flows have been demonstrated to be elastically unstable, primarily by experimental observations and measurements. Most of these flows involve curved streamlines and thus their instability is attributed to hoop-stress driven instabilities. As such, they are typically characterized, in some manner, by the M parameter. The geometric scaling has been enormously successful, as, for example, it has been shown that instability during flow in a serpentine channel is directly related to the Dean instability [50]. Remarkably, and perhaps surprisingly, the dependence of the instability threshold in Taylor-Couette flow predicted by the Pakdel-McKinley criterion is in a better agreement with the experimental values than the results of linear stability analysis carefully tailored to the fluid's rheology [109].

As the instability develops in time, or conditions beyond the critical conditions are considered, the dynamics of these purely elastic instabilities become increasingly complex, even at very small Reynolds numbers. In the late 1990s, Baumert and Muller [99–101] and Groisman and Steinberg [102–104] reported a series of experimentally observed transitions in Taylor-Couette flow involving axial vortices developing into localized "diwhirls" and "flame" patterns followed by oscillating states and finally disordered oscillations. Kumar and Graham [110,111] studied Taylor-Dean flow and computed stationary nontrivial solutions with the FENE-P model that strongly resemble some of

the experimentally observed diwhirls, showing that they arise in a nonlinear transition scenario. The self-sustaining mechanism is related to the mechanism of instability in viscoelastic Dean flow [43], arising from a finite-amplitude perturbation giving rise to a locally parabolic profile of the azimuthal velocity near the upper wall. The more complex time-dependent states were later simulated, at least qualitatively, by Khomami and coworkers [112–114]. These ideas of self-sustaining nonlinear interactions between the velocity field and the state of stress in the flow form a robust mechanistic basis for a transition to elastic turbulence [48].

As described further in Sec. IV, the first two decades of this century have focused on achieving a deeper understanding and progressively unraveling the complex viscoelastic dynamics for a range of different flow geometries and fluid rheologies. Furthermore, in more recent work, Khomami and coworkers have focused on examining through direct numerical simulations the connection between inertial and elastic turbulence, as well as the connection to curvature and curvature-induced elastic instabilities (of the type described by the Padel-McKinley criterion) in strengthening large-scale Taylor vortices at the expense of small-scale Görtler vortices as the curvature in the flow is increased while keeping the same Reynolds and Weissenberg numbers [115]. Additional work exploring these connections is described in Secs. IV–VI.

III. CONSTITUTIVE MODELS AND NUMERICAL SIMULATIONS OF ELASTIC FLOW INSTABILITIES

Author: A. N. Beris, with input from G. H. McKinley, R. J. Poole, and H. A. Stone

In addition to experimental characterization, many researchers are seeking insight into this large class of instabilities via large-scale numerical simulations. As an example, during the workshop M. Alves presented results from *RheoTool* (a numerical library based on the open-source OpenFOAM®) on cross-slot [116] and contraction flow instabilities that are purely elastic. Even though the flows have a large region of extensional flow, there is evidence that these instabilities are again driven by elastic hoop stresses. However, the evidence comes from calculating local fields of the M parameter in a flow and demonstrating that the flows break symmetry and/or become time dependent when the maximum value of M becomes sufficiently large, e.g., $M > 4$–5. In this context, there is a lack of linear (or energy) stability analyses for these extension-dominated flows such as the cross-slot geometry.

What are the underlying models used in theory/numerical simulations? For the analysis of flow instabilities and/or simulation of highly elastic viscoelastic flows, differential models are typically used that connect the stress and its time and space derivatives to the velocity gradient and its time derivatives [7,117]. The simplest of these models is the upper convected Maxwell (UCM), or Oldroyd-B model (when a Newtonian solvent viscosity contribution is added). This model originates from a simple mechanical analog of polymer solutions corresponding to a spring and dashpot in series, with the upper convected time derivative expressing the second-order (contravariant) tensor generalization of the material time derivative of the stress tensor, as beautifully shown first in the pioneering work of Oldroyd [118]. Most importantly, some time later, a formal connection was made to an idealized Hookean dumbbell polymer structure [119]. This image of a solution's microstructure has allowed a number of considerable generalizations to be obtained, like the Finitely Extensible Non-linear Elastic dumbbell with the Peterlin approximation (FENE-P dumbbell) that allows for a finite polymer extensibility [14,119]. Other notable generalizations of the Oldroyd-B model are the following: the Johnson-Segalman model [120] involving a nonaffine correction to the upper convected time derivative, first proposed by Gordon and Schowalter [121]; the Giesekus model involving a nonisotropic drag controlled by a mobility parameter [15]; and the Phan-Thien and Tanner (PTT) model involving a dependence of the relaxation time on the stress [122].

All of these models can be described conveniently using a time-evolution equation in terms of the stress tensor, $\boldsymbol{\tau}$. However, given the connection of microstructural models to kinetic and network theories the stress is assumed to be related to an internal structural parameter, $\mathbf{c}$, which is typically

TABLE I. List of commonly used models along with the corresponding expressions with respect to the conformation tensor, **c**, or values for materials parameters in Eq. (2). An earlier version of the FENE-P model used $f(c) = b/(b - \text{tr}\mathbf{c})$. Although for $b = L^2$ this expression reduces to asymptotically the same model for high L values, in general, it is a different model. The L^2 version is to be preferred as it is more physical, resulting in an equilibrium value for **c** that is the unity tensor, **I**, whereas that corresponding to the b model is **I** scaled by $b/(b + 3)$.

Model	ξ	$\lambda(\mathbf{c})$	α	$f(\mathbf{c})$	Remarks/References
Maxwell	0	λ_0	0	1	Hookean or linear dumbbell model [7];
Oldroyd-B					Oldroyd-B includes viscous stress
Johnson-Segalman	$0 \leqslant \xi \leqslant 2$	λ_0	0	1	[120]
FENE-P	0	λ_0	0	$\frac{L^2-3}{L^2-tr(\mathbf{c})}$	L represents the dimensionless maximum chain extensibility; $3 < L^2 < \infty$ [7]
Giesekus	0	λ_0	$0 < \alpha < 1$	1	α is an anisotropic mobility parameter [15]
Phan-Thien and Tanner	$0 \leqslant \xi \leqslant 2$	$\frac{\lambda_0}{1+\epsilon tr(\mathbf{c-I})}$	0	1	This is the linear PTT model [122]; for a nonlinear version use $\lambda = \lambda_0 e^{-\epsilon tr(\mathbf{c-I})}$; $\epsilon > 0$
Extended White-Metzner	0	$\lambda_0(\frac{1}{3}tr(\mathbf{c})^{-k})$	0	1	$k > 0$ [127]

identified as the second moment $\langle \mathbf{RR} \rangle$ of the end-to-end distance **R** vector if macromolecular chains are involved [7]; an elastic deformation strain [123,124] can also be described in terms of **c**. An advantage of this representation is that it allows for a connection to the theories of nonlinear elasticity [124], while providing for a nonlinear thermodynamics foundation [125,126] that allows for both a straightforward extension/mixing of models (like the extended White-Metzner model [127]) and an evaluation for their thermodynamic consistency and Hadamard-type instabilities [123].

Indeed, all of the above-mentioned models can be concisely represented as [126]

$$\frac{D\mathbf{c}}{Dt} - (\nabla\mathbf{v})^T \cdot \mathbf{c} - \mathbf{c} \cdot \nabla\mathbf{v} + \xi(\mathbf{D} \cdot \mathbf{c} + \mathbf{c} \cdot \mathbf{D}) = -\frac{1}{\lambda(\mathbf{c})}(\boldsymbol{\tau}^+ + \alpha\boldsymbol{\tau}^+ \cdot \boldsymbol{\tau}^+); \quad \boldsymbol{\tau}^+ = f(\mathbf{c})\mathbf{c} - \mathbf{I}, \quad (2)$$

where D/Dt is the material derivative, ξ is a dimensionless nonaffine motion parameter with $0 \leqslant \xi \leqslant 2$, $\mathbf{D} = \frac{1}{2}(\nabla\mathbf{v} + (\nabla\mathbf{v})^T)$ represents the rate of deformation tensor, $\lambda(\mathbf{c})$ represents the relaxation time (which may be a function of **c**), $\boldsymbol{\tau}^+$ is the dimensionless polymer extra stress, $\boldsymbol{\tau}^+ = \boldsymbol{\tau}/[G_0(1 - \xi)]$, with G_0 a characteristic elastic modulus, α an anisotropic mobility parameter, and $f(\mathbf{c})$ is a model-dependent parameter representing finite polymer extensibility effects. The left-hand side of Eq. (2) corresponds to the Johnson-Segalman derivative [120]. For most polymeric systems $\xi = 0$, in which case the left-hand side of Eq. (2) reduces to the Oldroyd upper-convected time derivative, as is appropriate for a structural material parameter connected to the Cauchy elastic strain tensor [124].

As discussed, Eq. (2) can represent all the above-mentioned constitutive models, with suitable choice of the model parameters, as shown in Table I; Table II summarizes the choices of the symbols used most commonly to describe various physical quantities in this article. We note that the highest elasticity (as, for example, determined by the magnitude of the normal stresses in shear flows) is obtained with the Maxwell/Oldroyd-B model. Alternatively, $\xi \to 0$, $L \to \infty$, $\alpha \to 0$ [see Eq. (2) and Table I], limits for which we recover the Maxwell/Oldroyd-B models, are values often selected in numerical simulations/analyses seeking to maximize the effects of elasticity, such as, for example, simulations of highly elastic, viscoelastic turbulent flow [128–131].

TABLE II. Due to the use of different symbolic conventions by different communities, here we summarize the choices of the symbols used most commonly in this article along with their meanings. Where relevant, the mathematical definitions are presented in the text as the symbols are introduced. Other symbols are also introduced in the text as needed for specific other quantities. Note that an overlying dot represents a time derivative, e.g., $\dot{\gamma}$ denotes the shear rate.

Symbol	Meaning
ρ	Density
σ	Interfacial tension
$\boldsymbol{v}$	Velocity vector
V	Velocity scale
t	Time
ℓ	Flow length scale
γ	Shear strain
τ	Stress (shear or extensional, as defined in the text)
η	Shear viscosity (dynamic)
ν	Shear viscosity (kinematic)
λ	Stress relaxation time
γ_y	Yield strain
τ_y	Yield stress
N_1	First normal stress difference
N_2	Second normal stress difference
Ψ_1	First normal stress coefficient
Ψ_2	Second normal stress coefficient
G	Shear modulus
G^*	Complex shear modulus
G'	Storage modulus
G''	Loss modulus
ϵ	Extensional Hencky strain
η_E	Extensional viscosity

Another advantage of the conformation tensor representation is that it allows checking for numerically induced instabilities as, from theory and its physical interpretation, **c** is a positive definite tensor [126]. Consequently, numerical schemes have been devised so that they guarantee that **c** always remains positive definite, such as the log-conformation tensor methodology proposed by Fattal and Kupperman [132,133] or the matrix decomposition proposed by Vaithianathan and Collins [134]. As such, when used, the approach significantly improves the numerical stability and allows reaching substantially higher values of elasticity (i.e., higher Wi or De numbers) [135]. Different types of stabilization techniques commonly used in computational rheology were reviewed recently by Alves and coworkers [136].

How successful have studies using these rather idealized single relaxation mode viscoelastic models been in describing highly elastic, viscoelastic flows? One could say fairly successful, judging from several important accomplishments. First and foremost, these include the capability of reproducing the polymer-induced drag reduction phenomenon in direct numerical simulations (DNS) of turbulent flows using the above-mentioned single relaxation viscoelastic models, when the elasticity in the flow was high enough [128–131]; e.g., see the discussion of elastoinertial turbulence in Sec. VI. The drag reduction is observed experimentally when high molecular weight polymers are added, usually in small concentrations, to a Newtonian solvent [137]. The DNS results, typically carried out in a channel geometry, showed, in addition to the drag reduction that increased with increasing elasticity in the flow, all of the main kinematic effects accompanying it, such as the

increase in the extent of the buffer layer, the widening of the streaky structure, and the enhancement of the larger, more coherent turbulent structures at the expense of the smaller scales, etc. [128–131].

Second, the detailed results and sensitivity analysis to the model parameters allowed one to deduce the main mechanism behind the drag reduction, namely, the weakening of the vortical structures (eddies) due to the enhancement of the resistance to extensional deformations induced by viscoelasticity [128,129], as originally proposed by Seyer and Metzner [138] and Lumley [139].

Third, in the most recent of these works [130,131] the analysis of the underlying mechanism revealed further details of the reasons for the experimentally observed maximum drag reduction [140]. In this respect, worth mentioning are the results of a recent linear stability analysis of a highly elastic viscoelastic pipe flow that showed it to be linearly unstable for a certain range of the parameters of the Oldroyd-B fluid model [141,142]. Moreover, linear stability analysis and direct numerical simulations of a highly elastic viscoelastic channel flow demonstrated the presence of an "arrowhead" 2D wave instability for a certain range of parameters of a FENE-P model [143,144]—see the relevant discussion in Sec. VI A.

The successes just described in extracting new physics out of highly elastic but rather idealized models raise the question as to how accurately the models, in the limit of high elasticity, can predict real polymer flow behavior. Of course, this depends on the complexity of the polymeric system. Research along these lines, involving much more accurate (but also much more highly time consuming from a computational stand point) microscopic models, along with a comparison to dilute polymer solutions [145,146], has shown that it may be possible to make quantitative predictions if some modifications are implemented to the description of the friction drag on the individual beads in the microscopic multibead models used. Thus, the fact remains that microscopic multibead models still need to be used, which is not very hopeful from a macroscopic, continuum mechanics, viewpoint. However, some early work on a modified FENE-P model (using two conformation tensor parameters instead of one) has shown that it may still be possible to capture those nonlinear effects, which arise primarily due to the non-Gaussian microscopic distribution of the deformation of the polymer chains and which are reflected in hysteresis phenomena [147]. This is therefore an avenue that still remains to be exploited. Still, for more complex physics, such as presented by concentrated polymer solutions and melts [148,149], or micellar solutions [150,151] or under confinement [152] and especially in the presence of entanglements [149], additional components in the models may be needed as outlined in the referenced papers. A particular outstanding challenge for these models are correct pressure-drop predictions for well-characterized dilute polymer solutions in mixed kinematics flows [68].

IV. TRANSITION TO ELASTIC TURBULENCE

We have seen that even relatively "simple" polymeric flows at low Reynolds numbers can become unstable. Beyond the instability we expect the flows to be more complicated; indeed, features consistent with "turbulence" have been identified. Here we describe some of the challenges and puzzles raised by recent research on elastic turbulence in 2D and 3D flows, especially parallel shear flows, such as pressure-driven flows in channels and pipes.

A. Taylor-Couette flow

Author: H. Stark

One archetypical geometry for studies of purely elastic instabilities in flows with curved streamlines is the Taylor-Couette geometry. In simulations of this configuration, what is especially surprising is that all unstable modes that have been computed so far rely on the 3D character of the flow. This topic was addressed during the workshop by H. Stark, who presented numerical simulations of two dimensional (i.e., zero axial wave number) elastic Taylor-Couette flow using *RheoTool*. At large enough Wi, the elastic turbulence that had been reported by Steinberg and coworkers in serpentine channel flow and plate-plate flows [50,87,96,153] appeared.
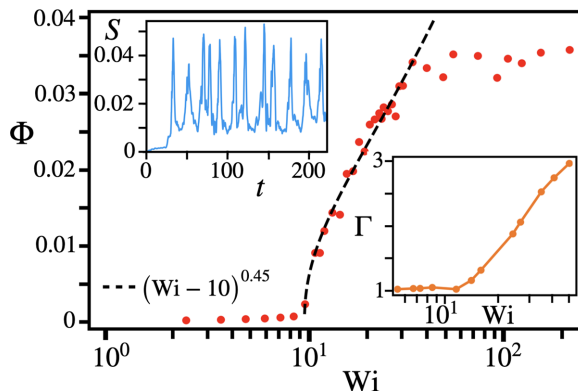
FIG. 6. Order parameter $\Phi = \overline{S(t)}$ vs Weissenberg number Wi for 2D Taylor-Couette flow with a wide gap. The dashed line indicates the fitted scaling law beyond the elastic instability. Upper inset: Secondary flow strength $S(t)$ plotted vs t for Wi $= 16.3$. Lower inset: Flow resistance quantified by the azimuthal stress on the outer cylinder plotted vs Wi. Adapted from Ref. [154] with permission from *EPL*, copyright (2018).

In particular, using the Oldroyd-B model for numerical simulations, van Buel and Stark reported the onset of the elastic instability towards elastic turbulence in the 2D Taylor-Couette flow with a wide gap [154]. They locate the instability by an order parameter $\Phi = \overline{S(t)}$, which is the time average of the secondary-flow strength $S(t)$ that measures the overall deviation from the Taylor-Couette base flow. The upper inset of Fig. 6 shows a typical example for $S(t)$ beyond the critical Weissenberg number $\mathrm{Wi}_c \approx 10$ and reveals the irregular nature of the secondary flow. The continuous increase of the order parameter with Wi in Fig. 6 indicates a supercritical instability that is accompanied by an increase in the flow resistance.

Furthermore, for the spatial power spectrum of the secondary flow along the azimuthal direction, a power-law decay $m^{-\zeta}$ with exponent $\zeta > 3$ for all Wi $>$ Wi$_c$ was reported [154]. This result is consistent with a theoretical bound on the exponent ζ [155]; note that we do not expect the Kolomogorov scaling $k^{-5/3}$ of inertial turbulence since elastic turbulence is initiated by elastic stresses. Also, the exponent α of the temporal power spectrum was found to be generally smaller than ζ [154], hence, does not obey Taylor's hypothesis for inertial turbulence that demands that the exponents are equal [156]. Only for small Wi was the exponent $\alpha > 3$, which is considered to be a signature for turbulent flow and was measured in several experiments [48,157]. Groisman and Steinberg suggested that the reduced value of the exponent α found in 3D Taylor-Couette flow indicates that the flow is transitional [153], and not fully in the elastic turbulence regime, due to the large shear strain component in Taylor-Couette flow with a small gap and a possible increase in the Wi needed to generate the coil-stretch transition of individual polymers [158].

Typically, changes to the flow geometry or boundary conditions are used to passively control the onset of the elastic instability and elastic turbulence [87,159–161]. In this spirit, van Buel and Stark realized active open-loop control in simulations of the 2D Taylor-Couette flow [162]. They apply a time-modulated shear stress by periodically reversing the rotational velocity of the outer cylinder. The modulation frequency is quantified by the Deborah number, the product of frequency times stress relaxation time. The insets of Fig. 7 show how the secondary-flow strength of the turbulent velocity field decreases with increasing De until a modulated laminar flow remains. For high modulation frequencies the elastic stresses cannot fully build up in order to generate turbulent flow. The transition from laminar to turbulent flow is again supercritical (Fig. 7) and for larger Weissenberg numbers a larger critical frequency (or De$_c$) is needed to suppress elastic turbulence. Note that the different curves in Fig. 7 collapse onto a master curve when plotting $\Phi/\mathrm{Wi}^{3/2}$ vs $\mathrm{De}^{-1} - \mathrm{De}_c^{-1}$.
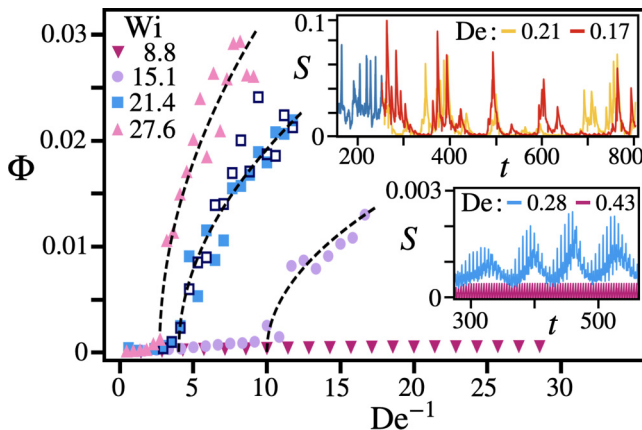
FIG. 7. Active control of elastic turbulence. Order parameter vs inverse Deborah number, De^{-1}, for different Wi; here De is defined as the product of the outer cylinder reversal frequency and the fluid stress relaxation time, while Wi is defined as the product of the outer cylinder maximum angular velocity and the fluid stress relaxation time. Insets: Secondary-flow strength vs time for different De at Wi = 21.4. The time-modulated driving is switched on at $t = 250$. Adapted from Ref. [162].

B. Parallel shear flows

In the sections that follow we discuss both experimental observations, including instabilities and later fully developed turbulence, and associated theoretical attempts to describe these flows in channels and pipes. The field has come a long way. In a prior version of this workshop that was held at the Princeton Center for Theoretical Science in 2018, the mere existence of sustained fluctuations in viscoelastic flows in straight channels was in doubt. Three years later, their existence is now well established, and researchers are now working on understanding the origins and mechanisms governing these observed instabilities. Even after much effort, however, there are different interpretations offered.

1. Theoretical analyses

Author: A. Morozov, with input from P. E. Arratia, M. D. Graham,
G. H. McKinley, V. Shankar, and G. Subramanian

Modal linear stability analysis. As we have discussed above, low-Reynolds-number, polymeric fluid flows with curvilinear streamlines are characterized by an elastic hoop stress that generates a bulk (body) force acting on the fluid in the direction of the center of curvature, which leads to an elastic instability and subsequently to elastic turbulence. This instability mechanism ceases to be effective at zero curvature in flows with straight streamlines, such as parallel channel shear flow, i.e., based on the criterion given in Eq. (1), purely elastic hoop stress-driven instabilities are not possible as the curvature of the streamlines decreases to zero ($\mathcal{R} \rightarrow 0$). Thus, a common assumption is that parallel or rectilinear shear flows of viscoelastic fluids, such as plane Couette and Poiseuille flows, are linearly stable in the absence of inertia [163]. This form of stability is described using linear stability analysis, which decomposes a perturbation in the flow into normal modes, familiar from studies of Fourier series. For solutions with the time dependence assumed to be of the form $e^{i\omega t}$, eigenvalues ω with negative imaginary parts correspond to perturbations that grow exponentially in time, thus leading to a linear instability in the limit $t \rightarrow \infty$.

There are a number of directions that have been pursued to examine the possible linear stability of viscoelastic flows. Motivated by the polymer extrusion instability and the problem of "melt fracture," Ho and Denn examined the stability of plane Poiseuille flow of a UCM fluid and concluded, based on an eigenvalue analysis, that the flow is stable to infinitesimal perturbations

[164]. The authors did acknowledge the possibility of the flow becoming unstable to finite amplitude perturbations, but it was deemed unlikely. Similar results were found by Lee and Finlayson for Poiseuille and planar Couette flows [165], by Renardy and Renardy for Couette flow using spectral methods [166], and by Gorodtsov and Leonov [163] for plane Couette flow. A rigorous proof that such rectilinear viscoelastic flows are indeed linearly stable was provided by M. Renardy [167], who studied the stability of plane Couette flow of a UCM fluid. Importantly, the author cautioned that artificial instabilities could arise from numerical discretization in simulations of viscoelastic flows.

Taken together, these results suggested that parallel shear flows of model viscoelastic fluids are indeed linearly stable [22,168], with the exception of fluids with strongly shear-thinning material properties [169,170]. So, it came as a surprise when Khalid *et al.* [171] recently reported a linear instability in purely elastic channel flows of Oldroyd-B fluids—described further in the next section. Although found only in a region of the parameter space that might be difficult to access experimentally [Wi $= O(10^3)$ and the ratio of the solvent to the total shear viscosity $\beta > 0.9$], these results suggest that the linear stability analysis of parallel shear flows of simple viscoelastic model fluids needs to be revisited. The recent work of Buza *et al.* [172] used the FENE-P model to show that the instability predicted by Khalid *et al.* extends down to Wi $= O(100)$, thereby making this instability potentially observable in experiments.

Transient nonmodal growth of nonnormal perturbations. While the linear stability analyses discussed above rule out the existence of a linear instability for a broad class of viscoelastic parallel shear flows, they do not automatically imply that such flows remain laminar. Indeed, there are several mechanisms that can potentially lead to flows that are very different than the corresponding laminar ones, even in the absence of a linear instability. One such mechanism was uncovered in the early 1990s in the field of Newtonian hydrodynamics. It relies on the observation that the dynamics of infinitesimal perturbations introduced to a laminar flow are governed by linear equations that often involve non-self-adjoint (nonnormal) operators [173–176]. Although the real parts of the associated eigenvalues can all be negative, the associated eigenmodes may not be "orthogonal" to each other, i.e., they do not represent unique, independent flow perturbations. Instead, some of the modes become almost parallel to each other, especially for sufficiently large Reynolds numbers [174]. For additional discussion of the transition to turbulence in inertially dominated flows, see Sec. VI.

This *nonnormality* has a profound implication for the short-time evolution of flow perturbations: an initial state, prepared as a combination of several such eigenmodes (in other words, a general random perturbation of the form expected to be experimentally relevant) will see its kinetic energy increase algebraically in time, reaching values that are many times larger than the initial value; in the framework of constant coefficient differential equations with repeated roots, there are solutions te^{-at}, where a is (in general) a complex constant with positive but small in magnitude real part, which grow at early times t. These solutions subsequently decrease exponentially in time, as predicted by the modal linear stability analysis of the previous subsection. It was shown that the maximum energy amplification that can be achieved through this mechanism in plane Couette and channel flows is $O(\text{Re}^2)$ [173]. For sufficiently large Reynolds numbers, such strong amplification can lead to perturbations becoming sufficiently large so that their dynamics are no longer described by the linearized equations on which the analysis is based. Thus, if a particular linearly stable flow is unstable to finite-amplitude perturbations (in other words, there exists a "bifurcation from infinity"), as is the case with plane Couette and pipe flows of Newtonian fluids, nonnormal growth can amplify small experimental noise helping to tip the system over the instability threshold.

The corresponding theory for viscoelastic nonnormal growth was developed by M. Jovanovich, S. Kumar, and colleagues during 2008–2018 [177,178] and T. Zaki and colleagues [179,180] in 2014–2018. Specifically, it was demonstrated that even in the absence of inertia, infinitesimal perturbations in plane Couette and channel flows can be significantly amplified [177]. Perturbations of the streamwise velocity achieve growth by a factor of $O(\text{Wi})$, while the streamwise component of the polymer stress tensor can be amplified up to $O(\text{Wi}^2)$ compared to its initial value; the time to reach the maximum values scales as $t_{\text{max}} \sim \lambda \text{Wi}$, where λ is the relaxation time of the fluid.

Similar to its Newtonian counterpart, the purely elastic nonnormal growth theory predicts that the most amplified initial flow structures comprise (almost) streamwise-independent vortices, leading to streamwise-independent streaks [177], although other forms of stress amplification have also been examined more recently [181].

The nonnormal growth mechanism provides a powerful pathway to significantly amplify small-amplitude experimental noise until it becomes large enough to ignite some nonlinear process that would sustain turbulent flow. However, the nonnormal growth mechanism does not provide any insight into the nonlinear process. As a linear theory, it cannot predict a critical Weissenberg number at which an instability might set in. We should also mention that although streamwise vortices and streaks are naturally produced by this theory, their experimental observation is not a proof that nonnormal amplification is at play in that particular flow: as discussed by Waleffe [182], these flow structures may also be produced by other, nonlinear mechanisms.

Weakly nonlinear analysis. As already discussed above, linear stability does not imply global stability. One of the classical examples of such behavior is Newtonian pipe flow that is linearly stable for all Reynolds numbers but is unstable when a sufficiently large perturbation is added to the flow [183]. In the early 2000s, Bonn, van Saarloos, Morozov, and collaborators [184,185] proposed that viscoelastic parallel shear flows exhibit analogous behavior. Using weakly nonlinear analysis, the authors in [184] tackled an interesting observation, namely that the fracture instability in polymer melts, which occurs when the solution flows out of a slit or "die," seems to occur at an approximately constant value of Wi. Using the UCM fluid model, it was then shown that viscoelastic Poiseuille flows could exhibit a nonlinear "subcritical" instability due to normal stress effects; the flow was predicted to become unstable at $\text{Wi}_c \approx 5$. This analysis was followed by experiments [185] that showed melt fracture instability at Wi values that are quantitatively similar to those predicted by the nonlinear expansion theory [184].

Subsequent analysis by Morozov and van Saarloos [186,187] for plane Couette and Poiseuille geometries showed that the viscoelastic flows could be unstable to finite-amplitude perturbations without curved streamlines or inertia. They developed a novel amplitude-equation technique that constructs a nonlinear solution as a power series in its amplitude (relative to the laminar flow), with the lowest-order term being the least-stable eigenmode of the linear stability analysis. Morozov and van Saarloos found that plane Couette and channel flows of Oldroyd-B fluids exhibit subcritical instabilities for $\text{Wi} \gtrsim 3$ and $\text{Wi} \gtrsim 5$, respectively. The nonlinear flow structures predicted by this analysis are traveling-wave solutions, similar to their Newtonian counterparts [183,188]; for channel flows their spatial profiles are reported in [187]. Their origin can be understood as a two-step process. While the underlying laminar flow has straight streamlines, and is thus linearly stable according to the Pakdel-McKinley criterion [6] [Eq. (1)], a slowly decaying perturbation with curvature in its streamlines can drive an instability. This *perturbation of a perturbation* scenario then leads to a finite-amplitude threshold.

To understand the relevance of these solutions to purely elastic turbulence in parallel shear flows, Morozov and van Saarloos yet again drew an analogy with Newtonian turbulence in pipes and rectilinear channels [183,188]. Our current understanding of the transition in these flows is centered on the exact solutions to the Navier-Stokes equations discovered by Nagata [189], Waleffe [190], Hof [191], and others. These solutions, often referred to as *exact coherent structures* or *exact coherent states* (ECS), are either traveling waves or periodic orbits that comprise streamwise streaks and vortices, and instabilities connecting them; they are generated through a self-sustaining process uncovered by Waleffe [190,192]. Importantly, ECS are linearly unstable: their vicinity in the phase space contains many attractive and a few repulsive directions [183,188], and a typical turbulent trajectory performs a pin-ball-type motion among those coherent structures. While each of them is regular in space (i.e., they visually appear to be relatively simple), an instantaneous snapshot of the flow caught between many ECS does look turbulent. This scenario is at the frontier of the current research in Newtonian turbulence and there are strong early indications that it persists sufficiently far away from the transition [193]; the role of ECS in the Newtonian transition is discussed further in Sec. VI below, in the context of elasto-inertial instabilities. Morozov and van Saarloos proposed

[187] that the solutions found in [186] are the viscoelastic counterparts to Newtonian ECS, and, while not being directly observable, they play a role in organizing the phase space dynamics of purely elastic turbulence in parallel shear flows.

It is important to note that the weakly nonlinear analyses presented above are the only theoretical results on nonlinear structures in purely elastic channel and pipe flows currently available, to our knowledge. Although suggestive, they are obtained by an approximate technique; also their linear stability is currently unknown. A significant amount of new research in this area is needed before the analogy with Newtonian turbulence, as proposed by Morozov and van Saarloos [187], can be made more exact. Indeed, to our knowledge, even for planar Couette flow, there are currently no results available beyond the work by Morozov and van Saarloos cited above.

2. Experimental results of Arratia and colleagues

Author: P. E. Arratia, with input from M. D. Graham, G. H. McKinley, A. Morozov, V. Shankar, and G. Subramanian

Experimental evidence of nonlinear instability has been hard to come by. While the hysteretic behavior presented in [185] is consistent with a nonlinear instability, it was unclear whether the instability originated inside or outside of the flow domain. A subsequent experimental study on the stability of viscoelastic flows inside a cylindrical straight pipe did find unusually large velocity fluctuations far downstream for the initial perturbation, but the subcritical nature of the instability was not established and no hysteretic behavior was reported [194].

Thus, it was particularly notable when in 2012, Arratia and coworkers [26] provided experimental evidence of such nonlinear subcritical instability in a straight microfluidic channel, as shown in Fig. 8. A linear array of upstream posts provided the initial (finite amplitude) perturbation, and the researchers found large and sustained velocity fluctuations far downstream from the initial perturbation; no fluctuations were found without perturbations, indicating that viscoelastic flows are indeed linearly stable. In addition, the transition to this nonlinear state was found to be hysteretic upon the increase or decrease of the flow rate, which is a typical behavior of a subcritical bifurcation. The flow became unstable at $Wi_c \approx 5$, in apparent agreement with the theory of Morozov and van Saarloos [186]. Subsequent work has shown that the nonlinear state possesses features of elastic turbulence [195], and a flow resistance law (pressure drop as a function of flow rate) that is nonlinear with Wi, followed by drag reduction [196] (which, intriguingly, seems to occur in other geometries as well [197,198]). However, experiments have yet to report the existence of traveling wave solutions predicted by Morozov and van Saarloos [186].

An important question is whether the evidence provided by Arratia and colleagues conform to the picture of nonnormal transient growth. Such a scenario predicts that a nonmodal perturbation should first grow algebraically before decaying exponentially in time. In the Lagrangian view, the scenario translates into a spatial region with large perturbations followed by a region where they decay. Experimental data, on the other hand, show that the velocity fluctuation levels remain essentially constant while moving downstream [26]. Nevertheless, one expects nonnormal growth to be a part of the mechanism that sustains elastic turbulence, but perhaps not the cause of it. This, however, is still an open question as the new results by Steinberg and colleagues suggest, as discussed next.

3. Experimental results of Steinberg and colleagues

Author: V. Steinberg

N. Jha and V. Steinberg undertook experiments similar to the Arratia group but with a somewhat different geometry. The experiments of Steinberg and colleagues were conducted in a long channel with the width/height ratio = 7 and length/height ratio = 950 using channels with a height of 0.5 mm, i.e., of a large aspect ratio compared with a square channel cross-section used in the Arratia group's experiment. It is possible that this difference is one of the reasons for the difference in some of the unexpected flow states observed both at transition and beyond, such as in the observed
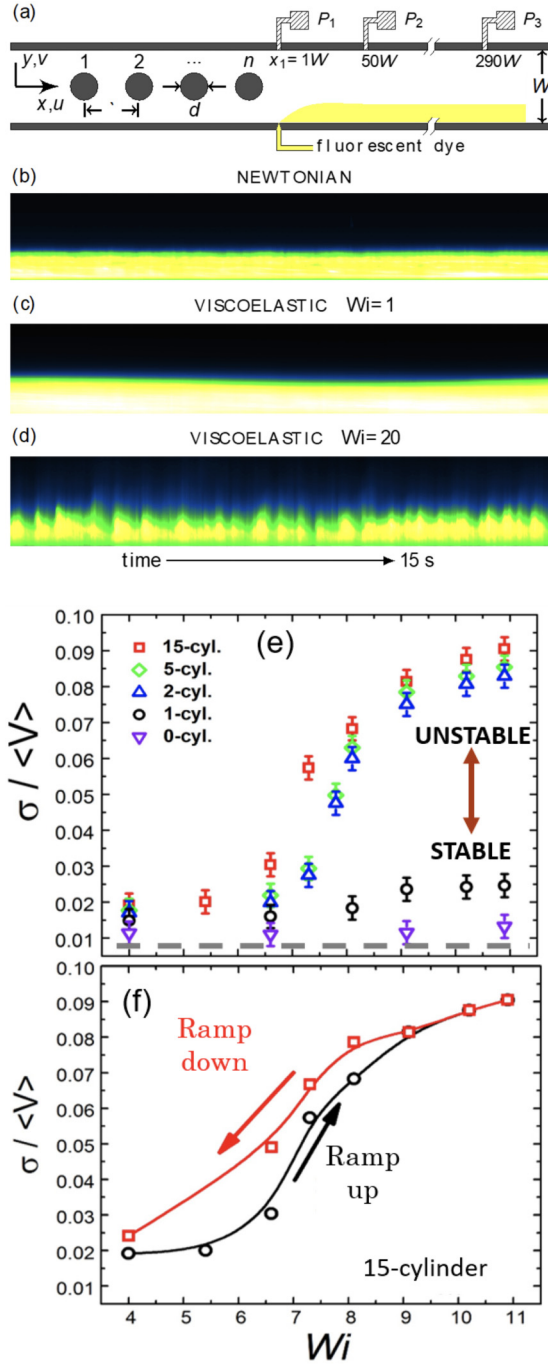
FIG. 8. Nonlinear elastic instability in a microfluidic channel flow. (a) Experimental setup showing the initial linear array of cylinders followed by a long parallel shear flow region. (b)–(d) Space-time dye patterns for the case with 15 cylinders for Newtonian and polymeric fluids measured far downstream. (e) Normalized velocity fluctuations as a function of initial perturbation (n) and Wi showing the appearance of two branches. (f) Hysteretic behavior, a hallmark of nonlinear subcritical instabilities, is found for polymeric fluids. Modified from [26].
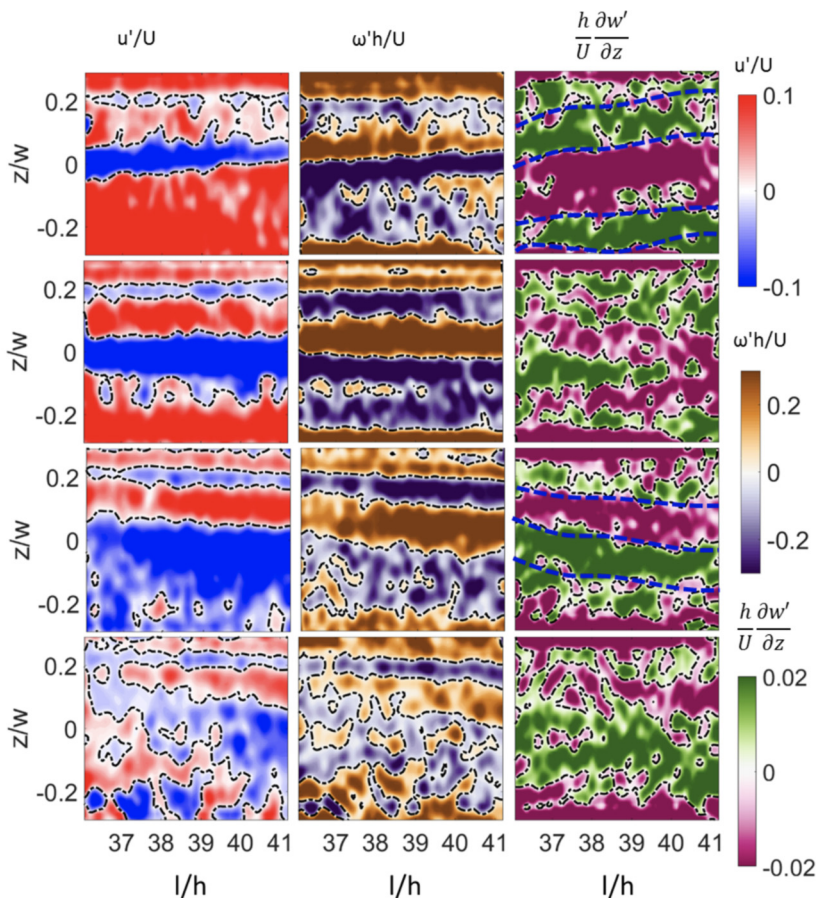
FIG. 9. A cycle of coherent structures in ET at Wi = 185 and downstream distances $l/h = 36$–41. The normalized time $t^* = t f_{el}$, where f_{el} is the elastic wave frequency. The quantities reported here are from PIV measurements of velocity fluctuations reported in a reference frame moving with the average fluid velocity. Fluctuating streamwise velocity (u'), vertical vorticity (ω'), and spanwise gradient of spanwise velocity ($\partial w'/\partial z$) are shown in each column with their scales shown on the right as marked in the plot [198].

coherent states (CSs) e.g., streamwise rolls and streaks, and self-sustained cycling processes (SSPs). We note that CSs are equivalent to the ECS introduced above, and discussed further later in this article; however, in this subsection we retain the term CSs given their use in the references cited here. Also, "elastic waves" (described further in Sec. IX) were found already at the onset to the elastically driven flow transition and up to the highest Wi, varying from Wi = 7 up to Wi = 3500, in this case defined as Wi = $\lambda U/h$ (instead of Wi = $U\lambda/w$, where h and w are the channel height and width, respectively) with a critical value Wi$_c$ = 140 [83]. The CSs are evident in PIV measurements of velocity fluctuations reported in a reference frame moving with the averaged fluid velocity profile, as shown in Fig. 9, which, remarkably, resemble those observed numerically and experimentally in Newtonian turbulence of a channel shear flow [198].

We next make remarks about the continuous transition and the manner in which the friction factor for the pressure drop in pipe flow varies with the flow speed (here quantified by Wi). The first key observation at Wi $\gg$ 1 and Re $\ll$ 1 (i.e., El $\gg$ 1) is the small magnitude of the exponent characterizing the power-law growth of the friction factor with the order parameter (Wi − Wi$_c$), which appears to have a value of 0.125 (in contrast to 0.5 for the normal mode instability) as shown
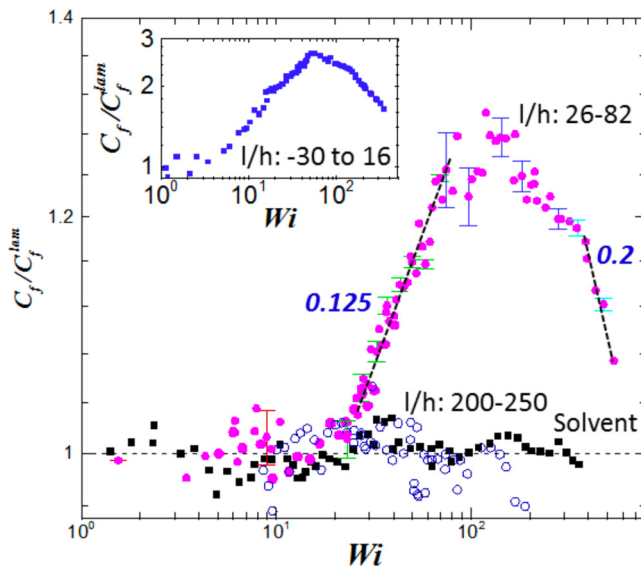
FIG. 10. Dependence of the normalized friction factor C_f/C_f^{lam} on Wi for three values of nondimensional distance from the third layer of cylinders (at $l/h = 0$) l/h: (i) -30 to 16 (inset), (ii) 26 to 82 (filled circle), (iii) 200 to 250 (open circle), and (iv) Newtonian solvent 26 to 82 (filled black square). Inset shows C_f/C_f^{lam} vs Wi across three rows of cylinders [198].

in the data reported in Fig. 10. This distinguishes the elastically driven transition in a straight channel flow from the continuous transition *via* the most unstable normal mode, where the exponent is 0.5.

Moreover, the velocity power spectra just above the instability threshold reveal the presence of a peak of elastic waves on the top of a continuous spectrum with the decay exponent -1.7 [198]. A continuous spectrum above an elastic instability signifies a direct transition to chaotic flow, contrary to a continuous linear instability resulting in a single, most unstable fastest growing normal mode, which is observed above the onset. Such a transition is characterized by algebraic growth of flow properties with the exponent 0.5 [275] and also occurs in viscoelastic flows with curved streamlines [96–98].Thus, another possibility of a nonnormal mode instability—which was first introduced in Sec. IV B 1) [177–181], and whose application to Newtonian parallel shear flows is further described in Sec. VI—should be considered.

Steinberg and colleagues characterize their experimental observations as weakly unstable non-normal modes selected by the flow from strong perturbations at the inlet, which are further amplified due to nonlinear self-interactions to generate CSs. The latter are self-organized into cycling SSP in particular in elastic turbulence, where CSs, namely, streamwise rolls and streaks, are clearly identified (Fig. 9). The SSPs are synchronized by the elastic wave frequency, and consequently the SSP cycling frequency is equal to the elastic wave frequency. The synchronization is critical for the existence of CSs and SSP, which is interpreted as the pumping of energy into CSs and supporting the SSP [198]. This feature distinguishes the CSs and SSP from those found in Newtonian turbulence in shear flows.

A surprising novel ingredient is the development of elastic waves above the flow transition, which are further amplified in ET and decay in the drag reduction regime. Moreover, elastic waves also pump energy into a secondary instability, whose dynamics destroy the counter-propagating streaks (compare the second and third rows in Fig. 9) and bring to mind the Kelvin-Helmholtz instability (KHI) in the flow of Newtonian fluids. However, in spite of the similarity of this KH-like instability to the conventional KHI, the instability mechanism is strikingly different for the purely elastic case, where the main destabilizing factor results from interaction of transverse elastic waves with wall-normal vorticity generated by perturbations of the streaks [199].

Finally, it should be pointed out that CSs and cycling SSP are localized only in a finite spatial range inside the channel flow. Further downstream, only chaotic velocity power spectra with power-law decay in frequency were observed. The reason for the finite spatial range of the existence of these structures is the spatial attenuation of the elastic waves; estimates of the attenuation length of the elastic waves show an agreement with the observation [198].

4. Perspective

Author: A. Morozov, with input from P. E. Arratia, M. D. Graham,
G. H. McKinley, V. Shankar, and G. Subramanian

One might think that understanding fluid flow in straight channels and pipes is easy. This is not the case at higher Reynolds numbers for Newtonian fluids, which produces inertial turbulence approximately when Re > 2000. As described in this section, it is also not the case for low-Reynolds-number flows of highly elastic (Wi ≫ 1) polymeric fluids.

To summarize, the early experimental observations of Arratia and colleagues demonstrate the existence of an elastically driven transition in a straight channel flow due to strong perturbations at the inlet [26]. Furthermore, their results suggest the existence of a subcritical instability, which can be viewed as the viscoelastic analog of turbulence in classical Newtonian pipe flows, except that it is controlled by the elasticity of the fluid and not by inertia. On the other hand, the experimental results of Steinberg and colleagues, also for a rectilinear channel flow—but with different cross-sectional dimensions and a distinct form of imposed perturbations—suggest that strong perturbations at the inlet are not a necessary condition to generate the elastic instability and subsequent ET in a straight channel flow [198,200]. Instead, their experiments provide evidence for an elastic instability even in a straight channel with a smoothed inlet and a small hole on the top plate at the middle of the channel for pressure measurements. As a result, the transition at $Wi_c = 125$ is observed with well-characterized "elastic waves" (described further in Sec. IX) at the onset, which are continued farther into the ET and drag reduction regions with the same elastic wave velocity dependence on $Wi - Wi_c$ on the top of continuous velocity and pressure spectra in the transition; the latter include ET and drag reduction regions with decay of the velocity spectra having an exponent with a magnitude smaller than 3. Moreover, in this case they were able to visualize elastic waves propagating in the spanwise direction towards the center by presenting them in spatiotemporal plots for three Wi values (Fig. 11). These features are consistent with the elastic instability occurring due to nonnormal modes similar to the channel flow with strong perturbations at the inlet, though the critical Weissenberg number Wi_c is about twice as large (taking into account the approximately 2× smaller value of the longest relaxation time). These results once more suggest a similarity to dynamics of Newtonian parallel shear flow; see also, e.g., [143], discussed further in Sec. VI.

With reference to the generic flow stability diagram sketched in Fig. 4, it is worth noting that the Weissenberg number values are quite different between these two experimental studies; while Arratia and coworkers focused on a regime where $Wi = O(10)$, Steinberg and coworkers, using the same polymer solutions, focused on much higher values, $Wi = O(10^3)$. Some part of the discrepancy may be due to significant differences in the reported (typically longest) polymer relaxation times, as different characterization methods were used—again highlighting challenges with understanding even relatively simple flows of complex fluids such as dilute polymer solutions. Taking these results together, as well as the results of the theoretical analyses described in the previous subsections, suggests that it is possible that viscoelastic flows in pipes and channels are nonlinearly unstable at low Wi, as suggested by Morozov and van Saarloos, but linearly unstable at moderate to high Wi. Recent linear stability analysis by V. Shankar and collaborators [171] seems to suggest such a possibility—but as summarized in this section, this question (and many others) remains unresolved.
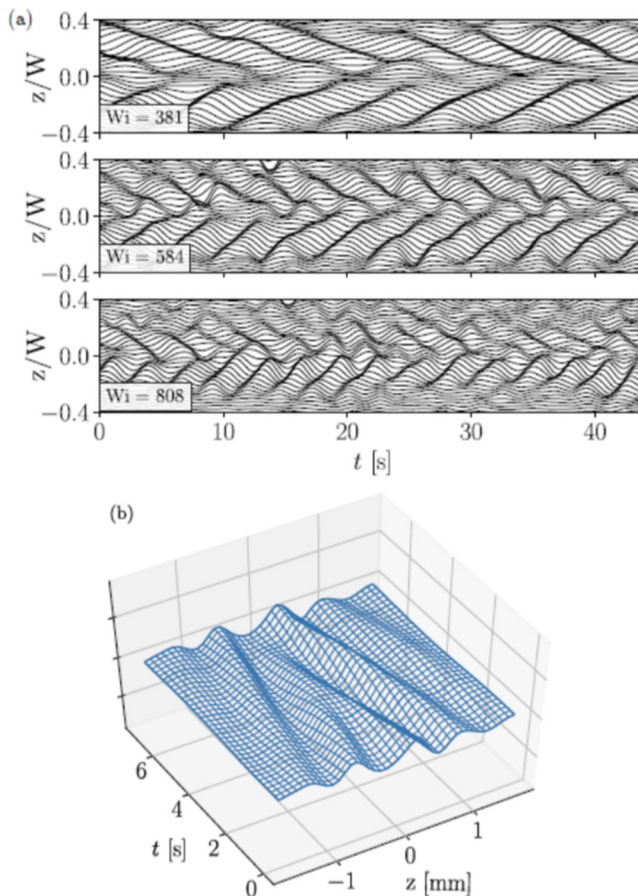
FIG. 11. (a) Space-time plots at $-0.4 < z/W < 0.4$ of the streamwise velocity fluctuations, $u'(z, t)$ exhibiting elastic wave structures for three values of Wi. The time series are filtered via a band-pass Butterworth filter centered on the spectral peaks to remove background noise. (b) Streamwise velocity, phase averaged at the elastic wave frequency for Wi = 407 [200].

V. ELASTIC INSTABILITIES IN MORE COMPLEX GEOMETRIES

A. Flow past cylinders

Authors: S. J. Haward and A. Q. Shen

A circular cylinder is arguably the most fundamental shape of an object that can be used for studying flows around obstacles. We note that extensive work has also focused on the related problem of flow past a sphere, e.g., [202–209]; here, we focus on the case of cylinders, since it was discussed at the workshop. Further discussion of flow past a sphere is given in Sec. VIII B. In viscoelastic fluid flows, circular cylinders are used frequently as building blocks to create complex geometries such as regular or random arrays that model aspects of porous media flows in 2D [64,161,210–216], although recent experiments have also explored aspects of these flows using sphere packings in 3D, as described in Sec. V B. Recently, there has also been interest in viscoelastic fluid-structure interactions, where elastic instabilities at high Wi (but negligible inertia, or small enough Re) drive the motion of flexible or cantilevered circular cylinders [217,218].

Our discussion thus far in this article has focused on polymer solutions; however, useful and related insights also arise from studies using viscoelastic wormlike micellar (WLM) solutions. Thus, we first describe work using WLMs to study flow past cylinders here; additional studies of WLMs
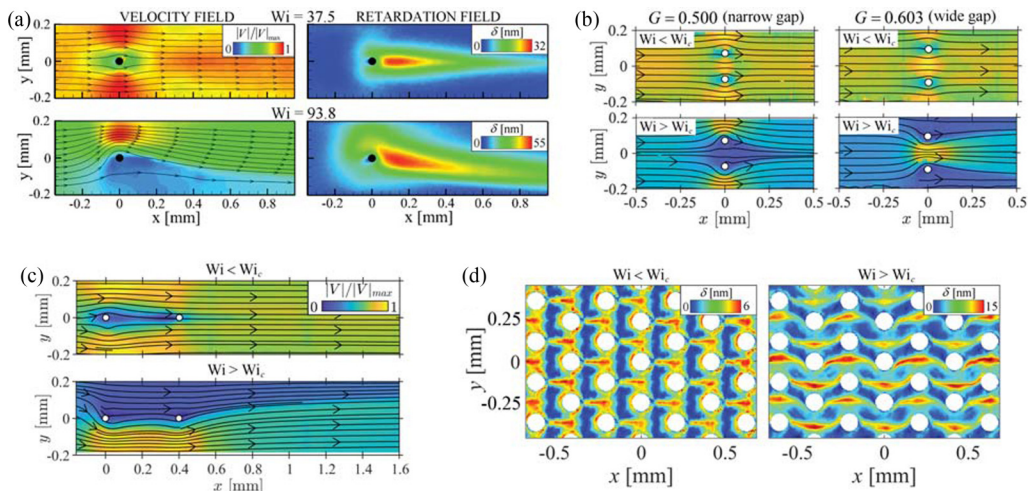
FIG. 12. Transitions to steady asymmetric flow states in various geometries constructed from microscale cylinders as the Weissenberg number is increased beyond a critical value Wi_c. (a) Flow past a single cylinder positioned on the flow axis. Reproduced from [222] with permission from the Royal Society of Chemistry. (b) Velocity fields for flow past side-by-side cylinders with different dimensionless intercylinder gap, $G = L_1/(L_1 + L_2)$, where L_1 and L_2 are the cylinder-cylinder and cylinder-wall gaps, respectively. Reproduced from [223] with permission. (c) Velocity fields for flow past two axially aligned cylinders. Reproduced from [218] with permission from John Wiley & Sons, Inc. (d) Retardation fields for flow through a hexagonal array of cylinders (unpublished data, S. Haward). All cases show the flow from left to right of a shear-thinning viscoelastic WLM solution.

are described in Sec. VIII B. In particular, using a model WLM solution consisting of 100 mM cetylpyridinium chloride (CPyCl) and 60 mM sodium salicylate (NaSal) [219,220], Haward, Shen, and coworkers examined flows past several different configurations of slender circular cylinders confined within microfluidic channels (see Fig. 12), with much larger depth aspect ratios than explored in previous studies. At $24\,^{\circ}$C (ambient laboratory temperature), the entangled WLM solution has a zero shear viscosity $\eta_0 \approx 47$ Pa s, exhibits a stress plateau (shear-banding region [221]), and in small-amplitude oscillation is well described by a single-mode Maxwell model with relaxation time $\lambda \approx 1.7$ s. The dimensions of the microfabricated glass geometries [channel height, $H = O(1\,\text{mm}) \gg$ width, $W \gg$ cylinder radius, $R = O(10\,\mu\text{m})$] ensure that inertia is always negligible, and that the flows are approximately uniform (or 2D) along the length of the cylinder. The Weissenberg number of the flow is defined by $Wi = \lambda U/R$, where the average flow velocity in the channel U is controlled by a syringe pump.

For flow around a single rigid cylinder located in the center of the microchannel [Fig. 12(a)], a flow bifurcation occurs as the Weissenberg number exceeds a critical value $Wi_c \approx 60$ [222]. For $Wi = 37.5 < Wi_c$, the fluid passes the cylinder symmetrically, with the same flow velocity profile on either side of the cylinder, and a straight elastic wake is observed along the flow axis downstream of the cylinder (as seen in the retardation field). However, for $Wi = 93.8 > Wi_c$, the fluid selects a preferred path around the cylinder, with a higher average velocity on one side than the other, and the elastic wake becomes correspondingly distorted downstream. This symmetry-breaking transition has been characterized as a supercritical pitchfork bifurcation [222].

The bifurcation at one cylinder influences (and is influenced by) the bifurcation occurring at neighboring cylinders positioned adjacently [Fig. 12(b)] [223] or downstream [Fig. 12(c)] in the channel [218]. In a hexagonal array of circular cylinders, the bifurcation at each obstacle results in
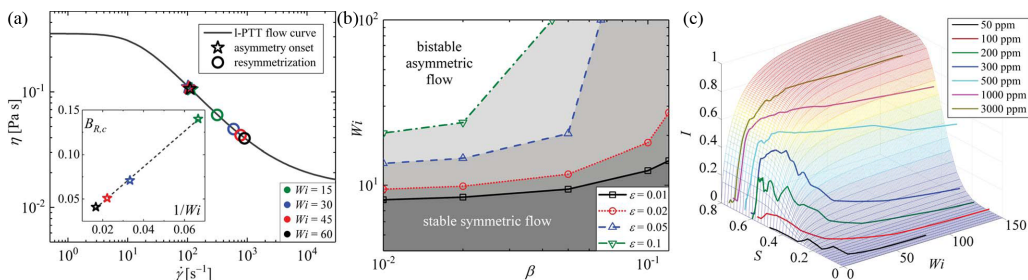
FIG. 13. Influence of shear thinning and elasticity on the onset and development of asymmetric flow states around a single cylinder. (a) Flow asymmetry occurs only when characteristic shear rates near the cylinder correspond to the shear-thinning region of the flow curve. (Inset) The onset of instability is consistent with the scaling predicted by McKinley *et al.*, indicating that elasticity and curved streamlines in the downstream wake provide the initial perturbation to destabilize the flow [74,225]. (b) Stability diagram constructed from simulation results with the l-PTT model examining the interplay between shear thinning and strain hardening (ε) [225]; in this literature shear thinning in the l-PTT model is denoted β (the label of the horizontal axis). Panels (a) and (b) are reprinted from [225] with the permission of AIP Publishing. (c) Experimental measurements with polymer solutions over a range of concentration also show that the asymmetric flow around a cylinder (characterized by the magnitude of I plotted on the ordinate axis) requires both shear-thinning and elastic effects in the fluid. Reproduced from [91] with permission.

a regular pattern of asymmetric wakes where the handedness of the asymmetry alternates between rows [Fig. 12(d)].

We note that in all the cases illustrated in Fig. 12, the flow becomes time dependent and apparently chaotic as Wi becomes sufficiently large. However, instability progresses from an initial transition to a steady asymmetric flow around each cylinder. These flows all appear to be governed primarily by the bifurcation that occurs at each obstacle for $Wi > Wi_c$. Therefore, to correctly interpret phenomena observed in more complex flows, e.g., path selection through arrays of cylinders representing porous media, we consider it crucial to first understand how instability develops around a single cylinder.

Accordingly, Haward, Shen, and colleagues have invested significant efforts in this direction, employing rheologically diverse fluids and a combination of experiments and numerical simulations [91,222,224,225]. The comprehensive studies indicate that the instability is initiated by random fluctuations in the downstream wake due to a combination of high elasticity and streamline curvature close to the downstream stagnation point, i.e., a purely elastic instability of the type described by Pakdel and McKinley [6,74,225] [Eq. (1)]. As shown in the inset to Fig. 13(a), from numerical simulations with the simplified linear Phan-Thien and Tanner (l-PTT) model (Table I with $\xi = 0$), the onset Weissenberg number for asymmetric flow scales with the blockage ratio, $B_R = 2R/W$, in excellent agreement with the prediction of McKinley *et al.* [74,225]. However, from the same set of simulations, performed by varying B_R at fixed Wi, asymmetric flows are supported only when the characteristic shear rate near the cylinder lies on the shear-thinning region of the flow curve [Fig. 13(a)]. As the shear rate approaches the high-shear-rate plateau region, symmetry is recovered.

By fixing the blockage ratio $B_R = 0.1$ and varying the degrees of strain hardening, ε, and shear thinning, denoted β, in the l-PTT model, a stability diagram is obtained in Wi-β parameter space, where the boundaries marking the onset of asymmetric flows can be followed along lines of constant ε [Fig. 13(b)]. The instability is clearly affected by an interplay between the shear thinning and the elasticity of the fluid: if strain hardening is reduced, more shear thinning is required to induce the asymmetric flow state (and vice versa) [225].

These observations are paralleled in experimental measurements using polymer solutions with a range of rheological characteristics [i.e., by varying the shear thinning and elasticity; see Fig. 13(c)]. Here, to understand the role of shear thinning, Haward, Shen, and colleagues employ the "shear-thinning parameter" defined in Sec. II C, $\mathcal{S} = 1 - (d \ln \tau / d \ln \dot{\gamma})$, which is evaluated from the flow

curve measured in steady shear [89–91]. The quantity "I" reported in Fig. 13(c) is a measure of the degree of asymmetry in the flow obtained from the difference in flow velocity on either side of the cylinder [91,222]. Elasticity in the wake of the cylinder is considered to depend on the magnitude of Wi. Note that both $\mathcal{S}$ and Wi depend on the imposed flow velocity through the microchannel.

The colored lines in Fig. 13(c) show the trajectories of fluids with different polymer concentrations through the 3D space, while the fitted surface is formed from a combination of sigmoidal curves in $\mathcal{S}$ and Wi [91]. From Fig. 13(c), it can be observed that fluids with low polymer concentrations (e.g., 50 or 100 ppm) never show significant flow asymmetry ($I \cong 0$); shear-thinning is high only when elasticity is low. Fluids with higher polymer concentrations (e.g., 200 or 300 ppm) show the onset of asymmetry as Wi is initially increased, but the flow recovers symmetry at very high Wi due to the loss of shear thinning in the high shear-rate plateau. Fluids of very high polymer concentration (e.g., 1000 or 3000 ppm) develop strong flow asymmetries ($I \to 1$), which can persist up to high Wi since the degree of shear thinning $\mathcal{S}$ remains significant.

The development of the steady flow asymmetry in the cylinder geometry depends on both the degree of shear-thinning and the elasticity of the fluid in question, and the two rheological properties share an interplay whereby strong shear thinning can compensate for weak elasticity (and vice versa). In light of these results, it may be worthwhile revisiting the role of shear thinning in other instances of steady viscoelastic flow asymmetries (for instance in the cross-slot geometry [52,53,90,226]), where the initial onset of instability gives rise to regions in the flow field with disparate shear rates.

B. Flow in porous media

Authors: A. Ardekani, S. S. Datta, and J. S. Guasto

Studies of the flow of a polymer solution through an isolated constriction or across a single cylinder give some insight to the pore-scale flow dynamics in porous media, as noted in the previous subsection [91,225,227,228]. However, the higher connectivity and elevated disorder inherent in natural porous media introduce new complexities to such flows [229,230]. Being able to predict and control viscoelastic fluid flow through porous media has several important industrial applications, as reviewed previously in [231]. Notable examples are enhanced oil recovery (EOR) [232] and groundwater remediation [233,234], in which addition of polymers to a displacing fluid leads to enhanced recovery of a trapped nonwetting fluid [235–237]. Several mechanisms for this phenomenon have been proposed: adding polymers is thought to (i) increase the viscous drag on trapped immiscible fluid droplets that helps to mobilize them [238,239]; (ii) suppress viscous fingering instabilities during fluid displacement [240]; (iii) impart strong spatial and temporal velocity fluctuations induced by elastic instabilities, potentially also helping to mobilize trapped droplets [63,241–243]; and (iv) reduce the permeability of the medium locally due to polymer retention at solid surfaces, leading to large and heterogeneous local changes in flow that may also help mobilize trapped droplets [244]. However, systematic studies in porous media of varying geometries are needed to parse the influence of these different possible instability mechanisms.

The accumulation of stresses as polymers traverse successive pores can produce spatial variation in the dominant flow features [161,197,225,245–249]. For example, when flowing around closely separated obstacles, polymer chains can be advected from an upstream to a downstream obstacle faster than they can relax. This interaction leads to a bifurcation of the unstable polymeric fluid flow into two coexisting flow states between the two obstacles [214]. More recent work has shown that in tightly ordered (lower porosity) one-dimensional (1D) arrays of *multiple* pores, with resemblance to natural porous media, this interaction can produce an unexpected bistability in the unstable flow in which the flow in each pore switches stochastically between two distinct primary structures: an eddy-dominated structure and an eddy-free structure [65] (Fig. 14).

Numerical simulations have corroborated these experimental results, showing that even more patterns (i.e., multistability) can arise above a critical Weissenberg number: (i) eddy on both the top and bottom of the pore, (ii) eddy-free pore, (iii) eddy-free top of the pore, and (iv) eddy-free bottom
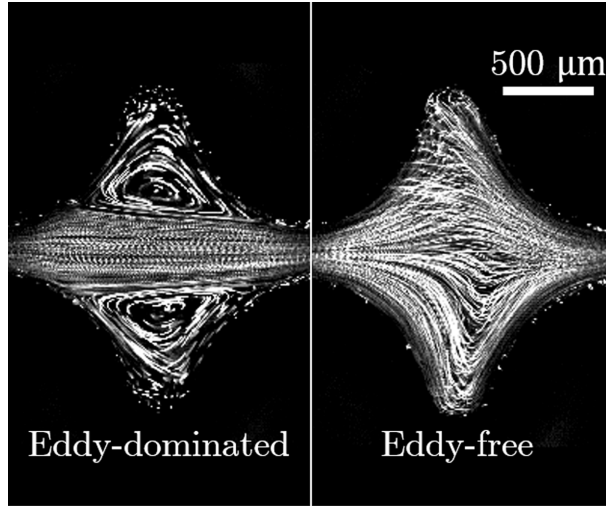
FIG. 14. Experimental images of two distinct unstable flow states observed for elastic polymer solution flow through ordered 1D arrays of pore constrictions. Images show fluid pathlines and are adapted from [65] with permission.

of the pore [197] [Figs. 15(a)–15(c)]. This multistability reflects the formation of different regions of high polymeric stress in the pores [Fig. 15(b)]: the accumulation of stresses as the polymeric chains cross successive pores creates streaks of high polymeric stress that are closely coupled to the flow structures inside the pores. Polymeric chains are highly stretched in the regions of high polymeric stresses, preventing the flow crossing these streaks and inducing eddy formation in different parts of the pore. Intriguingly, the simulations suggest that this multistability can actually reduce the
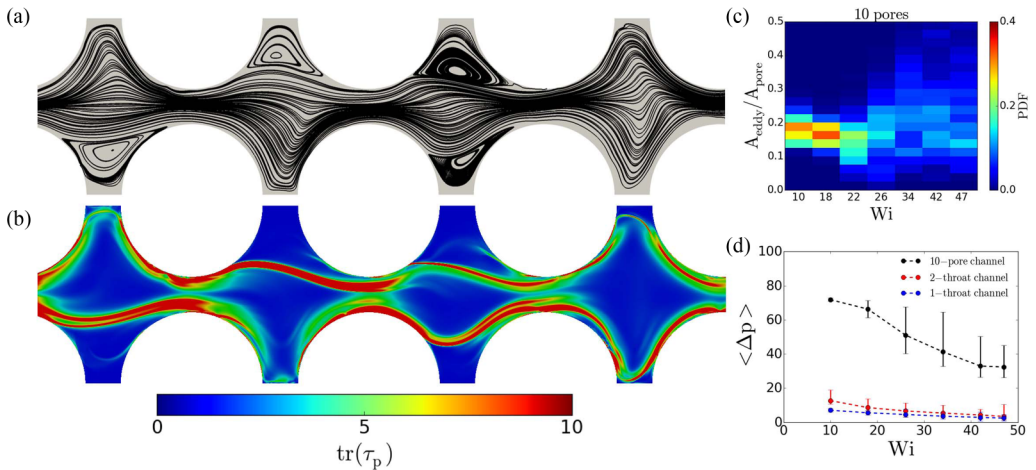
FIG. 15. (a) Multistability of the unstable flow of polymeric fluid through the pores of a converging-diverging channel. (b) Trace of polymeric stress tensor inside the pores. (c) Probability density function (PDF) of the ratio of eddies to pore area (A_{eddy}/A_{pore}) at different Wi for a channel of 10 closely located pores. A_{eddy} represents the total area occupied by eddies in an individual pore and A_{pore} is the total area of the pore. Above a threshold Wi, multistability occurs, and the eddy areas take on a broad range of values. (d) Time-averaged pressure drop ($\langle \Delta p \rangle$) across the channels at different Wi. Images are reproduced from [197].
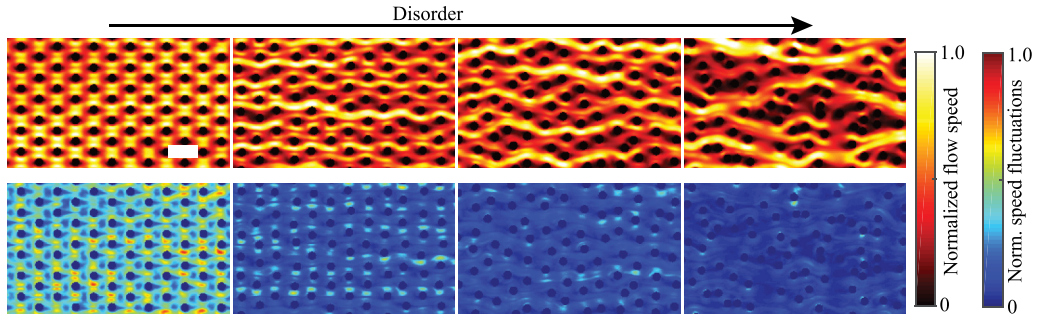
FIG. 16. Experiments in which disorder reduces chaotic fluctuations in viscoelastic flows through porous media. (Top row) Normalized, time-averaged speed field in a microfluidic pillar array for a range of geometric disorders (Wi ≈ 4). Scale bar, 150 μm. (Bottom row) Local, normalized speed fluctuations as a function of increasing disorder, corresponding to speed fields above. Images are reproduced from [161].

pressure drop across the channel [197] [Fig. 15(d)] because the eddies do not contribute to the net volumetric flow through the channel; therefore, an eddy-free pore has a larger apparent width to allow the net volumetric flow than the pore with eddies, which leads to a smaller pressure drop across the eddy-free pore. Further experimental tests of this behavior will be an interesting direction for future work.

Recent experiments have shown that disorder may also play a fundamental role in the stability of viscoelastic flows through porous media [161]. Similar to single obstacles, viscoelastic flow through an ordered 2D array of cylinders readily transitions to chaos at a critical $Wi_{cr} = O(1)$. However, the introduction of small deviations from crystalline order in the porous medium can delay the transition to higher Wi_{cr}, and strongly disordered media can have largely suppressed random velocity fluctuations (Fig. 16). The mechanism by which disorder may promote stability is by causing a shift in the flow type [250] from extension- to shear-dominated flow. In the work of Walkama *et al.* [161], as geometrical disorder increases, stable preferential flow paths emerge and promote shear, which weakly stretches polymers in comparison to extensional flow [251,252]. This work also emphasizes the importance of Lagrangian stretch that is accrued along a polymer's flow path in triggering viscoelastic instability, and inspires further studies of the influence of pore geometry on the flow behavior.

Exploring how insights developed in 1D and 2D systems relate to flows in more complex 3D porous media [229,232–234] is an active frontier of current research. In the stable creeping flow regime considered here, spatial correlations of velocity and pore space have been shown to be almost identical between 2D and 3D media [229]. However, pore-scale flow instabilities in 3D geometries can exhibit different patterns than 2D instabilities [62,81,253], inducing differences in macroscopic flow and transport as well [254–256].

Indeed, given the observation that disorder can suppress the transition to elastic turbulence in 2D porous media [161], it has been unclear whether and how this transition manifests in disordered 3D media—though elastic turbulence has been speculated to underlie the long-standing observation that the macroscopic flow resistance of an injected polymer solution can abruptly increase above a threshold flow rate in a porous medium, but not in bulk solution [242,243,257–261]. By directly visualizing the flow in a transparent, disordered, 3D porous medium, the authors of [262] directly verified that elastic turbulence does arise within a disordered 3D porous medium and used flow velocimetry to link chaotic pore-scale flow fluctuations to the macroscopic flow resistance. In particular, the authors found that the transition to unstable flow in each pore is continuous, arising due to the increased persistence of discrete bursts of instability above a critical value of the characteristic Wi; however, the onset value varies from pore to pore.
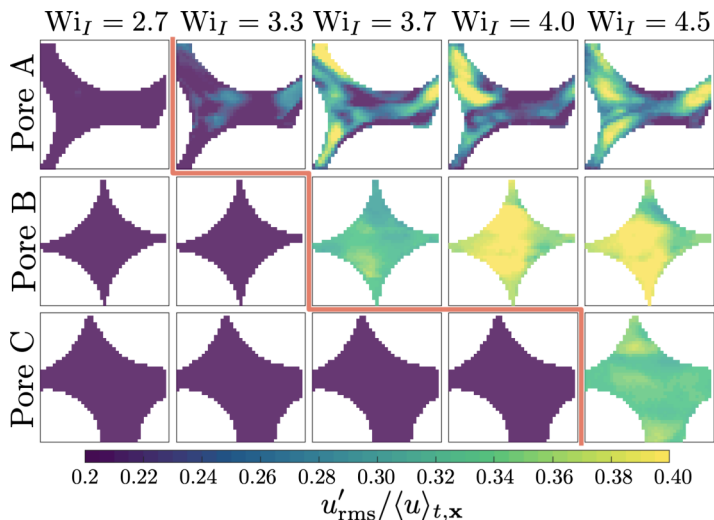
FIG. 17. The occurrence of elastic turbulence is spatially heterogeneous throughout a porous medium, reflecting "porous individualism." Images show the normalized magnitude of root mean square flow fluctuations in different pores and at different flow rates, parameterized by a characteristic Weissenberg number Wi_I. Applied flow is from left to right. Pore A becomes unstable at the lowest flow rate, as shown by the red line in the first row. Pore B becomes unstable at the next highest flow rate, shown by the red line in the second row. Pore C becomes unstable only at even higher flow rates. Note that flow velocity magnitude is denoted by u instead of v as in the rest of the text. Modified from [262].

This observation that single pores exposed to the same macroscopic flow rate become unstable in different ways provides a fascinating pore-scale analog of "molecular individualism" [263], in which single polymers exposed to the same extensional flow elongate in different ways; the authors therefore termed it "porous individualism," although it is important to note that here this effect is still at the continuum (not molecular) scale. Thus, unstable flow is spatially heterogeneous across the different pores of the medium, with unstable and laminar regions coexisting (Fig. 17). Guided by these findings, and inspired by the analysis of recent simulations [264], the authors quantitatively established that the energy dissipated by unstable pore-scale fluctuations generates an anomalous increase in flow resistance through the entire medium that agrees well with macroscopic pressure drop measurements.

Thus, by linking the onset of unstable flow at the pore scale to transport at the macroscale, such research is beginning to yield generally applicable guidelines for predicting and controlling unstable flows of polymer solutions in porous media. Indeed, experimental developments using confocal microscopy in model 3D porous media [210,230,265], defocusing particle tracking velocimetry [266], holographic particle tracking velocimetry [267], and fast synchrotron-based x-ray computed microtomography in real porous rocks [268,269] provide access to flows *in situ* that will likely continue to refine our understanding of these complex systems.

VI. ELASTOINERTIAL FLOW INSTABILITIES

Authors: M. D. Graham, V. Shankar, and G. Subramanian, with input from A. Morozov

Ever since the iconic experiments of Osborne Reynolds in 1883 [270], it has been well known that Newtonian pipe flow undergoes a laminar-turbulent transition when the eponymous dimensionless parameter (the Reynolds number, Re) exceeds a threshold. The complexity of this transition was already understood by Reynolds, as evidenced by the following remark in Ref. [270]: "it was observed that the critical velocity was very sensitive to disturbance in the water before entering

the tubes." Later experiments have indeed shown that the laminar state in Newtonian pipe flow can be maintained up to Re $\approx 10^5$ [271]; this behavior is consistent with the current consensus that Newtonian pipe flow is linearly stable at all Reynolds numbers [272]. The Newtonian pipe flow transition from laminar to turbulent flow is therefore very different from that observed in the Taylor-Couette geometry (with the inner cylinder rotating) discussed earlier in Sec. II. In the latter case, the transition is marked by a sequence of reasonably well-defined bifurcations starting from the initial linear instability, and leading to a gradual increase in the spatiotemporal complexity [273]. In stark contrast, in Newtonian pipe flow (and indeed in the other canonical shear flows such as plane Couette and Poiseuille flows), transition is abrupt, and is marked by the appearance of localized structures known as turbulent puffs and slugs (or turbulent spots in the aforementioned plane shear flows) that already exhibit the full spatiotemporal complexity of the ensuing turbulent state [183,188]. Indeed, the original paper by G. I. Taylor [9] on the centrifugal instability in the geometry that now (partly) bears his name involved a successful comparison between theory and experimental observations of the transition from the base-state azimuthal flow. However, as discussed below, more than a century was required after the original paper of Reynolds for the emergence of a rigorous theoretical understanding of the Newtonian pipe flow transition.

Transition to turbulence in canonical rectilinear shearing flows, e.g., plane Couette, and plane- and cylindrical-Poiseuille flows, of a Newtonian fluid, beyond a threshold Re is a complicated process [183,274], largely due to the absence (plane Couette and pipe flow) or irrelevance (plane Poiseuille) of an underlying linear instability [275]. Note that Re here is the Reynolds number based on the half-height/pipe radius, maximum velocity of the laminar flow, and the total solution viscosity and density. The Weissenberg number, Wi, is based on the polymer relaxation time, maximum velocity of the laminar flow and the half-height/pipe radius. Nevertheless, the Newtonian transition is now regarded as well understood from a dynamical systems perspective, with the eventual transition being presaged by the appearance of nontrivial 3D solutions (the so-called exact coherent states or "ECS" in short, which were first introduced in Sec. IV B 1 by way of analogy to the possibility of nonlinear elastic structures in the inertialess limit) of the Navier-Stokes equations [276–279]. These are disconnected from the trivial laminar state and serve as a scaffold, in an appropriate phase space, for the turbulent dynamics after transition [130,280,281]. These ECSs contain the basic self-sustaining ingredients of transitional Newtonian turbulence, i.e., quasi-streamwise vortices and streaks. A comprehensive review of ECS can be found in [130,188].

While the transition to inertial turbulence in Newtonian pipe and plane Poiseuille flow is now relatively well understood as described above, recent experimental, theoretical, and computational studies have shown that the transition scenario in viscoelastic counterparts of the above flows may be markedly different. Both linear and nonlinear mechanisms, with no analogues in the Newtonian realm, have been proposed for viscoelastic rectilinear shearing flows. Thus, while the focus in Sec. IV was on instabilities of rectilinear shearing flows pertaining to the low-Re regime, this section emphasizes the crucial role played by both fluid inertia *and* elasticity in destabilizing the laminar base state, and the focus is on what may be appropriately referred to as "elastoinertial" instabilities. In Sec. VI A below, we begin with the well-known drag-reducing effect of polymers on fully developed Newtonian turbulence, before moving on to the mechanistic underpinnings of turbulent drag reduction in Sec. VI B. We then summarize in Sec. VI C various transition scenarios for viscoelastic pipe and plane Poiseuille flows for different fixed values of the ratio between solvent and total viscosity, denoted β.

A. Turbulent drag reduction and elastoinertial turbulence (EIT)

Author: M. D. Graham, with input from V. Shankar and G. Subramanian

The addition of long chain polymer molecules to a fluid has tremendous effects on wall-bounded turbulence, the most dramatic being the substantial reduction of the friction factor [140,282,283], which is proportional to the pressure drop for a given flow rate (or Reynolds number). This phenomenon has found wide use in various applications that seek energy efficiency in flow processes
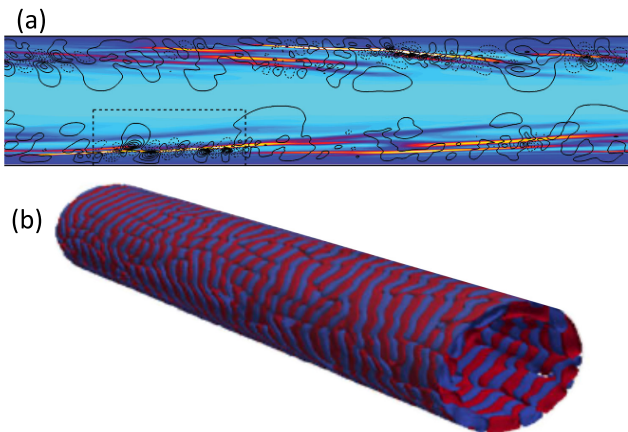
FIG. 18. Snapshots of simulations of EIT in (a) channel flow [298] and (b) pipe flow [297]. (a) Color contours indicate polymer stretching, and lines indicate the magnitude Q of the second invariant of the velocity gradient tensor; reproduced with permission from [298]. (b) Isosurfaces indicate Q; licensed under a Creative Commons Attribution (CC BY) license.

[284–286]. Not surprisingly, there is also a large literature seeking to understand and/or exploit this phenomenon.

Hence, in this section, we now broaden our perspective and focus on situations in which fluid inertia is nonnegligible. We focus on high-Reynolds-number channel flow of a dilute solution of high molecular weight polymer, so the ratio between solvent and total viscosity, β satisfies $1 - \beta \ll 1$, and the Trouton ratio (i.e., the ratio between extensional and shear viscosities) Tr $\gg 1$. For the FENE-P constitutive model with chain length parameter (there should be a space inserted here) $b (\equiv L^2)$, this requires that $b(1 - \beta) \gg 1$. This is the regime of primary relevance for drag reduction, where as a practical matter it is desired to keep the shear viscosity of the fluid low (i.e., $1 - \beta \ll 1$), but the extensional viscosity high [i.e., $b(1 - \beta) \gg 1$]. The Reynolds number regime considered is Re $\sim 10^3$–10^4, i.e., near transition.

Important features of turbulent flow when the degree of polymer-induced drag reduction is large include a very small Reynolds shear stress and a mean velocity profile that closely approaches the so-called Virk maximum drag reduction (MDR) asymptote [140]. It is interesting that this profile is nearly independent of the composition or concentration of the polymer.

With respect to mechanism, it is well known that viscoelasticity suppresses the near-wall streamwise vortices that dominate Newtonian turbulence [287,288]. A number of studies have captured this phenomena by studying the effect of viscoelasticity on the aforementioned ECS solutions [289–295]. In particular, Li and coworkers [291,293] found that the ECS are so weakened by viscoelasticity that they are no longer self-sustaining and so should fail to exist. However, recognizing that, in general, viscoelasticity is not experimentally observed to drive relaminarization of the flow, these authors suggested the possibility of new viscoelastic mechanisms for sustaining turbulence and becoming unmasked as the Newtonian structures are suppressed [293].

Indeed, instead of complete relaminarization of the flow (except in narrow parameter ranges at transitional Re as detailed later), recent studies have unearthed a polymer-driven chaotic flow state dubbed elastoinertial turbulence (EIT), which dominates high-Reynolds-number flows at high levels of viscoelasticity [296]. In this parameter regime EIT displays multilayered sheets of polymer stretch emanating from near the walls [see Fig. 18(a)] and very weak, spanwise-oriented vortices, which is in sharp contrast to the 3D quasi-streamwise vortex structures of Newtonian wall turbulence. Similarly, near-wall localized, nearly axisymmetric vortex and stress structures [Fig. 18(b)] have been reported in pipe flow simulations of EIT [297].

Using computations in channel flow at Re $= 1500$, Shekar *et al.* [299] observed a narrow zone of Wi, roughly 10–18, where the only attractor was the laminar base state. This zone separated drag-reduced Newtonian turbulence at lower Wi and EIT at higher Wi, corroborating the experimental observations of [300]. In this case, the laminar flow remains linearly stable in the EIT regime, but only very small (but finite) perturbations are required to drive the flow to EIT. This observation suggests that extreme care must be taken in interpreting experimental observations of a transition to a very weak EIT state: what appears to be a linear instability may not be.

Before discussing the theory to understand these observations, as well as others described below, it is first useful to recall the known structure, and the associated features, of the Newtonian eigen-spectrum for plane- and pipe-Poiseuille flows [307]. The spectrum has a characteristic "Y"-shaped structure, with the two arms of the Y comprising the wall modes (the so-called A branch with modal phase speeds and decay rates approaching zero) and the center modes (the so-called P branch with phase speeds approaching the centerline maximum and decay rates approaching zero) for Re ~ 1000 and higher. The (lower) stem of the Y structure corresponds to the S branch that consists of a denumerable infinity of modes that propagate at two-thirds of the base-flow maximum and with progressively increasing decay rates down the stem. Note that, with increasing Re, the underlying Y template remains unchanged, while there is a progressive increase in the number of modes along each of the three branches. This Y template characteristic of the Newtonian spectrum is henceforth referred to as the "A-P-S" template. The Tollmien-Schlichting (TS) mode in Newtonian plane-Poiseuille flow corresponds to a wall mode belonging to the A branch that becomes unstable at Re ≈ 5772; Newtonian pipe-Poiseuille flow, in contrast, is known to be stable for all Re.

For large Re, the streamwise velocity eigenfunction for the TS mode displays a sharp localization at wall-normal locations called "critical layers," near the top and bottom walls (thus the term "wall mode"), where the base-flow velocity equals the phase speed. A balance of inertial and viscous effects shows that the thickness of the critical layer decreases as Re$^{-1/3}$, consistent with the aforementioned localization. Critical layers can be thought of as the most favorable positions for energy exchange between the base flow and the fluctuations, because they are the positions where both the fluctuations and the base flow have the same speed.

Returning to the observations of [299], EIT in this parameter regime displays polymer stretch fluctuations localized near the wall. In particular, a resemblance was noted between the EIT structure and the viscoelastic extension of the classical TS mode, which at the chosen parameters is the slowest decaying mode from linear stability analysis. This viscoelastic TS mode displays polymer stretch fluctuations that are sharply localized to critical layers near the top and bottom walls. Similarly, resolvent analysis predicts strong amplification of this structure in the presence of viscoelasticity. This strong amplification implies, consistent with the fully nonlinear results, that even very weak disturbances may be sufficient to trigger EIT. We note that Page and Zaki [302] present computations, and Haward *et al.* [301,303] present corresponding experiments for viscoelastic flow over a wavy wall that illustrate amplification of perturbations in the critical layer. Building on the above observations, Shekar *et al.* [304] performed direct simulations of 2D plane channel flow with the FENE-P constitutive equation at Re $= 3000$, revealing the existence of an attractor family denoted the "viscoelastic nonlinear Tollmien-Schlichting attractor" (VNTSA), whose structure is virtually identical to the linear TS mode and in particular exhibits strongly localized stress fluctuations at the critical layer position of the TS mode, as illustrated in Fig. 19. At the parameter values chosen, this solution branch is not connected to the nonlinear TS solution branch found for Newtonian flow and thus represents a solution family that is nonlinearly self-sustained by viscoelasticity: the laminar state remains linearly stable, though again, as in [299], only an extremely small perturbation is required to drive the solution away from the laminar state. This attractor loses stability subcritically, and edge tracking can be used to show that it connects through an unstable solution family to 2D EIT.

The results of [304] strongly suggest, but do not directly indicate, the existence of a continuous path in parameter space between the Newtonian TS wave and EIT in channel flow. To clarify this issue, Shekar *et al.* [305] used DNS to continue the VNTSA solution branch of [304] from
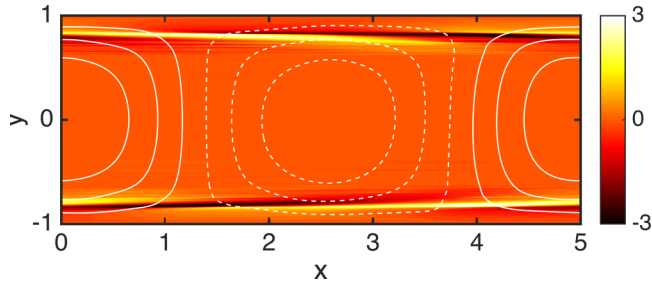
FIG. 19. Snapshot of the finite amplitude Tollmien-Schlichting wave solution at Re = 3000, Wi = 10 [304]. White contours are wall-normal velocity, colors are deviations of *xx* polymer stretch from laminar values. Reproduced with permission from [304].

Re = 3000 up to Re = 10 000, and then down to Wi = 0, to recover the Newtonian nonlinear Tollmien-Schlichting attractor. Conversely, starting with the Newtonian TS attractor at Re = 10 000, the Newtonian TS attractor evolves continuously and without hysteresis into EIT as Wi is increased from zero to about 13—*the two flows are part of the same solution family*. Figure 20 illustrates the evolution of the flow and stress fields as Wi increases. Note the resemblance between Fig. 20(d) and Fig. 18(a). The simple sheet structures that originate with the TS critical layer structure evolve into the multilayered structure of EIT through a process that has been denoted "sheet shedding":
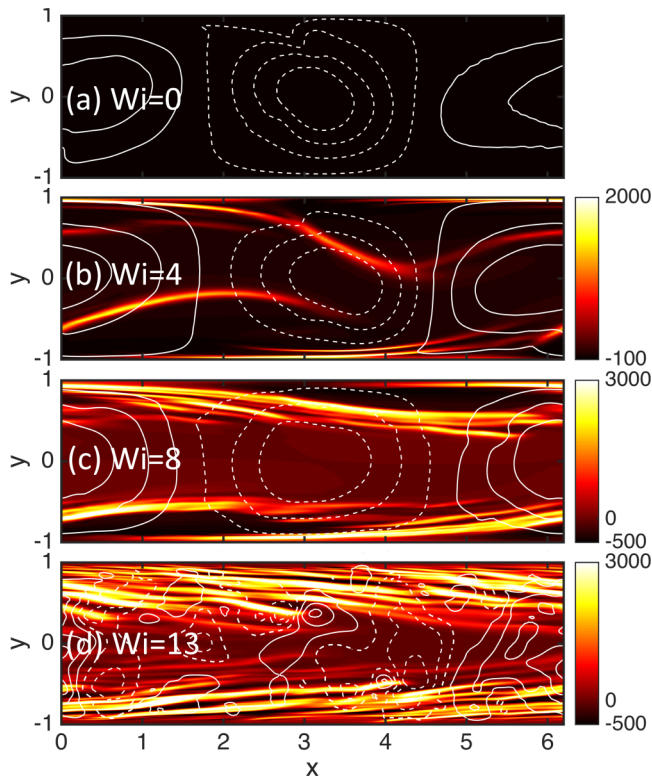

FIG. 20. Snapshots of the finite amplitude Tollmien-Schlichting wave solution at Re = 10 000 and (a) Wi = 0, (b) Wi = 4, (c) Wi = 8, (d) Wi = 13 [305]. White contours are wall-normal velocity, and colors are deviations of *xx* polymer stretch from laminar values.

Individual sheets associated with the critical layer structure break up, with the fragments further sheared as they travel downstream.

The linear instability to Tollmien-Schlichting waves does not arise for pipe or plane Couette flow, so the scenario described here does not directly apply to those geometries. On the other hand, in these geometries elastoinertial turbulence with very similar features does arise in simulations in the same general parameter regime: namely, fluctuations localized in a layer near the wall, with a sheetlike stress structure and little to no activity in the center of the flow as illustrated in Fig. 18(b) [297,306]. Furthermore, while linearly stable, wall modes analogous to the TS wave do exist in these other geometries [307] and may be subject to nonlinear critical layer excitation, and subsequent evolution into EIT, just as the TS mode is in the channel flow case. Indeed, Zhang [308] performed resolvent analysis for pipe flow in the same parameter regime considered here, demonstrating that the most amplified mode has strong stress fluctuations localized in a critical layer near the wall, just as is found by Shekar *et al.* [299]. See [304] for further discussion of these issues.

The work described here demonstrates a direct connection between a wall mode (the TS mode) and EIT structures. At the same time, in more strongly viscoelastic regimes, typically $El \gtrsim 10^{-1}$ and extremely high molecular weight ($L^2 \gtrsim 10^5$), Garg *et al.* [141], Chaudhary *et al.* [142], and Khalid *et al.* [309] have found a linear center-mode instability for pipe flow and channel flow respectively, as described in Sec. VI C. In channel flow Page *et al.* [143] computed the finite amplitude nonlinear traveling wave solution that originates in the center-mode instability, finding that at finite amplitude it exhibits an "arrowhead" structure of polymer stretching. Dubief *et al.* [144] study this state with direct numerical simulations. In an experimental study, Choueiri *et al.* [310] also note the appearance of "chevron"-shaped velocity fluctuation structures resembling the unstable center mode in pipe flow up to $Re = O(100)$ before being taken over by near-wall modes at higher Re. These results open up the possibility that other states unrelated to the nonlinear excitation of a wall mode may play a role in elastic and/or elastoinertial turbulence, with Reynolds numbers in the aforementioned range. Section VI C extensively elaborates on this point.

B. Linking back to drag reduction

Author: M. D. Graham

Next, we return to the issue of the maximum drag reduction phenomenon (MDR). Based on the results described above, the following scenario can be hypothesized: In the MDR regime, the flow cannot stay classically turbulent because streamwise vortices are so strongly suppressed by viscoelasticity that they cannot persist, but on the other hand the flow cannot fully laminarize either, because viscoelastic TS waves (or something else) are nonlinearly excited by small but finite perturbations even when the laminar flow is linearly stable. Nevertheless, weak quasi-streamwise vortex and streak structures are experimentally observed to exist at MDR [288]. Based on these points, MDR may be a marginal state where weak critical layer (or other) excitations keep the flow from laminarizing and provide sufficient perturbations to the flow for the mean shear to generate weak quasistreamwise vortices.

We provide two further comments on this hypothesis. First, for Newtonian and viscoelastic channel flows, Xi and Graham [311] computed "edge states," which are dynamical trajectories that are marginal in the sense that they lie on the state-space boundary between laminar and turbulent flow. Near transition, these states display a mean velocity profile very close to the Virk MDR profile. Furthermore, very recent computations by Zhu and Xi [131] indicate the presence of an intermittent process in viscoelastic channel flow involving quasi-2D structures with near-wall critical layer characteristics and 3D quasi-streamwise structures, again with a mean velocity profile that lies on or above the Virk MDR profile.

C. Elasticity-induced transition scenarios in Re-Wi space

Authors: V. Shankar and G. Subramanian, with input from M. D. Graham

In this section, we focus on the role of polymer on the incipient transition from the laminar state. Transition for viscoelastic fluids such as polymer solutions, even within the framework of the simplest constitutive equations (the Oldroyd-B equation, for instance), is characterized by at least two additional parameters: Wi and β [142,312]. Transition from the steady laminar base state, to states characterized by nontrivial spatiotemporal dynamics, can occur along multiple pathways in the Re-Wi-β space; for example, the work on purely elastic instabilities described in Sec. IV and the opening of this section, Sec. VI, explored pathways characterized by Re = 0.

The recent prediction of a linear center-mode instability for both viscoelastic pipe and channel flows (alluded to above) [141,142,309] is qualitatively different from the Newtonian scenario, where pipe flow is linearly stable at all Re, while plane Poiseuille flow becomes unstable to the TS mode at Re = 5772, a value that is much higher than the observed threshold for transition. It is important to note that this center mode does not bear a direct relation to the Newtonian center mode, and this in turn is due to the elastoinertial spectrum being very different, and significantly more complicated, than its Newtonian counterpart (which has the A-P-S template described earlier in Sec. VI A). One of the reasons for this is the presence of continuous spectra, which happen to be branch cuts, and discrete eigenmodes can appear and disappear out of the branch cut with variation in the different parameters. The structure of the elastoinertial spectrum in plane- and pipe-Poiseuille flows has been discussed, in some detail, in Refs. [142,309].

The discovery of a linear instability in viscoelastic pipe flow, in particular, marks a radical departure from the earlier literature, which had assumed this flow to be stable in the Re-Wi-β parameter space [26,186,313]. The existence of a linear pathway to transition was also strongly suggested by the earlier experiments of Samanta *et al.* [296], where the threshold Reynolds number was independent of whether the flow was forced at the inlet or not, beyond polymer concentrations of 200 ppm. Both recent computations of Page *et al.* [143] and experiments of Choueiri *et al.* [310] have pointed to the connection of the center-mode eigenfunction to the eventual nonlinear state (a novel EIT coherent structure in the computations) that emerges above threshold.

We now attempt to bring together the ideas described above, both in this section that deals with elastoinertial transition and turbulence and in the earlier sections that focused on elastic instabilities and transition in rectilinear shearing flows, via Figs. 21 and 22. These attempt to summarize the transition scenarios for pipe and plane Poiseuille flows, respectively, in the Wi-Re plane for different fixed values of β. The linearly unstable regions in the interior of the Wi-Re plane, corresponding to the center-mode instability, are marked by thick black lines (solid, dashed, or dash-dotted) for specific values of β, while those for other values of β are depicted by light gray lines. In both figures, regions adjacent to the Re and Wi axes correspond to the onset of predominantly inertial and elastic instabilities, respectively, with the former underlying the subcritical Newtonian transition.

We begin with a brief discussion of the features common to both figures, before going on to describe those unique to Fig. 22, which make the transition in plane Poiseuille flow a potentially richer playground for both linear and nonlinear transition mechanisms. The 3D ECS-driven mechanism that triggers the Newtonian transition becomes less relevant for weakly elastic flows on account of the Newtonian ECSs being suppressed by increasing elasticity [289–293]. While this suppression has been demonstrated specifically for plane Poiseuille flow, it is reasonable to conjecture that a similar scenario should prevail for pipe flow on account of the similarity of the underlying ECSs [142]. The suppression and eventual disappearance of the ECSs is thought to be responsible for a delayed transition to, and eventual disappearance of, the Newtonian turbulent state. In both Figs. 21 and 22, the Newtonian-turbulent-like state is therefore confined to a region between the Re axis and a curve that corresponds to a Re-dependent critical value of the Weissenberg number Wi_c. At higher levels of elasticity, the aforementioned linear center-mode instability becomes operative.

Although the extent of the linearly unstable region depends sensitively on flow type and β, the unstable regions for both pipe and channel flows, shown in Figs. 21 and 22, respectively, bear a
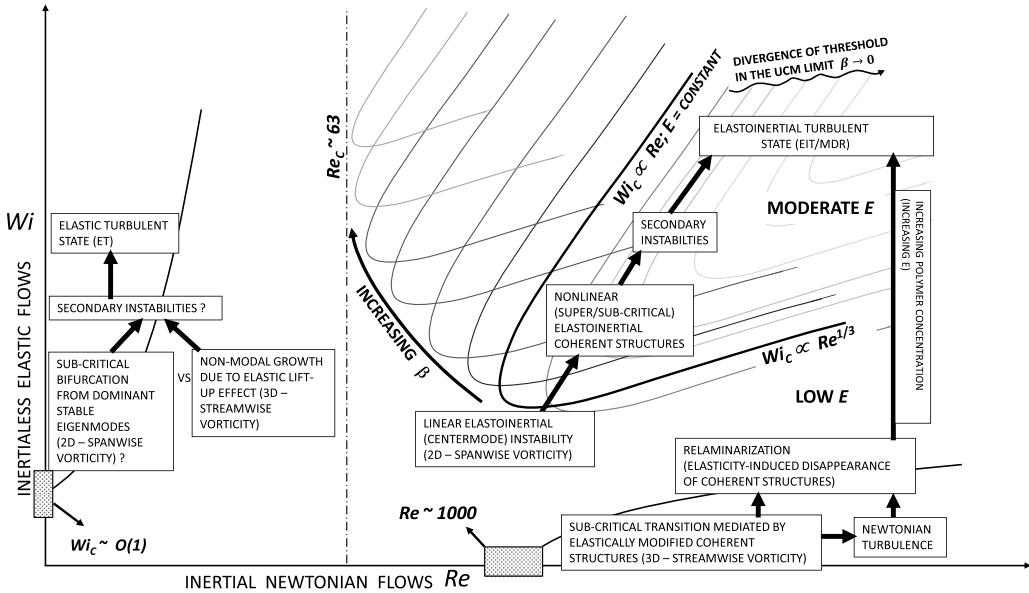
FIG. 21. Schematic representation of various transition scenarios for viscoelastic pipe flow in the Re-Wi plane. The laminar flow is characterized by the Poiseuille velocity profile with rectilinear streamlines. The linearly unstable regions in the interior of the Wi-Re plane, corresponding to the center-mode instability, are marked by a thick black line (solid) for one specific values of β, while those for other values of β are depicted by light gray lines.
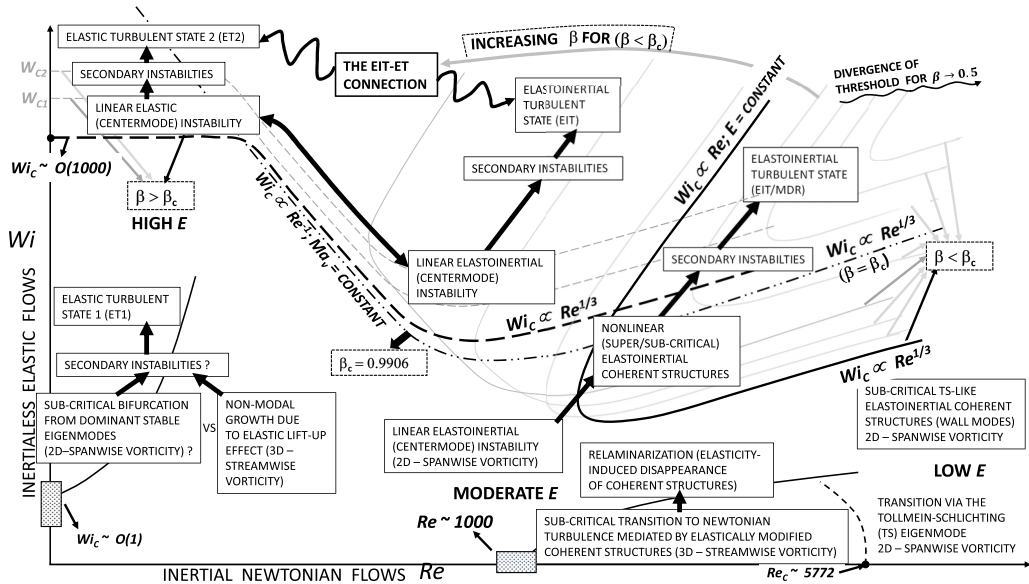

FIG. 22. Schematic representation of various transition scenarios for viscoelastic plane Poiseuille flow in the Re-Wi plane. The linearly unstable regions in the interior of the Wi-Re plane, corresponding to the center-mode instability, are marked by thick black lines (solid, dashed, or dash-dotted) for specific values of β, while those for other values of β are depicted by light gray lines. Note that the critical value Re$_c$ $\sim$ 5772 is defined using the laminar equivalent centerline velocity.

close resemblance in the range $0.5 < \beta < 0.98$. Specifically, $\text{Wi}_c \propto \text{Re}^{1/3}$ along the lower branch of the unstable region, while $\text{Wi}_c \propto \text{Re}$ along the upper branch; the latter corresponds to a constant elasticity number El, and represents an experimental path for a given flow geometry and polymer solution. For both geometries, the center-mode eigenfunction likely gives way to supercritical nonlinear structures that, either directly or via secondary instabilities, might underlie the observed EIT dynamics. In this sense, the center-mode instability, for both pipe and channel flows, provides a continuous pathway from the laminar state to the EIT (and the eventual MDR) regime. Although not shown, the EIT and Newtonian turbulence domains overlap at higher Re, where the original center mode gives way to a wall mode—indeed, this overlap has been found by several authors [131,306,314]—implying that the latter transitions in a continuous manner to the former, without an intervening relaminarization. This was believed to always be the case in earlier literature. The vertical path shown on the right in Fig. 21 corresponds to the one in Ref. [300], which first accessed an intermediate quasi-laminar state with increasing Wi at a fixed Re ($= 3600$), thereby contradicting the aforesaid long-held belief. A vertical path at fixed Re in the Wi–Re plane implies an increase in elasticity number $\text{El} = \lambda\nu/R^2$, introduced earlier in Sec. II C, but defined here with the pipe radius R as the relevant length scale and $\nu \equiv \mu/\rho$. In this context, it is useful to note that in the dilute limit, strictly speaking, both the relaxation time λ and ν are independent of polymer concentration. Thus, in this regime, an increase in El can be accomplished only by decreasing the pipe radius R. However, in the experiments of Choueiri *et al.* [300], the pipe radius R is fixed; instead, the authors increase the polymer concentration in the vicinity of the overlap value, which results in an increase in both λ and ν, and thence El (while, presumably, adjusting the flow rate to keep Re fixed).

Despite the above similarities, there remain significant differences between the instabilities of pipe and plane Poiseuille flows outside of the aforementioned range of β. The center-mode instability disappears for $\beta < 0.5$ for channel flow, while it persists down to $\beta \approx 10^{-3}$ for pipe flow. The opposite limit of $\beta \to 1$, discussed above in the drag reduction context, is also of particular interest from the linear stability viewpoint. While the center-mode instability appears to be restricted to $\text{Re} > 63$ for pipe flow (Fig. 21), remarkably, it morphs into a purely elastic instability for channel flow, continuing to arbitrarily small Re for $\beta > \beta_c \approx 0.9905$ [171]. As a result, the "nose" of the original unstable region in Fig. 22 begins to broaden for $\beta \to \beta_c$, eventually opening out into a plateau that extends right up to the Wi axis for $\beta > \beta_c$. Rather intriguingly, for β close to β_c, the lower branch ($\text{Wi}_c \propto \text{Re}^{1/3}$) and the small-Re plateau are separated by an intermediate asymptotic regime with $\text{Wi}_c \propto \text{Re}^{-1}$; this corresponds to a constant viscoelastic Mach number, $\text{Ma}_v = V/V_{\text{shear}} = O(1-\beta)^{-1}$, with $V_{\text{shear}} = \sqrt{\frac{(1-\beta)\eta}{\rho\lambda}}$ being the shear wave speed. However, the implied shear-wave signature may not be relevant to the recent observation of "elastic waves" in sheared dilute polymer solutions [83,171]. Considerations of continuity imply that the crossover from the intermediate scaling regime to the creeping-flow instability must pass through a special $\beta = \beta_c$ for which the scaling $\text{Wi}_c \propto \text{Re}^{-1}$ should persist down to $\text{Re} \to 0$! (As shown by the dash-dotted line in Fig. 22.) Importantly, the aforementioned transformation of the original center-mode instability into a purely elastic one—that in turn might give way to a turbulent state—highlights the existence of an EIT-ET connection for channel flow (via an underlying modal pathway). This might serve as a novel template in a search for purely elastic coherent structures.

In regions of the Re-Wi-β space where the center mode is linearly stable, novel subcritical mechanisms likely dominate the transition process. In this regard, and as discussed in Sec. VI A, recent work [299,304] has identified a nonlinear mechanism closely related to the stable Newtonian Tollmein-Schlichting mode (although still disconnected from it in phase space until a Re of 10^4). The fact that there is no analog of the TS instability in Newtonian pipe flow, and no evidence of a corresponding nonlinear solution branch in the Newtonian limit, suggests that the TS-mode-based subcritical mechanism could be specific to plane Poiseuille flow. On the other hand, as noted in Sec. VI B, the direct simulations of EIT by Lopez *et al.* [297] display strong localization of fluctuations near the wall, and the resolvent analysis of Zhang [308] demonstrates strong linear amplification of a mode with near-wall critical-layer stress fluctuations. Both of these observations

are fully consistent with those described by Shekar *et al.* [299,304] in channel flow, wherein subcritical transition to EIT is driven by the amplification of fluctuations with near-wall critical layer structure, suggesting a similar mechanism for EIT in pipe and channel flows. Indeed, in the work of [299], the Reynolds number is so low that no subcritical TS branch exists in the Newtonian limit. Returning to the case of channel flow, the recent subcritical continuation of the unstable center mode to a nonlinear EIT structure [143] implies that subcritical mechanisms based on the center mode might also be operative in certain regions of Re-Wi-β space, and thus the relevance of the center mode might extend outside of the linearly unstable regions indicated in Figs. 21 and 22.

In the opposite limit of Re $\ll$ 1, viscoelastic pipe and Poiseuille flows are linearly stable for Wi $= O(1)$ and when β is not very close to unity [142,315]. One of the proposed transition scenarios is that of a subcritical 2D nonlinear instability [186,187], although this has been demonstrated only for Wi $= O(1)$ and $\beta \rightarrow 0$. The existence of a linear instability at the other extreme, Wi $= O(1000)$ and $\beta \rightarrow 1$ [171], implies the possibility of a bifurcation to a distinct elastic turbulent state. It is therefore possible to envisage (at least) two different ET states (labeled ET1 and ET2 in Fig. 22), in inertialess plane Poiseuille flow, depending on Wi. Even in this limit, however, there is a wide intermediate range of β ($0 < \beta < \beta_c$) for which the nature of the subcritical transition remains an open question.

It is worth summarizing, in a succinct manner, the implications of the findings detailed in this section with respect to transition to EIT in pipe and channel flows of polymer solutions. For moderate-to-strongly elastic polymer solutions (El > 0.1, $\beta \sim 0.5$–0.9), where transition to EIT occurs directly from the laminar state, both experiments and theory point to the relevance of the center mode at onset [141–143,309,310]. On the other hand, for weakly elastic dilute polymer solutions of the type investigated in the context of drag reduction (El < 0.02, $\beta \rightarrow 1$), when the primary transition to turbulence is akin to the Newtonian one, the eventual EIT state is dominated by wall modes that appear to be closely related to the nonlinear traveling-wave solutions identified in [299,304]. It is worth noting that there are vast tracts of the viscoelastic parameter space that remain to be understood from the transition perspective. For instance, for dilute solutions (with $\beta = 0.97$) at higher El ($0.02 < $ El < 0.5), it is the continuous spectrum that is the least stable [see Fig. 19(b) of Ref. [309]] and may perhaps be expected to play a dominant role in the (subcritical) transition dynamics. Future research will be necessary to disentangle the roles of wall- and center-mode-based structures, and perhaps other structures (e.g., modes belonging to the continuous spectrum) as well, for EIT in various geometries and parameter regimes.

D. Nonmodal scenarios

Authors: V. Shankar and G. Subramanian, with input from A. Morozov

As explained in Sec. IV B 1, "nonmodal" scenarios refer to nonexponential, algebraic growth of perturbations at relatively early times when the flow is linearly stable—implying that the perturbations will decay exponentially at large times. The above discussion of transition scenarios is restricted to either new modal pathways induced by elasticity or the elastic modification of essentially Newtonian nonmodal pathways. There also exist efforts that have highlighted novel nonmodal pathways due to elasticity alone [177,178], or due to a nontrivial interplay of elasticity and inertia [316]. The nonmodal pathways, in the inertialess limit in particular, point to the importance of spanwise varying disturbances (much like the Newtonian case) that are amplified by an elastic analog of the lift-up effect, and by an amount that increases with increasing Wi. The significance of the essentially 3D nonmodal pathways [177,178] relative to the aforementioned 2D nonlinear modal mechanism [186,187] requires more detailed examination; in light of this, Figs. 21 and 22 indicate both nonmodal and modal pathways leading to the ET state (ET1 for channel flow).

The experiments reported so far [195,196] cannot reliably be used to emphasize either pathway especially because the nonlinear elastic state accessed is for a channel with a cross-sectional aspect ratio of unity; the sensitivity of this state to the precise form ("shape") of the inlet disturbance, including the relative significance of streamwise *vis-à-vis* spanwise variations, remains to
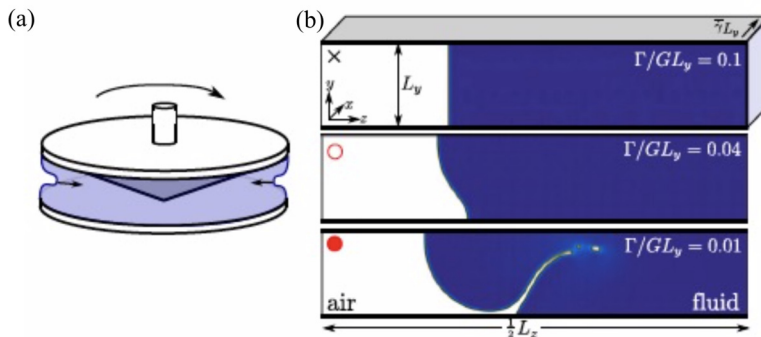
FIG. 23. Free surface instabilities in edge fracture. (a) Schematic of a cone and plate device where the interface undergoes an instability. (b) Snapshots from simulations of the Giesekus model between rigid walls. Note that in this figure, Γ is used to denote interfacial tension, while in the corresponding text we use σ instead, and G is the elastic modulus; reproduced with permission from [333].

be established. Although the ET state has been reasonably well characterized statistically in the aforementioned experiments, recent experiments [198] have, in channels with higher aspect-ratio cross sections, begun exploring the underlying structural motifs that might help identify the elastic analogs of the Newtonian ECSs. In contrast to the above, the EIT state accessed in both pipe and channel geometries exhibits minor only spanwise variations, and this essential two-dimensionality is consistent with the underlying modal picture [141,142,309].

VII. FREE SURFACE INSTABILITIES IN POLYMERIC FLUIDS

The previous sections described flow instabilities within bounded domains. In this section, we address flow instabilities that arise at the free surface between a polymeric fluid and the outside air. We do not attempt a comprehensive review, but instead focus on three specific instabilities. The first, often termed "edge fracture," is widely observed when a highly viscoelastic polymeric fluid is sheared in a torsional (cone-plate or plate-plate) flow device (Fig. 23). The second concerns the necking of a filament of viscoelastic polymeric fluid in which the constituent polymer chains are highly entangled, in the regime where the bulk viscoelastic stresses dominate surface tension (Fig. 24). The third concerns the breakup of a thread of high molecular weight elastic polymer in the regime where surface tension dominates (Fig. 25).

A. Edge fracture in sheared complex fluids

Author: S. M. Fielding

Measurements of a fluid's shear rheology are commonly performed in a torsional rheometer, often using either a cone-plate or plate-plate flow cell. In the linear viscoelastic regime, measurements are generally well controlled and reproducible. The measurement of stronger flows is often hindered by flow instabilities. For example, above a critical value of the imposed rate of shear, $\dot{\gamma}$, the free surface where the fluid sample meets the outside air can destabilize towards a more complicated profile, e.g., Fig. 23, despite having been neatly trimmed initially, forming an indentation of the interface that can then invade the bulk. Part of the sample can even be ejected from the flow cell, leading to unreliable data. This phenomenon is known as "edge fracture" [317–324]. Several experimental strategies have been developed aimed at mitigating its effects [317,325–330].

From a theoretical viewpoint, an early insightful work [331,332] argued that edge fracture must be driven by the second normal stress difference N_2 in the fluid, positing instability to arise above a critical magnitude $|N_2(\dot{\gamma})| > \sigma/R$, where σ is the surface tension of the fluid-air interface and R

a preassumed surface indentation radius. Experimental work later confirmed this important role of N_2 in driving edge fracture [319,332].

More recent theoretical studies have revisited this phenomenon [333–336]. By means of linear stability analysis, an updated criterion for the onset of edge fracture was put forward (note that the notation has been adjusted slightly to be consistent with usage in this paper) [333,334],

$$\frac{1}{2}\Delta\tau\frac{d|N_2(\dot{\gamma})|}{d\dot{\gamma}}\bigg/\frac{d\tau}{d\dot{\gamma}} = \frac{1}{2}\Delta\tau\frac{d|N_2|}{d\tau} > \frac{2\pi\sigma}{L_y}, \tag{3}$$

where $\tau = \tau(\dot{\gamma})$ is the shear stress in the fluid, $\Delta\tau$ the jump in shear stress between the fluid and outside air ($\Delta\tau \approx \tau$, given the low viscosity of air), and L_y the gap size in the rheometer. This updated criterion was shown to agree with the instability threshold found in direct nonlinear simulations at low shear rates, which is the regime in which it was developed [333,334].

In the limit of low shear rates, in fluids in which the shear stress scales linearly with shear rate and N_2 scales quadratically, the criterion (3) predicts the same scaling as that of the earlier Refs. [331,332], if the preassumed indentation radius in the earlier work is now instead identified as the rheometer gap size. It is, however, worth noting that the updated criterion correctly predicts the prefactor and identifies the important role of shear stresses in contributing to instability. Importantly, the new criterion also departs markedly from the early ones in stronger shear.

The linear stability analysis of Refs. [333,334] also elucidated for the first time the basic physical mechanism of edge fracture, which can be understood as follows. Were the interface between the fluid and air to remain flat, the jump in shear stress across it would be consistent with force balance. It is helpful to recognize that, with x as the flow direction, were the interface oriented with its normal in the flow-gradient direction y, then the shear stress τ_{xy} would have to be continuous across it. However, this perturbed interface has its normal in the vorticity direction (z) so the shear stress τ_{xy} can jump across it. (This structure is actually the same as allowing vorticity bands with layer normals in the vorticity direction, with a jump in shear stress τ_{xy} between the bands, which has been discussed in the literature [337].) So imagine that a small disturbance from a planar state now develops in the interfacial profile. This exposes the jump in shear stress, potentially disturbing the force balance across the interface. To recover local equilibrium, a perturbation is needed in the shear stress, and so in the shear rate. This in turn perturbs the second normal stress, which must be counterbalanced by a perturbation to the extensional stresses in the vicinity of the interface. The imbalance then requires a perturbation to the velocity gradient and therefore velocity near the interface, which can be shown to enhance the original interfacial disturbance, giving the runaway positive feedback of the edge fracture instability. The mechanism just described resembles that of other interfacial instabilities between layered viscoelastic fluids [338–340].

The work of Refs. [333,334] also suggested a possible route to mitigating edge fracture experimentally. In particular, the left-hand side of Eq. (3) contains the term $\Delta\tau$, which is the jump in shear stress between the fluid and outside medium. By immersing the flow cell in an immiscible Newtonian fluid with a viscosity more closely matched to that of the original fluid, the jump $\Delta\tau$ will be reduced, thereby potentially mitigating the instability. Another strategy could be to engineer a larger interfacial tension σ, again by suitable choice of the (Newtonian) bathing medium.

In addition, the interplay of edge fracture with the bulk flow instability known as shear banding has been considered [335,336,341]. These works show that modest edge disturbances that constitute a precursor to edge fracture can lead to a noticeable apparent shear banding effect that can penetrate far into the bulk, for a fluid with a relatively flat underlying constitutive relation of shear stress as a function of shear rate [335]. Conversely, shear banding can lead to edge fracture [341]. More generally, a complicated interplay is expected to exist between the two effects [336], potentially informing the long standing debate concerning whether bulk shear banding occurs in entangled polymers [321,322,342–346].
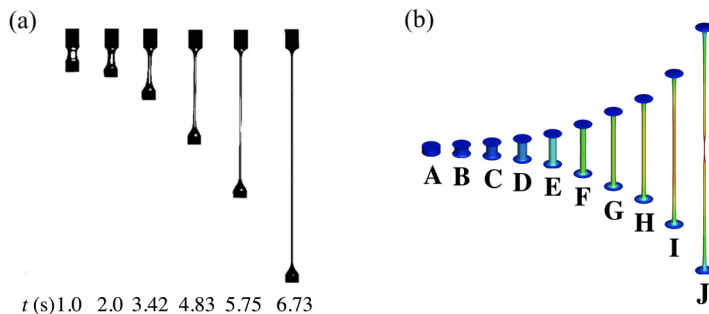
FIG. 24. Extensional necking. (a) Experiments of exponential elongation of a filament of a viscoelastic fluid (0.31 wt% polyisobutylene in polybutene) [348]. Modified from [349], with permission from Elsevier. (b) Numerical simulations of the so-called pom-pom model for an imposed strain rate $\dot{\epsilon}$, with the color scale indicative of the tensile stress [368]; see Fig. 9 of the original reference for the time of each image. Modified from [368], with the permission of the Society of Rheology.

Notable challenges in understanding edge fracture remain. For example, the work of Refs. [333–336] considered only fluids with a negative second normal stress difference; it would be interesting in future studies to consider the case of a positive N_2. Furthermore, these works considered only fluids with a finite terminal relaxation time, λ, for which the shear stress $\tau \sim \dot{\gamma}\lambda$ and second normal stress $N_2 \sim -(\dot{\gamma}\lambda)^2$ for low shear rates, $\dot{\gamma}\lambda \ll 1$. Future work should consider non-Brownian suspensions [347], in which N_2 scales linearly with shear rate.

The criterion discussed above also assumes an underlying base flow of steady shear, while edge fracture is widely seen in transient rheological protocols, the modeling of which would require a time-dependent underlying base state. Finally, the phenomenon of wall slip arises widely in strongly sheared entangled polymers, and is therefore likely often to occur alongside edge fracture. The interplay of these two widely occurring phenomena remains to be considered theoretically.

B. Extensional necking in entangled polymeric fluids

Author: S. M. Fielding

Extensional flows provide a key benchmark for the development of rheological constitutive models of highly entangled polymeric fluids, with many nonlinear flow features being apparent only in extension. A common experimental protocol consists of stretching out in length an initially cylindrical filament of material in a filament stretching rheometer; see, e.g., Fig. 24. Such experiments can be performed by switching on a Hencky strain rate $\dot{\epsilon}$, which is held constant thereafter, or a tensile stress τ_E [350–353], or a tensile force F (which provides a closer model of some industrial processes, such as fiber spinning [354,355]). Note that $\tau_E \equiv \tau_{zz} - \tau_{rr}$, with direction z along the filament's length and r along its radius. In many such experiments, the region of the filament farthest from the sample ends will often thin more quickly than the sample as a whole, forming a "necked" region and finally even causing the filament to fail [356–362]. This necking instability has been observed at constant tensile stress [363], constant Hencky strain rate [358,364], and during the process of stress relaxation after an initial Hencky strain ramp [365].

From a theoretical viewpoint, recently criteria for the onset of necking have been developed [366–370], separately for the flow protocols of constant imposed tensile stress, tensile force, and Hencky strain rate, and considering necking during stress relaxation after an initial extensional strain ramp. These criteria were initially derived analytically within a constitutive model written in a highly generalized form, then checked to indeed apply in numerical calculations performed in several different widely used polymer constitutive models [371] (the Oldroyd B, Giesekus, FENE-

CR, Rolie-poly [372], and pom-pom [373] models). The focus throughout these studies was on the case of highly viscoelastic filaments of sufficient radius that bulk stresses dominate surface tension.

For a filament subject at time $t = 0$ to the switching on of a constant tensile stress τ_E, the Hencky strain rate $\dot{\epsilon}$ quickly attains its value prescribed by the underlying steady state extensional constitutive curve before any appreciable necking develops. The criterion for a neck subsequently to develop was then found to be [369]

$$\frac{d\tau_E}{d\dot{\epsilon}} > 0. \tag{4}$$

This shows that, in fact, any highly viscoelastic material with a positively sloping extensional constitutive relation $\tau_E(\dot{\epsilon})$ must ultimately be unstable to necking in filament stretching.

For a filament subject instead to the switch-on of a constant tensile force F, a filament was predicted to become unstable to necking in any regime where the extensional creep curve $\epsilon(t)$ simultaneously has positive slope and positive curvature [369]:

$$\frac{d^2\epsilon}{dt^2} \bigg/ \frac{d\epsilon}{dt} > 0. \tag{5}$$

A filament subject to the switch-on of a constant Hencky strain rate was shown to be unstable to necking if the tensile stress response shows negative curvature as a function of the accumulating Hencky strain [366],

$$\frac{d^2\tau_E}{d\epsilon^2} < 0. \tag{6}$$

A full discussion of these criteria can be found in Refs. [366–370]. They were derived within a so-called "slender filament" approximation, in which the wavelength of necking variations along the filament's length is assumed long compared with the filament radius. They furthermore ignore any effects of the endplates, beyond their role in seeding an initial heterogeneity in the way that the filament starts to deform. In future work, it would be interesting to perform fully 3D simulations using microscopically motivated rheological models, move beyond the slender filament approximation, and incorporate endplate effects.

C. Instabilities in polymeric pinching

Author: J. G. Eggers

The breakup of a solution of high molecular weight, elastic, polymers, driven by surface tension, is very different from its Newtonian counterpart, even at concentrations as low as 10 ppm in weight [364,374]. Polymers are stretched by the extensional flow leading to breakup and resist it, resulting in a strong increase of the extensional viscosity η_E (the extensional stress $\tau_{zz} - \tau_{rr}$ divided by the elongation rate $\dot{\epsilon}$). What would have been two or a whole series of isolated drops in the Newtonian case, are now connected by thin threads of highly stretched material of almost uniform radius. This is known as the "beads-on-a-string" (BOAS) structure, characterized by a strong buildup of stress inside the threads, the extensional viscosity growing by several orders of magnitude in the process. Since the capillary pressure inside a thread is much higher than inside a drop, the thread empties into the drop and thins further [375], limited by the buildup of stress. In a regime where inertia is important, it is known from the Newtonian case that so-called satellite drops of smaller size are formed between two main drops [376]. The same is true in the elastic case, but with threads connecting the main and satellite drops [84,377,378].

Taking into account stress relaxation, an analysis of the Oldroyd-B viscoelastic equations [379] with a single relaxation time λ shows that the thinning of the thread (radius h_{thr}) is exponential [380]:

$$h_{\text{thr}} = h_0 e^{-t/(3\lambda)}. \tag{7}$$

Although even monodisperse polymer solutions are known to exhibit a spectrum of relaxation times rather than a single λ [381], (7) works remarkably well for a wide range of flexible polymer systems, in both low- and high-viscosity solvents. The reason is that (7) is dominated by the longest relaxation time [382], which can be estimated as the Zimm time [383]. Good agreement between λ found from fitting Eq. (7) to experimental data and the Zimm time is found for dilute solutions [383–385], but the case of higher concentrations is often more complicated. For example, [384,386] found a strong (power-law) dependence of λ on polymer concentration, with an exponent that depends on the quality of the solvent.

In order to relate the prefactor h_0 in (7) to the stress, one needs to match the thread to the drop into which it is emptying [387], as has recently been done on the basis of the full 3D, axisymmetric Oldroyd-B equations [386,388]. Thus one can determine the extensional viscosity by measuring the thread radius alone, knowing the surface tension σ:

$$\eta_E \equiv \frac{\tau_{zz} - \tau_{rr}}{\dot{\epsilon}} = \frac{3\sigma\lambda}{h_{\mathrm{thr}}} = -\frac{\sigma}{\dot{h}_{\mathrm{thr}}}. \tag{8}$$

The remarkable feature of (8) is that it is independent of the history of the filament (for example any prestretch), or the geometry (a dripping geometry or a free jet). Of course, this is true only in an asymptotic sense, such that the regime of exponential thinning is long. However, eventually the polymer reaches full stretch, and crosses over to a faster thinning law, which is observed to be linear instead of exponential, with η_E saturating at a constant value [383,389,390].

The physical idea is that at full stretch of the polymer, the viscosity can grow no longer, and the polymeric solution behaves once more like a Newtonian fluid, but with an elevated value of the elongational viscosity. Indeed, a theoretical analysis [391,392] of the FENE-P model [379], which incorporates finite extensibility, predicts an *instability* of the uniform thread, leading to localized pinch solutions of the same self-similar form as for a Newtonian thread [393], but with an effective viscosity that grows linearly with the length of the polymer. By observing the minimum radius of the localized pinch $h_{\min}(t)$, the extensional viscosity can be inferred from $\eta_E = -3\alpha\sigma/\dot{h}_{\min}$, where $\alpha = 0.0709$ for symmetric pinching (inertia subdominant), and $\alpha = 0.0304$ for asymmetric pinch solutions (the asymptotic case for small $h_{\min}$) [393].

The latter case predicts an extensional viscosity more than a factor of 10 smaller than (8), which indeed is for a uniform thread, which is at best an unstable solution once finite extensibility comes into play. In order to interpret thread radius data correctly, it therefore seems important to monitor the radius of the thread in space, which can no longer be assumed uniform. A theoretical analysis of the crossover between a uniform thread and localized pinching remains to be done.

However, as first reported in [394], uniform polymeric threads are frequently subject to a more complicated, delocalized instability, leading to the sudden growth of many small droplets all along the thread. The instability can proceed through several generations [394,395], producing drops of different sizes, but the initial instability was observed to follow an exponential growth law [396], indicative of a linear instability. While there is a superficial resemblance to the original BOAS structure, the physical process is the opposite: a localized relaxation of stress, leading to droplets. To differentiate between the two processes, "blistering instability" has been proposed as a name for the instability of a highly stretched polymeric thread.

The blistering instability cannot be understood as the linear (Rayleigh-Plateau) instability of a Newtonian thread, but with an elevated elongational viscosity: the growth rate is at least an order of magnitude faster than a Newtonian instability would predict [396,397]. Instead, the authors of [395] proposed an instability localized at the end of the thread, resulting in a relaxation of stress, followed by elastic recoil, and triggering the formation of a thinner filament. While such localized instabilities have also been seen by others [397], they are distinct from the linear instability leading to quasi-simultaneous growth along the entire thread.

To explain the observed linear instability, it has been proposed [398] that the coupling between stress and the local polymer density [399,400] has to be taken into account. Density fluctuations are automatically part of the description when deriving continuum models using kinetic theory [401],
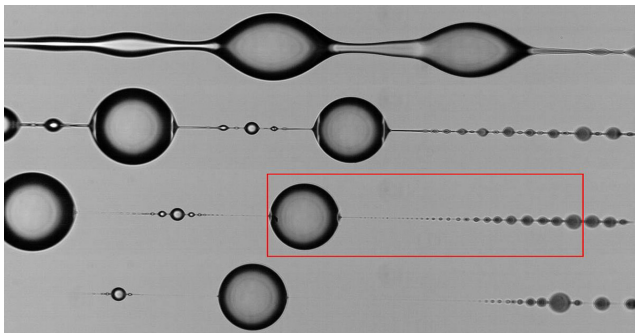
FIG. 25. The late stages of the blistering process of an aqueous 1000 ppm PEO solution [397]. The first image is at $t = 250$ ms after the formation of the cylindrical filament; subsequent images are taken every 30 ms. A thin fiber with the small beads is drawn out of the large droplet (red box). The width of the image is about 300 μm. Image is from R. Sattler, S. Gier, J. Eggers, and C. Wagner, Phys. Fluids **24**, 023101 (2012); licensed under a Creative Commons Attribution (CC BY) license.

but are usually neglected in continuum descriptions. The stress-density coupling results in a flow of polymers toward regions of high stress—this is true independent of the flow type [399]—leading to further stress relaxation in polymer-poor parts of the thread, driving an instability. The idea of a nonuniform polymer density is consistent with the observation that for polymer concentrations of above 1000 ppm, threads eventually solidify and never break [396,397,402,403].

Based on the linear stability analysis of a uniform thread in the exponentially thinning regime (7) [398], a transition is expected to take place when the thread radius is smaller than the "blistering" radius

$$h_{bl} \approx \sqrt{D\lambda}, \tag{9}$$

where $D = k_B T/(6\pi \eta_s a)$ is the diffusion constant of the polymer [381]. Here η_s is the solvent viscosity and $a \propto M_w^{1/2}$ the polymer radius, so that D decreases strongly with molecular weight M_w. The prediction (9) has been confirmed experimentally in [385], varying D and λ independently. This was achieved using two different polymers, whose relaxation times have a different dependence on temperature.

It is, however, worth pointing out that as nonlinear effects become more important, and phase separation progresses, the blistering dynamics can become remarkably complicated, as illustrated by the sequence shown in Fig. 25. As the thread evolves, droplets of widely varying size are created on the thread, in a manner that seems difficult to predict. However, there are also some organizing features, like the sequence of smaller and smaller drops highlighted in the red box, which a partially solidified thread draws out of a drop. Relating such small-scale features to a fundamental description of polymer solutions appears to be a daunting yet worthy challenge!

VIII. FLOW INSTABILITIES IN NONPOLYMERIC SYSTEMS

The previous sections focused on flow instabilities of polymeric fluids (with a brief discussion of some instabilities exhibited by viscoelastic wormlike micellar solutions in Sec. V A). In this section we discuss briefly some features of the flow and instability of three other classes of materials with complex rheological characteristics: yield stress fluids, wormlike micelle solutions, and liquid crystals.

A. Yield stress fluids

Author: S. Hormozi

In many industrial and natural settings, we often deal with yield stress fluids. Examples include natural muds, cement pastes, injectable hydrogels, biological fluids, and hygiene products. Yield stress fluids have a threshold in stress, namely the yield stress, above which they flow like a nonlinear viscous fluid. In the past, the main research activities have been focused on yield stress fluids with inelastic properties (e.g., natural muds). Therefore, ideal yield stress models or viscoplastic models, such as Bingham and Herschel-Bulkley, have been used by researchers to address flows involving a yield stress [404]. In the ideal yield stress models the shear rate is set to zero when the second invariant of the deviatoric stress tensor falls below the yield stress. In these flow regions, the effective viscosity becomes infinite, the material is unyielded, and the state of stress is undetermined. We refer the reader to the recent book edited by Ovarlez and Hormozi [405], which includes several lectures on theoretical, computational, and experimental approaches in viscoplastic fluid mechanics.

However, recent experimental studies show that even a slight elasticity in polymer-based yield stress test fluids has an essential role in the flow dynamics. For example, in the absence of inertia, the loss of the fore-aft symmetry and the formation of the negative wake are observed when a sphere settles in a yield stress fluid (see, e.g., [406,407]). Also, Firouznia *et al.* showed an asymmetric disturbance velocity field around a neutrally buoyant sphere in Carbopol gels (i.e., an accepted model yield stress test fluid) subjected to linear shear flows. Additionally, the authors showed that the trajectories of two spheres are asymmetric in the absence of contact [408]. None of the aforementioned observations can be explained *via* ideal yield stress models that produce symmetric flow solutions. However, the loss of symmetry and reversibility can be explained by including viscoelastic effects in modeling flows of yield stress fluids around obstacles [409,410]. In addition, applications in industry frequently utilize yield stress fluids for rheological innovation, e.g., designing injectable hydrogels and engineering inks for additive manufacturing, which are advantageous as these materials are self-supporting and hence preserve their shape. These new polymer-based gels have substantial elasticity as well as a yield stress.

It is only relatively recently that soft matter scientists have begun to incorporate elastic effects into constitutive equations for yield stress fluids. For example, Saramito proposed a constitutive law in which the material behaves as a nonlinear viscoelastic fluid above the yield stress and as a nonlinear viscoelastic solid below the yield stress [18]. Modeling practical yield stress fluids via this constitutive description results in an unrealistic zero value of the loss modulus below the yield stress since the deformation of an ideal Hookean solid remains in phase with the imposed strain. This issue has been resolved in recent models where McKinley and coworkers have developed a class of elastoviscoplastic constitutive models adapted from ideas in the nonlinear plasticity literature, collectively known as isotropic and kinematic hardening (IKH) [411,412]. The evolution of the yield stress is captured through an internal tensorial back stress, which describes the residual stresses that develop in the microstructure as it is deformed elastoplastically prior to yield. This framework results in a set of Oldroyd-type evolution equations that contain up to nine material constants, which can be determined using a sequence of steady and time-varying viscometric flows. The aforementioned constitutive laws can be used in numerical simulations to predict nonviscometric flow fields. The comparison of the results with experimental observations then provides a basis for further improvement of such constitutive laws.

To our the best of our knowledge, the stability analysis of elastoviscoplastic fluids has not yet been performed. As far as the yield stress property is concerned, the first study of the hydrodynamic stability of a Bingham fluid came more than a century after the Newtonian equivalent, and even plane channel flow was studied only recently [413]. The primary assumption in these efforts is that yielded surfaces remain invariant as instabilities develop, which is an approximation that leads to mathematical anomalies [414]. There is a dearth of literature in this area, with only a few weakly nonlinear and nonlinear (energy) stability results [415–418]. The difficulty arises because, for yield stress fluids, the nonlinearity of the problem is not only in the inertial terms, if the Reynolds number

is finite, but also in the shear stress/shear rate relationship and in the existence of unyielded regions, which are defined in a nonlocal fashion even for simple flows. Therefore, the gap between linear and nonlinear theories is much broader and more complex than with Newtonian fluids. Therefore, it is essential to study how the knowledge of the stability of the ideal yield stress models can be extended to practical elastoviscoplastic fluids. To further our ability to design, predict, and optimize flows of elastoviscoplastic fluids, we must first build new scientific knowledge regarding the behavior of these fluids.

B. Wormlike micellar solutions

Author: J. Esteban López-Aguilar

Wormlike micellar solutions (WLMs) are materials of wide use in industrial and technological applications due to their versatile rheological properties, i.e., they are thixotropic, shear-thinning, strain-hardening, and softening viscoelastic fluids, capable of displaying shear banding and plasticity [419–422]. WLMs are utilized in home-care and health-care products, such as shampoos, soaps, detergents, pharmaceuticals, and biocompatible drug-delivery systems; in the oil industry, WLMs are used as drilling and reservoir stimulation fluids, drag-reducing agents in pipelines and lubricants, and emulsifiers, among other numerous uses [419–421]. The rheological properties and applications of WLMs are promoted by their time-dependent internal structure, which may be broken down and rebuilt under deformation. Accordingly, WLMs are also referred to as "living polymers," since they can relieve stress, in addition to undergoing reptation, with a mechanism of dynamic construction-destruction of their internal structure [421,423]. Indeed, wormlike micellar fluids appear as one example of soft matter that intimately links the internal structure of the fluid with its macroscopic response [423].

Instabilities in wormlike micelles. These complex fluids display a large variety of instabilities ranging from classical flow segregation in the form of shear banding in simple shear flow [422] to complex spatiotemporal instabilities accompanying complex deformations [419,423]. Here the interplay between viscoelasticity (common with polymeric systems) and the complex internal-structure dynamics triggers fascinating macroscopic responses when using typical surfactants, e.g., cetyltrimethylammonium bromide (CTAB), cetylpyridinium chloride (CPyCl), cetyltrimethylammonium tosylate (CTAT), combined with salts, such as sodium salicylate (NaSal) or sodium chloride (NaCl), in water [419–423].

The following benchmark non-Newtonian fluid mechanics flows have been studied experimentally and theoretically for WLM solutions:

(i) *Sphere sedimentation.* Experimental studies of the sedimentation of smooth spheres in WLM solutions report a common phenomenology of sphere oscillations beyond a critical speed threshold and strong negative wakes behind the sphere [206,207]. Such observations have been attributed to complex dynamics in the construction and destruction of the fluid's internal structure and its viscoelasticity, described using an extensionally based Deborah number, which permits consistent steady-to-unsteady flow classification [209,424–429]. These features have been little explored computationally, with the first studies provided by Sasmal [430], using the Vasquez-Cook-McKinley (VCM) [151,431–433] and Giesekus models, and by López-Aguilar *et al.* for the BMP $+$ $_\tau_p$ model [434].

(ii) *Flow past a cylinder.* This benchmark flow has attracted attention in single and multiple-unit arrays, in which transitions occur from liquidlike symmetric flow regimes at relatively low flow rates or cylinder velocities up to gellike tearing responses, which have been observed experimentally by Gladden and Belmonte [435]. Moss and Rothstein [436] performed experiments keeping the cylinder fixed in a channel and the WLM solutions flowing around it with pressure-drop measurements revealing three distinct phases: (1) at low Deborah numbers, a constant normalized pressure-drop is recognized, (2) at intermediate Deborah numbers, shear thinning provokes a reduction in pressure drop driven by the WLM solution's shear-thinning response, and (3) an elastic instability is observed in the wake of the cylinder, promoted by the extensional features of the micellar solutions. As

discussed in Sec. V A, for geometries at the microscale, the studies of Haward and coworkers [222] recorded different instabilities with an increase in Wi, where (1) symmetric flow fields occur at relatively small Wi, while (2) an increase in flow rate to moderate levels triggers an asymmetric flow regime in which the fluid takes a preferential path around the cylinder, to finally (3) development of a time-dependent flow at larger flow rates. Numerically, some features of these elastic instabilities have been captured using the VCM model [437].

(iii) *Contraction-expansion geometries.* Different contraction and contraction-expansion flow settings have been studied experimentally for planar and axisymmetric geometries with sharp and round corners, and for hyperbolic profiles [438–441]. In a circular sharp-corner contraction flow of tube-to-capillary aspect ratio 10.7-to-1, Hashimoto *et al.* [438] identified four different flow regimes with (1) a Newtonian-like response appearing as symmetrical salient-corner vortices, (2) a steady vortex regime, in which growth and strengthening of such vortices occurred, (3) a periodic oscillatory flow, in which time-dependence of size and strength of the vortices was recorded, and (4) an unstable flow, where a chaotic response was obtained; for the two last phases, a turbid appearance of the fluid was observed. For a planar configuration of a contraction slit channel, a detailed flow-structure study based on small angle neutron scattering (SANS), particle image velocimetry (PIV), and birefringence visualization provided by Lutz-Bueno *et al.* [439] revealed a complex interaction between micellar structure and deformation in the flow field, with development of various vortex-formation phases that evolved depending on the solute concentration and the solution rheological properties. More recently, Salipante *et al.* [440] studied the WLM flow structure in hyperbolic contraction-expansion geometries of aspect ratio 3.7-to-1 and 8.5-to-1 and reported an instability from steady to unsteady flow beyond critical flow rates in the form of fluctuations of pressure drop linked to jetting flow-rate jumps that happened at similar dimensionless extension-rate conditions across experiments, and for which the characteristic scale is given by the micelle relaxation time. Matos *et al.* [441] used a microscale configuration with a planar sharp-corner and tapered contraction-expansion settings to study the flow of typical WLM solutions under aspect ratios of 2:1:2, 4:1:4 and 8:1:8. Their findings reveal flows that evolve from (1) symmetric steady behavior at low flow rates, followed by (2) asymmetry about the contraction plane at intermediate shear rates, and (3) unstable time-dependent response with further flow rate increases.

In computations, the variety of settings is also wide. For example, the work by Sasmal [442] uses the VCM model to simulate the response of WLM solutions in expansion-contraction configuration, perhaps representative of a porous medium. Taking the Bautista-Manero family of fluids as a base, a series of simulation exercises by López-Aguilar and collaborators [434,443–448] proposed modifications of a group of constitutive equations to predict the response of WLMs in different contraction-expansion settings. Here axisymmetric rounded and sharp-cornered and hyperbolic geometries under the benchmark 4:1 and a more stringent 10:1 aspect ratio have been studied. In line with experimental findings, a complex kinematic evolution is recorded, with (1) a Newtonian-like symmetric salient-corner vortex response at small flow rates that evolves into (2) coexistence of lip-to-salient-corner vortices at intermediate flow rates, to finally reach (3) an elastic-corner vortex phase at large flow rates, driven by a competition between viscoelasticity and thixotropy. Such vortex phasing correlates with normal-stress fields in the recess zones and, for highly concentrated WLM solutions, where a yield stress may be displayed by the WLMs, asymmetric yield fronts are predicted.

(iv) *Flow through cross-slot geometries.* Building on earlier work [449], studies from Shen, Haward, and colleagues [90,450] in microfluidic cross-slots display a extensionally dominated deformation that provokes an intricate relationship between the flow field and WLM rheology, reporting flow transitions with increases in flow rate: the first transition happens from a symmetric stable to an asymmetric flow, with strong alignment of the micelles along the shear-free line in the geometry; the second flow transition appears at higher flow rates and is characterized by a 3D time-dependent response. Numerical predictions using the VCM model have been put forward recently by Kalb *et al.* [451,452], which capture qualitatively the main features and flow phases

observed experimentally, such as asymmetry about the stagnation point and the formation of lip vortices at the walls of the inlet arms.

(v) *Extensional deformation under filament stretching extensional (FiSER) and capillary break-up extensional rheometers (CaBERs).* The extensional response of WLM solutions has been extensively studied [453–459]. For example, Rothstein and coworkers recorded the evolution of the filament in both FiSER and CaBER configurations, and found that the filament rupture appeared related to a micellar-scission process, in contrast to the elasto-capillary thinning observed in polymer solutions [453,454,459]. Yesilata *et al.* [455] studied the WLM response in shear and extensional CaBER deformations, for which they found a highly nonlinear response of such materials in extension—with Trouton ratios increasing up to two orders of magnitude—and revealed relaxation times in extension smaller than those in their shear tests; the results were confirmed recently by Omidvar *et al.* [458]. In subsequent work, Kim *et al.* [456] used a CaBER apparatus to evaluate the effect of the end-plate diameter and concluded that this configuration is appropriate to measure the fluid's relaxation time and transient extensional viscosity. More recently, Sachsenheimer *et al.* [457] performed CaBER experiments on typical WLM fluids and found the formation of extension-induced structures that correlate with the linear or branched structure of the wormlike micelles. Computational modeling by Cromer *et al.* [460] using the VCM model confirmed the experimental observations of the fast rupture of the WLM filaments as being related to a scission mechanism of entangled micelles.

(vi) *Fluid-structure interaction.* Dey and Rothstein [461] performed experiments on flow of a WLM solution past a cantilevered beam as a function of Weissenberg number. They reported the development of an instability in the bending of the beam with increase of Wi, triggered by the periodic formation of fluid jets upstream of the beam and accompanied by vortices.

(vii) *Shear banding.* Shear banding is an important instability observed in concentrated WLM solutions under simple shear flow. Typically, two or more bands with different viscosity coexist for a fixed shear rate. A second modality of such a flow-segregation phenomenon, identified as vorticity banding, occurs when the sample is subjected to a given shear rate and arranges itself spontaneously into bands with different stress in the vorticity direction [422,462]. Due to the growing interest on shear banding in the 1990s, wormlike micellar flows started to be scrutinized with an increasing degree of precision. This led to the discovery of unexpectedly large *fluctuations*, in particular of the stress at an imposed shear rate within the banding plateaued regime. These fluctuations were first interpreted as the result of an instability of the banded state due to coupling with structural variables. Basically, the fluctuations were thought to be connected with changes in the microstructure of the fluids.

A different, more hydrodynamic, perspective eventually emerged, interpreting the fluctuations as the result of flow instabilities [423]. At first, the hydrodynamic perspective focused on instabilities due to jumps in normal-stress differences (N_1 or N_2) at the interface between the bands [150]. The instability mechanisms due to jumps in normal stresses are analogous to the elastic version of the Kelvin-Helmoltz instability [336]. Using a novel visualization technique, Lerouge *et al.* [463] showed that the interface between the bands of a wormlike micellar solution exhibited clear undulations, displaying different spatiotemporal dynamics. The hypothesis that these undulations could be the result of an underlying vortex flow was first formulated by Lerouge and coworkers [464], whilst the presence of a vortex flow in the high shear-rate band was demonstrated in [465]. The existence of a turbulent state analogous to elastic turbulence was found shortly after [466].

In theory, the vortex flow could be due to a Taylor-like bulk elastic instability of the high shear rate (induced) band, or to a Kelvin-Helmoltz-like instability of the interface between bands. Fielding [467] and Nicolas and Morozov [468] showed that the bulk mode dominates except for very thin bands, where the effective curvature is too small to produce a Pakdel-McKinley-type instability. By taking this point into consideration and realizing that the interface between bands can act as a soft boundary, it was shown that shear-banding flows could follow three instability scenarios according to the Pakdel-McKinley criterion, as demonstrated theoretically in [469] and experimentally in [470]. The experimental studies cited above showed that elastic instabilities could be at play for shear banding of semidilute solutions of wormlike micelles. Finally, it was shown that elastic

instabilities could also be present for dilute shear-thickening solutions [471], non-shear-banding semidilute solutions [472], and concentrated shear-banding solutions [473].

Constitutive models for wormlike micelles. There are two main streams of constitutive modeling for WLM rheology, i.e., models based on a microstructural description of the dynamic construction-destruction of micelles, and the other based on a evolution of a structural parameter. In the first classification, one of the first modeling paradigms stands on the grounds of chemical-like interactions between micelles put forward by Cates and coworkers [474]. Another approach based upon the microstructural evolution is the VCM model, proposed by Vázquez *et al.* [151,431–433], which uses a two-species mechanism intended to describe the rheology of concentrated solutions and successfully predicts key shear and extensional features of such complex fluids in steady and transient flows. More recently, the reactive-rod model (RRM) of Graham and collaborators [475,476] was proposed to model the rheological response of dilute WLMs based on a construction-destruction mechanism given by suspended rigid Brownian rods that link across alignment undergoing reversible scission and growth.

On the side of structure-parameter-based models, the Bautista-Manero-Puig (BMP) family of fluids, whose novel BMP $+\ _\tau{}_p$ model variant was proposed recently [434], brings in the interaction of the wormlike micellar network dynamics in a viscoelastic framework. The BMP $+\ _\tau{}_p$ model is embodied in a generalized differential equation of the Oldroyd-B type in stress-split form that feeds the thixotropic internal structure into the polymeric viscosity η_p via an evolution equation for a dimensionless fluidity $f = \frac{\eta_{p0}}{\eta_p}$; here η_{p0} represents the polymeric first Newtonian-plateau level. Such a structure equation considers rates of internal-structure construction and destruction of wormlike micelles involving viscoelasticity in such dynamics, where destruction of structure is promoted by the energy dissipated by the solute in flow. This constitutive equation predicts a rheological response of shear thinning, finite strain hardening, and softening, alongside a nonlinear first normal-stress difference in shear [434], which are all common features of WLM systems [419–421].

In addition, the BMP $+\ _\tau{}_p$ model predicts flow segregation, such as shear banding and an apparent yield stress [434,477]. Such flow-segregation features, i.e., shear banding, are imbued in the BMP family of fluids in the form of a deformation-rate-dependent structure-destruction coefficient that, in simple shear flow, has a nonmonotonic flow curve [477–479]. Here the shear-banding instability has been studied in ideal simple shear flow [478,479], and in complex contraction-expansion flow [477], this being the first instance of a complex flow where shear banding has been studied. Such efforts in modeling shear banding were followed by Germann and coworkers for flow in a tube [480] and in complex flow for planar contraction flow [481] with WLMs characterized under the VCM paradigm. In addition, shear banding has been modeled through different mechanisms, as in the diffusive Johnson-Segalman model [482], with its stress-diffusion extra term, and the Giesekus model, with its ability to trigger banding through its anisotropy parameter [483]. To motivate banded flow regimes, the Germann-Cook-Beris (GCB) model proposes a structure breakage rate depending explicitly on the trace of the conformation tensor [151,484], while the soft glassy rheology (SGR) model has been proposed to model shear banding under LAOS [485,486].

In the workshop, López-Aguilar presented numerical solutions of complex flows of WLMs in an axisymmetric contraction-expansion flow and flow past a sphere, produced with an in-house hybrid finite-element/volume algorithm ([434] and references therein). Particular attention was paid to the flow structure and its correlation with the rheological properties of WLMs characterized by the BMP $+\ _\tau{}_p$ model [434]. In an axisymmetric abrupt 10:1 contraction-expansion setting, distinct flow transitions are observed for WLMs (studying extension-hardening and solute-concentration variations [434]). Strong correlation is recorded between vortex evolution and the normal-stress distribution in the recess zones. Here, for solutions with solvent fraction $\beta \leqslant 1/9$ and high flow rates, strain-hardening WLM flow structures evolve to have upstream elastic-corner vortex phases, which is a step before there is strong time dependence of the numerical solutions with further increase of the flow rate (see [487] and references therein). In contrast, for dilute solutions, upstream lip vortices are captured at intermediate deformation rates.
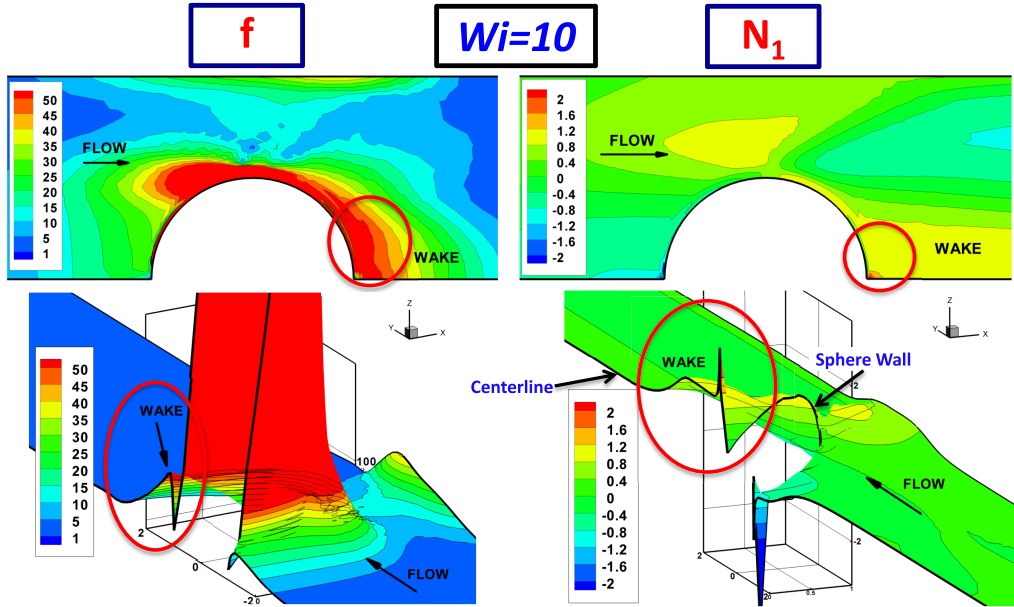
FIG. 26. Dimensionless fluidity and first normal-stress difference N_1 in flow past a sphere (sphere-to-tube aspect ratio 1:2) of a WLM solution; solvent fraction $\beta = 5 \times 10^{-3}$ and moderate hardening features, Wi = 10; see López-Aguilar *et al.* [434] for further details of the rheology used.

For flow past a sphere, the BMP + $\_\tau_p$ dimensionless fluidity f is used to analyze the internal structural changes that are suffered by extremely concentrated WLMs in the wake of a sphere. In the 3D plots of Fig. 26, for $\beta = 5 \times 10^{-3}$, moderate hardening features and Wi = 10, coinciding maxima are captured in N_1 and f, and are located on the symmetry line downstream of the sphere. In the companion 2D representation, a highly unstructured fluid (red fringe level of high f values) is recorded on the sphere wall, reflecting a shear-thinned material with relatively small N_1 values. Such a red fringe of fluid connects to the centerline downstream of the sphere, where extensional deformation prevails and the fluid develops a N_1-hardening peak. This N_1 peak coincides in location with a fluidity maximum, which, under extensional deformation and the BMP + $\_\tau_p$ formalism, reflects an evolution in the increase of Wi that follows the strain hardening/softening of extensional viscosity [434]. Such a complex interplay between the change in a localized material property and mixed deformations may take a role in further understanding the instabilities observed experimentally when a sphere settles in WLMs [206,207,209,419,424–429] and polymer solutions [488].

C. Liquid crystals

Author: I. Bischofberger

Nematic liquid crystals are a class of fluids with intrinsic orientational order. In equilibrium, nematics tend to uniformly align their anisotropic constituents as a means to minimize energy, which annihilates topological defects. When driven away from equilibrium by an externally applied flow, the continual injection of energy can destabilize the defect-free alignment. The primary control parameter for the effect of shear on the orientation of the director field is the Ericksen number $\text{Er} = \frac{\eta \dot{\gamma} L^2}{K}$, which denotes the ratio between the viscous torques and the elastic ones. Here η is the dynamic viscosity, $\dot{\gamma}$ the shear rate, L the typical scale of deformation (often the thickness of the liquid crystal layer), and K the Frank elastic constant. The condition $\text{Er} \approx 1$ is typically reached for corresponding Reynolds numbers of order 10^{-6}; thus, hydrodynamic instabilities in the

usual inertially driven sense are not expected to take place in nematic liquid crystals. However, the emergence of shear-induced structures has attracted significant attention in studies of nematic thermotropic liquid crystals and liquid crystal polymers [8,489–492], and was therefore a topic of discussion at the workshop.

Most nematic thermotropic liquid crystals are shear-aligned nematics, in which the director evolves towards an equilibrium polar angle. The shear-alignment in the bulk flow leads to an irreconcilable alignment of the directors with those in the surface-anchored region. The high elastic stresses of the director gradient at the boundary between the two regions are released through the formation of defects beyond a critical Ericksen number. Liquid crystal polymers, by contrast, are typically tumbling nematics characterized by a nonzero viscous torque for any orientation of the director. Their tumbling characteristics facilitate the nucleation of singular topological defects. Recently, topological structures and their dynamics have been described in 3D active nematics, where disclination loops undergoing complex dynamics and recombination events are identified as the primary unstable structure [493].

The flow behavior of lyotropic chromonic liquid crystals has so far remained largely unstudied. Lyotropic chromonic liquid crystals (LCLCs) are aqueous dispersions of organic, disklike molecules that self-assemble into cylindrical aggregates, which form nematic and columnar phases beyond a certain concentration [494]. Due to their biocompatibility, they have opened paths for controlling assembly and dynamics of biological systems when used as a replacement for isotropic fluids in microfluidic devices [495,496]. At rest, LCLCs exhibit unique properties distinct from those of thermotropic liquid crystals and liquid crystal polymers. In particular, LCLCs have significant elastic anisotropy and their twist elastic constant, K_2, is much smaller than the bend and splay elastic constants, K_1 and K_3 [497]. The resulting relative ease with which twist deformations occur can lead to a spontaneous symmetry breaking and the emergence of chiral structures in static LCLCs under spatial confinement, despite the achiral nature of the molecules [498,499].

A recent study by Baza *et al.* has revealed a variety of complex textures that emerge in Couette flow in the nematic LCLC disodium cromoglycate (DSCG) [500]. The liquid crystal tends to tumble, which leads to a high sensitivity to shear rate; with increasing shear rate the materials transitions from a log-rolling state, where the director realigns perpendicular to the flow direction, to polydomain textures and finally to periodic stripes in which the director is predominantly along the flow direction.

For pressure-driven flow of nematic DSCG, during the workshop Bischofberger discussed the emergence of pure-twist disclination loops for a certain range of shear rates, which form as a consequence of the smallness of the twist elastic constant K_2. Their characteristic size is governed by the balance between the nucleation force and the annihilation force acting on the loop [501]. Remarkably, chiral domains spontaneously form at lower shear rates, suggesting that not only topological confinement, but also weak shear can induce chiral structuring in achiral materials. These observations hint towards the wealth of phenomena that are still awaiting to be discovered in flows of lyotropic chromonic liquid crystals.

IX. OUTLOOK AND OPEN QUESTIONS

With contributions from all authors

A reader who has even read only one or two sections of this wide-ranging perspective will note that, in spite of substantial progress in the field over the past 30 years, including advances in experimental measurements, theory, and detailed numerical simulations by computational rheologists, where each brings their own insights, there remain important areas where the integration of ideas is needed and new discoveries remain to be made. This is true for the flow transition that occurs in channel and pipe flows of polymeric fluids (Sec. IV, Sec. VI) and wormlike micelle solutions (Sec. VIII). It is also the case for more complex configurations, such as the cross-slot geometry [52,53,90,226]), where shear-thinning apparently triggers flow asymmetries so that the initial onset

of instability gives rise to regions in the flow field with disparate shear rates. Similar issues are at the heart of unstable flows at the pore scale for a wide range of heterogeneous and porous media; recent experimental developments seeking to provide *in situ* access to these flows are mentioned in Sec. V. Not surprisingly, observations of other microstructurally complex fluids Sec. VIII, such as lyotropic chromonic liquid crystals, or free-surface flows of complex fluids that are impacted by surface tension Sec. VII, hint at a wealth of discoveries that are yet to be made.

Models of viscoelastic flows. Throughout the workshop there was discussion surrounding the fact that elastic instabilities are typically discovered at "high Weissenberg number" in polymer solutions—where the veracity of constitutive equations at the requisite shear rates always comes into serious question. Indeed, when modeling highly elastic viscoelastic flows, the Oldroyd-B model is almost never quantitative at high Weissenberg number either in shear flows or in extensional flows of polymer solutions. This can also be said of nonlinear extensions of this model, including the FENE models as well as the Giesekus and PTT (see Sec. III). In particular, detailed molecular studies have demonstrated that internal degrees of freedom cannot be neglected in these flows if one wants to accurately capture the extra polymer stress. Thus, progress in understanding elastic instabilities must almost, by the definition of the phenomena, be made hand in hand with advancements in the rheological modeling of elastic fluids.

Spectral properties of elastic turbulence. There was also significant discussion surrounding the fact that the eigenspectrum of elastic 2D Taylor-Couette flow was essentially unstudied. Many of the attendees thought that such a study deserved attention in an effort to further understand the work described in Sec. IV, especially since the beginnings of instability at values of Wi ∼10, albeit at large gap ratio, had been found.

Importance of a Lagrangian perspective. Remarkably, shear plays an important role in all detailed mechanisms worked out for purely elastic instabilities so far. This is despite the fact that purely elongational flows can have a dramatic effect on single molecules, with a strong dependence on individual histories, as exemplified by the coil-stretch transition of a single polymer, which can be sharp and hysteretic. Moreover, typically a dependence on the history does not play any role in the currently understood instability mechanisms, as most of the flows considered have been viscometric, e.g., the flows have been such that each infinitesimal fluid element sees effectively a steady shear; the extensional necking described in Sec. VII B is an example of other possibilities that exist.

Consequently, the history of the flow and stress experienced by a fluid element should enter considerations for flows that are Lagrangian unsteady; see, e.g., Ref. [503] for a description of 3D particle tracking experiments exploring elastic turbulence from such a Lagrangian perspective. In particular, even the notion of extension- or shear-dominated flow may depend on Lagrangian properties such as the residence time of fluid elements. Beyond classification, it would be interesting to see if new, purely Lagrangian, instability mechanisms could be found, e.g., using insights from bead-spring models to inform the expected stresses and the coupling to the base flow. A Lagrangian perspective might be useful also at the next level of complexity, when conceptually the flow is made up of many coupled flow units; e.g., see Sec. V on flows in different porous systems. Indeed, stress correlations over the path of a fluid element can play a nontrivial role in coupling the flow units and determining the overall stability of the flow, which largely remain to be understood.

Another perspective on elastic waves. Because the topic of elastic waves was actively discussed at the workshop, here we include another perspective put forward by V. Steinberg. Three main features characterize the elastic waves observed by Varshney and Steinberg [83], as described by the group of Steinberg: (i) the waves are transverse and manifest as a peak in the power spectrum of spanwise velocity fluctuations; (ii) the velocity of wave propagation depends on $(\text{Wi} - \text{Wi}_c)^\beta$ with $\beta = 0.73$; (iii) the measured wave dispersion relation is linear [200]. Given these three features, and given the apparent agreement with the predictions of [502], the authors propose that such waves are indeed elastic waves. Moreover, they note that they observed these waves exclusively in random flows: either in chaotic flows above the nonnormal mode bifurcation and further in ET in a straight channel with and without strong perturbations [198,200,201] or only above the transition to ET in

a flow past an obstacle or between two obstacles hindering a channel flow [83,504]. In addition, the elastic waves were not found in flow geometries with curvilinear streamlines including ET.

Because of these apparent similarities as the elastic waves predicted in [502], the authors use the expression for the wave velocity $c_{el}^2 = \tau/\rho$ to estimate an elastic stress, τ, which depends on the flow, in the direction of wave propagation. In the experiments of [83], c_{el} varied from 2 to 17 mm/s, yielding an estimate for τ ranging from $\sim 5 \times 10^{-3}$ to 0.375 Pa, and a corresponding viscoelastic Mach number $\mathrm{Ma}_V = V/c_{el}$ of the order $0.3 < 1$. In a later paper [198], the Steinberg group reported reaching $c_{el} \approx 45$ mm/s corresponding to $\tau \approx 10$ Pa, whereas in [200], much smaller wave velocities close to the onset were measured from 0.05 to 0.2 mm/s corresponding to τ between 3×10^{-6} and 5×10^{-5} Pa. Thus, summarizing these experiments, the range of the elastic stress derived from c_{el} is $\sim 3 \times 10^{-6}$ up to 10 Pa—considerably smaller than the values noted in Sec. II C, where the shear wave speed is tied to a flow-independent material property. Clarifying the underlying physics will be an important direction for future research.

Open questions regarding EIT. Substantial progress has been made, both experimentally and computationally, in understanding the nature of the turbulent drag reduction phenomenon, and more broadly in nonlinear viscoelastic dynamics in straight pipes and channels. The mechanism by which viscoelasticity suppresses near-wall coherent structure are understood, and the discovery of elastoinertial turbulence helps explain why flows remain turbulent even when the Newtonian near-wall structures are strongly suppressed. Many questions about EIT remain, however. In channel flow, it is directly connected to the Tollmien-Schlichting instability mode and corresponding near-wall critical layer, and is known to subcritically excite this mode, driving flow away from the laminar state even when that state is linearly stable. A simple mechanistic explanation of this viscoelastic excitation of the TS mode does not yet exist. Simulations reveal similar near-wall critical layer fluctuations in plane Couette and pipe flows, even though they do not display a linear instability of Tollmien-Schlichting type—perhaps, in analogy to channel flow, wall modes are highly susceptible to amplification, driving bypass transition.

Additionally, a new mode of linear instability, with a critical layer near the centerline, arises in both pipe and channel flows. This mode also appears to be strongly subcritical, leading to flows with substantial polymer stretch fluctuations near the centerline. This may be the dominant mode at low Reynolds numbers and high Weissenberg numbers, helping explain experimental observations in this regime.

In addition, the maximum drag reduction asymptote may be a marginal flow regime in which Newtonian and elastoinertial flow structures coexist, perhaps in an intermittent fashion. These issues are ripe for future study.

Controlling and using flow instabilities. Finally, an interesting research direction for the future will be to connect this emerging understanding of the physics underlying elastic instabilities and turbulence to applications of viscoelastic fluids. For example, one of the most fundamental descriptors of such flows in applications is the relationship between the overall pressure drop and the volumetric flow rate, often described using an "apparent viscosity" η_{app} that quantifies macroscopic flow resistance; however, prediction and control of this quantity remains challenging, despite its central importance in applications. Recent work has made progress in doing so for flows in porous media [262], and further research along these lines will be important in the rational application of viscoelastic flows in diverse settings.

Another important direction for future work will be in exploring ways to *control* elastic instabilities and turbulence as well as *engineer* spatiotemporal flow patterns in viscoelastic fluids. So far, mostly geometric control has been employed such as the flow between two cylinders [214], in a cross-slot geometry [160], in disordered obstacle arrays [161], or in designed porous media [65,262]. An attractive alternative is to employ time-dependent or modulated shear rates for active open-loop control of viscoelastic fluid flow. As demonstrated in Ref. [162], this allows tuning or control of the occurrence of elastic turbulence and therefore, for example, the mixing of complex fluids. Exploring this and other approaches (e.g., employing deformable structures [461]) will be a useful direction for future work.

In terms of direct applications of elastic turbulence, a number of different research groups have shown that, in addition to enhancing passive scalar mixing as was originally demonstrated in the earlier works of Steinberg and collaborators [49,96,505,506], these kinds of viscoelastic chaotic flows can also be used to effectively enhance heat transfer at low Reynolds numbers both in macroscale "von Kármán flow" [507] and also at the microscale in serpentine and wavy channel geometries [508–510]. Finally, elastic turbulence has been used to create emulsions from immiscible viscous liquids in a simple shear mixing device [511]. In the absence of elasticity, but at identical viscosity ratio, Reynolds and capillary numbers, no mixing was observed and the immiscible liquids remain separated. Elastic turbulence thus offers a unique pathway to create dispersions in viscous liquids at low Reynolds numbers in nominally shear-dominated flows. Further studies of these phenomena, and other potential applications, would be a fruitful avenue for additional research.

In conclusion. Any reader that has gotten this far will hopefully agree that the subject is fascinating, both from the standpoint of fundamentals, but also because the materials that make up the complex fluids field find a wide range of applications. Thus, we hope this article serves future researchers as a basis for next steps in advancing research and understanding of the flows and instabilities of complex fluids.

---

[1] G. V. Vinogradov and A. Y. Malkin, *Rheology of Polymers* (Springer-Verlag, Berlin, 1980).

[2] P. E. Rouse, A theory of the linear viscoelastic properties of dilute solutions of coiling polymers, J. Chem. Phys. **21**, 1272 (1953).

[3] B. H. Zimm, Dynamics of polymer molecules in dilute solution: Viscoelasticity, flow birefringence and dielectric loss, J. Chem. Phys. **24**, 269 (1956).

[4] P. G. de Gennes, Coil-stretch transition of dilute flexible polymers under ultrahigh velocity gradients, J. Chem. Phys. **60**, 5030 (1974).

[5] E. J. Hinch, Mechanical models of dilute polymer solutions in strong flows, Phys. Fluids **20**, S22 (1977).

[6] P. Pakdel and G. H. McKinley, Elastic Instability and Curved Streamlines, Phys. Rev. Lett. **77**, 2459 (1996).

[7] R. B. Bird, R. C. Armstrong, and O. Hassager, *Dynamics of Polymeric Liquids*, 2nd ed. (John Wiley & Sons, New York, 1987), Vol. 1.

[8] R. G. Larson, *The Structure and Rheology of Complex Fluids* (Oxford University Press, New York, 1999).

[9] G. I. Taylor, VIII. Stability of a viscous liquid contained between two rotating cylinders, Philos. Trans. R. Soc. London A **223**, 289 (1923).

[10] D. V. Boger, A highly elastic constant-viscosity fluid, J. Non-Newtonian Fluid Mech. **3**, 87 (1977/78).

[11] D. F. James, Boger fluids, Annu. Rev. Fluid Mech. **41**, 129 (2009).

[12] G. Prilutski, R. K. Gupta, T. Sridhar, and M. E. Ryan, Model viscoelastic liquids, J. Non-Newtonian Fluid Mech. **12**, 233 (1983).

[13] S. L. Anna, G. H. McKinley, D. A. Nguyen, T. Sridhar, S. J. Muller, J. Huang, and D. F. James, An inter-laboratory comparison of measurements from filament-stretching rheometers using common test fluids, J. Rheol. **45**, 83 (2001).

[14] J. M. Rallison and E. J. Hinch, Do we understand the physics in the constitutive equation? J. Non-Newtonian Fluid Mech. **29**, 37 (1988).

[15] H. Giesekus, A simple constitutive equation for polymer fluids based on the concept of deformation-dependent tensorial mobility, J. Non-Newtonian Fluid Mech. **11**, 69 (1982).

[16] L. M. Quinzani, G. H. McKinley, R. A. Brown, and R. C. Armstrong, Modeling the rheology of polyisobutylene solutions, J. Rheol. **34**, 705 (1990).

[17] R. G. Larson and P. S. Desai, Modeling the rheology of polymer melts and solutions, Annu. Rev. Fluid Mech. **47**, 47 (2015).

[18] P. Saramito, A new elastoviscoplastic model based on the Herschel-Bulkley viscoplastic model, J. Non-Newtonian Fluid Mech. **158**, 154 (2009).

[19] C. J. Dimitriou and G. H. McKinley, A canonical framework for modeling elasto-viscoplasticity in complex fluids, J. Non-Newtonian Fluid Mech. **265**, 116 (2019).

[20] E. S. G. Shaqfeh and B. Khomami, The Oldroyd-B fluid in elastic instabilities, turbulence and particle suspensions, J. Non-Newtonian Fluid Mech. **298**, 104672 (2021).

[21] J. M. Dealy, Weissenberg and Deborah numbers—Their definition and use, Rheol. Bull. **79**, 14 (2010).

[22] E. S. G. Shaqfeh, Purely elastic instabilities in viscometric flows, Annu. Rev. Fluid Mech. **28**, 129 (1996).

[23] S. J. Muller, R. G. Larson, and E. S. G. Shaqfeh, A purely elastic transition in Taylor-Couette flow, Rheol. Acta **28**, 499 (1989).

[24] R. G. Larson, E. S. G. Shaqfeh, and S. J. Muller, A purely elastic instability in Taylor-Couette flow, J. Fluid Mech. **218**, 573 (1990).

[25] E. S. G. Shaqfeh, S. J. Muller, and R. G. Larson, The effects of gap width and dilute solution properties on the viscoelastic Taylor-Couette instability, J. Fluid Mech. **235**, 285 (1992).

[26] L. Pan, A. Morozov, C. Wagner, and P. E. Arratia, Nonlinear Elastic Instability in Channel Flows at Low Reynolds Numbers, Phys. Rev. Lett. **110**, 174502 (2013).

[27] M. D. Graham, Effect of axial flow on viscoelastic Taylor-Couette instability, J. Fluid Mech. **360**, 341 (1998).

[28] K. Arora and R. Sureshkumar, A viscoelastic flow instability near the solid body rotation limit, J. Non-Newtonian Fluid Mech. **132**, 36 (2005).

[29] J. J. Magda and R. G. Larson, A transition occurring in ideal elastic liquids during shear flow, J. Non-Newtonian Fluid Mech. **30**, 1 (1988).

[30] G. H. McKinley, J. A. Byars, R. A. Brown, and R. C. Armstrong, Observations on the elastic instability in cone-and-plate and parallel-plate flows of a polyisobutylene Boger fluid, J. Non-Newtonian Fluid Mech. **40**, 201 (1991).

[31] G. H. McKinley, A. Oztekin, J. A. Byars, and R. A. Brown, Self-similar spiral instabilities in elastic flows between a cone and a plate, J. Fluid Mech. **285**, 123 (1995).

[32] J. A. Byars, A. Oztekin, R. A. Brown, and G. H. McKinley, Spiral instabilities in the flow of highly elastic fluids between rotating parallel disks, J. Fluid Mech. **271**, 173 (1994).

[33] H. Yamaguchi, J. Fujiyoshi, and H. Matsui, Spherical Couette flow of a viscoelastic fluid Part I: Experimental study of the inner sphere rotation, J. Non-Newtonian Fluid Mech. **69**, 29 (1997).

[34] H. Yamaguchi and H. Matsui, Spherical Couette flow of a viscoelastic fluid Part II: Numerical study for the inner sphere rotation, J. Non-Newtonian Fluid Mech. **69**, 47 (1997).

[35] H. Yamaguchi and B. Nishiguchi, Spherical Couette flow of a viscoelastic fluid—Part III: A study of outer sphere rotation, J. Non-Newtonian Fluid Mech. **84**, 45 (1999).

[36] J. R. Stokes, L. J. W. Graham, N. J. Lawson, and D. V. Boger, Swirling flow of viscoelastic fluids. Part 1. Interaction between inertia and elasticity, J. Fluid Mech. **429**, 67 (2001).

[37] J. R. Stokes, L. J. W. Graham, N. J. Lawson, and D. V. Boger, Swirling flow of viscoelastic fluids. Part 2. Elastic effects, J. Fluid Mech. **429**, 117 (2001).

[38] P. Pakdel and G. H. McKinley, Cavity flows of elastic liquids: Purely elastic instabilities, Phys. Fluids **10**, 1058 (1998).

[39] A. M. Grillet and E. S. G. Shaqfeh, Viscoelastic instabilities in recirculation flows of Boger fluids, J. Non-Newtonian Fluid Mech. **64**, 141 (1996).

[40] A. M. Grillet, E. S. G. Shaqfeh, and B. Khomami, Observations of the viscoelastic instabilities in lid driven cavity flow, J. Non-Newtonian Fluid Mech. **94**, 15 (2000).

[41] J.-H. Kim, A. Oztekin, and S. Neti, Instabilities in viscoelastic flow past a square cavity, J. Non-Newtonian Fluid Mech. **90**, 261 (2000).

[42] Y. L. Joo and E. S. G. Shaqfeh, Viscoelastic Poiseuille flow through a curved channel: A new elastic instability, Phys. Fluids A **3**, 1691 (1991).

[43] Y. L. Joo and E. S. G. Shaqfeh, A purely elastic instability in Dean and Taylor-Dean flow, Phys. Fluids A **4**, 524 (1992).

[44] Y. L. Joo and E. S. G. Shaqfeh, The effects of inertia on the viscoelastic Dean and Taylor-Couette flow instabilities with application to coating flows, Phys. Fluids A **4**, 2415 (1992).

[45] Y. L. Joo and E. S. G. Shaqfeh, Observations of purely elastic instabilities in the Taylor-Dean flow of a Boger fluid, J. Fluid Mech. **262**, 27 (1994).

[46] J. A. Pathak, D. Ross, and K. B. Migler, Elastic flow instability, curved streamlines, and mixing in microfluidic flows, Phys. Fluids **16**, 4028 (2004).

[47] K. Arora, R. Sureshkumar, and B. Khomami, Experimental investigation of purely elastic instabilities in periodic flows, J. Non-Newtonian Fluid Mech. **108**, 209 (2002).

[48] A. Groisman and V. Steinberg, Elastic turbulence in a polymer solution flow, Nature (London) **405**, 53 (2000).

[49] T. Burghelea, E. Segre, I. Bar-Joseph, A. Groisman, and V. Steinberg, Chaotic flow and efficient mixing in a microchannel with a polymer solution, Phys. Rev. E **69**, 066305 (2004).

[50] J. Zilz, R. J. Poole, M. A. Alves, D. Bartolo, B. Levache, and A. Lindner, Geometric scaling of a purely elastic flow instability in serpentine channels, J. Fluid Mech. **712**, 203 (2012).

[51] J. Soulages, M. S. N. Oliveira, P. C. Sousa, M. A. Alves, and G. H. McKinley, Investigating the stability of viscoelastic stagnation flows in T-shaped microchannels, J. Non-Newtonian Fluid Mech. **163**, 9 (2009).

[52] P. E. Arratia, C. C. Thomas, J. Diorio, and J. P. Gollub, Elastic Instabilities of Polymer Solutions in Cross-Channel Flow, Phys. Rev. Lett. **96**, 144502 (2006).

[53] R. J. Poole, M. A. Alves, and P. J. Oliveira, Purely Elastic Flow Asymmetries, Phys. Rev. Lett. **99**, 164503 (2007).

[54] L. Xi and M. D. Graham, A mechanism for oscillatory instability in viscoelastic cross-slot flow, J. Fluid Mech. **622**, 145 (2009).

[55] S. J. Haward and G. H. McKinley, Instabilities in stagnation point flows of polymer solutions, Phys. Fluids **25**, 083104 (2013).

[56] S. J. Haward, G. H. McKinley, and A. Q. Shen, Elastic instabilities in planar elongational flow of monodisperse polymer solutions, Sci. Rep. **6**, 33029 (2016).

[57] F. A. Cruz and M. A. Alves, Characterization of superimposed instabilities in the planar extensional flow of viscoelastic fluids, Phys. Rev. Fluids **3**, 113301 (2018).

[58] B. Thomases and M. Shelley, Transition to Mixing and Oscillations in a Stokesian Viscoelastic Flow, Phys. Rev. Lett. **103**, 094501 (2009).

[59] A. M. Afonso, M. A. Alves, R. J. Poole *et al.*, Viscoelastic flows in mixing-separating cells, J. Eng. Math. **71**, 3 (2011).

[60] M. S. N. Oliveira, F. T. Pinho, R. J. Poole, P. J. Oliveira, and M. A. Alves, Purely elastic flow asymmetries in flow-focusing devices, J. Non-Newtonian Fluid Mech. **160**, 31 (2009).

[61] I. M. Dris and E. S. G. Shaqfeh, On purely elastic instabilities in eccentric cylinder flows, J. Non-Newtonian Fluid Mech. **56**, 349 (1995).

[62] G. H. McKinley, R. C. Armstrong, and R. A. Brown, The wake instability in viscoelastic flow past confined circular cylinders, Philos. Trans. R. Soc. London A **344**, 265 (1993).

[63] A. M. Howe, A. Clarke, and D. Giernalczyk, Flow of concentrated viscoelastic polymer solutions in porous media: Effect of M_W and concentration on elastic turbulence onset in various geometries, Soft Matter **11**, 6419 (2015).

[64] S. De, J. van der Schaaf, N. G. Deen, J. A. M. Kuipers, E. A. J. F. Peters, and J. T. Padding, Lane change in flows through pillared microchannels, Phys. Fluids **29**, 113102 (2017).

[65] C. A. Browne, A. Shih, and S. S. Datta, Bistability in the unstable flow of polymer solutions through pore constriction arrays, J. Fluid Mech. **890**, A2 (2020).

[66] M. A. Alves and R. J. Poole, Divergent flow in contractions, J. Non-Newtonian Fluid Mech. **144**, 140 (2007).

[67] J. V. Lawler, S. J. Muller, R. A. Brown, and R. C. Armstrong, Laser Doppler velocimetry measurements of velocity fields and transitions in viscoelastic fluids, J. Non-Newtonian Fluid Mech. **20**, 51 (1986).

[68] J. P. Rothstein and G. H. McKinley, Extensional flow of a polystyrene Boger fluid through a 4:1:4 axisymmetric contraction-expansion, J. Non-Newtonian Fluid Mech. **86**, 61 (1999).

[69] D. G. Hassell, J. Embery, T. C. B. McLeish, and M. R. Mackley, An experimental evaluation of the formation of an instability in monodisperse and polydisperse polystyrenes, J. Non-Newtonian Fluid Mech. **157**, 1 (2009).

[70] E. M. Ekanem, S. Berg, S. De, A. Fadili, T. Bultreys, M. Rucker, J. Southwick, J. Crawshaw, and P. F. Luckham, Signature of elastic turbulence of viscoelastic fluid flow in a single pore throat, Phys. Rev. E **101**, 042605 (2020).

[71] A. Groisman and S. R. Quake, A Microfluidic Rectifier: Anisotropic Flow Resistance at Low Reynolds Numbers, Phys. Rev. Lett. **92**, 094501 (2004).

[72] P. C. Sousa, F. T. Pinho, M. S. N. Oliveira, and M. A. Alves, Efficient microfluidic rectifiers for viscoelastic fluid flow, J. Non-Newtonian Fluid Mech. **165**, 652 (2010).

[73] R. J. Poole, Three-dimensional viscoelastic instabilities in microchannels, J. Fluid Mech. **870**, 1 (2019).

[74] G. H. McKinley, P. Pakdel, and A. Oztekin, Rheological and geometric scaling of purely elastic flow instabilities, J. Non-Newtonian Fluid Mech. **67**, 19 (1996).

[75] G. H. McKinley, Dimensionless groups for understanding free surface flows of complex fluids, Rheol. Bull. 6 (2005), Society of Rheology.

[76] D. W. Beard, M. H. Davies, and K. Walters, The stability of elastico-viscous flow between rotating cylinders Part 3. Overstability in viscous and Maxwell fluids, J. Fluid Mech. **24**, 321 (1966).

[77] R. F. Ginn and M. M. Denn, Rotational stability in viscoelastic liquids: Theory, AIChE J. **15**, 450 (1969).

[78] M. Renardy, Y. Renardy, R. Sureshkumar, and A. Beris, Hopf-Hopf and steady-Hopf mode interactions in Taylor-Couette flow of an upper convected Maxwell liquid, J. Non-Newtonian Fluid Mech. **63**, 1 (1996).

[79] D. D. Joseph, Hyperbolic phenomena in the flow of viscoelastic fluids, in *Viscoelasticity and Rheology*, edited by A. S. Lodge, M. Renardy, and J. A. Nohel (Academic Press, Orlando, 1985), pp. 235–321.

[80] V. Delvaux and M. J. Crochet, Numerical prediction of anomalous transport properties in viscoelastic flow, J. Non-Newtonian Fluid Mech. **37**, 297 (1990).

[81] B. Qin, P. F. Salipante, S. D. Hudson, and P. Arratia, Upstream vortex and elastic wave in the viscoelastic flow around a confined cylinder, J. Fluid Mech. **864**, R2-1 (2019).

[82] Y. Zhao, A. Q. Shen, and S. J. Haward, Flow of wormlike micellar solutions around confined microfluidic cylinders, Soft Matter **12**, 8666 (2016).

[83] A. Varshney and V. Steinberg, Elastic Alfvén waves in elastic turbulence, Nat. Commun. **10**, 652 (2019).

[84] P. P. Bhat *et al.*, Formation of beads-on-a-string structures during break-up of viscoelastic filaments, Nat. Phys. **6**, 625 (2010).

[85] C. Clasen *et al.*, Dispensing of rheologically complex fluids: The map of misery, AIChE J. **58**, 3242 (2012).

[86] U. A. Al-Mubaiyedh *et al.*, Effect of viscous heating on the stability of viscoelastic Taylor-Couette flow, J. Fluid Mech. **462**, 111 (2000).

[87] J. P. Rothstein and G. H. McKinley, Non-isothermal modification of purely elastic flow instabilities in torsional flows of polymeric fluids, Phys. Fluids **13**, 382 (2001).

[88] M. M. Denn *et al.*, Shear thickening in concentrated suspensions of smooth spheres in Newtonian suspending fluids, Soft Matter **14**, 170 (2018).

[89] V. Sharma and G. H. McKinley, An intriguing empirical rule for computing the first normal stress difference from steady shear viscosity data for concentrated polymer solutions and melts, Rheol. Acta **51**, 487 (2012).

[90] S. J. Haward and G. H. McKinley, Stagnation point flow of wormlike micellar solutions in a microfluidic cross-slot device: Effects of surfactant concentration and ionic environment, Phys. Rev. E **85**, 031502 (2012).

[91] S. J. Haward, C. C. Hopkins, and A. Q. Shen, Asymmetric flow of polymer solutions around microfluidic cylinders: Interaction between shear-thinning and viscoelasticity, J. Non-Newtonian Fluid Mech. **278**, 104250 (2020).

[92] W. Ostwald and R. Auerbach, Ueber die Viskosität kolloider Lösungen im Struktur-, Laminar- und Turbulenzgebiet, Kolloid Z. **38**, 261 (1926).

[93] H. Giesekus, Nicht-Lineare Effekte beim Strömen viskoelasticher Flüssigkeiten Schlitz- and Lochdüsen (Nonlinear effects for viscoelastic liquids flowing through rectangular and circular ducts), Rheol. Acta **7**, 127 (1968).

[94] J. R. A. Pearson, Instability in non-Newtonian flow, Annu. Rev. Fluid Mech. **8**, 163 (1976).

[95] M. M. Denn, Extrusion instabilities and wall slip, Annu. Rev. Fluid Mech. **33**, 265 (2001).

[96] V. Steinberg, Elastic turbulence: An experimental view on inertialess random flow, Annu. Rev. Fluid Mech. **53**, 27 (2021).

[97] M. Avgousti and A. N. Beris, Non-axisymmetric modes in viscoelastic Taylor-Couette flow, J. Non-Newtonian Fluid Mech. **50**, 225 (1993).

[98] R. Sureshkumar, A. N. Beris, and M. Avgousti, Non-axisymmetric subcritical bifurcation in viscoelastic Taylor-Couette flow, Proc. R. Soc. London A **447**, 135 (1994).

[99] B. M. Baumert and S. J. Muller, Flow visualization of the elastic Taylor-Couette instability in Boger fluids, Rheol. Acta **34**, 147 (1995).

[100] B. M. Baumert and S. J. Muller, Flow regimes in model viscoelastic fluids in a circular Couette system with independently rotating cylinders, Phys. Fluids **9**, 566 (1997).

[101] B. M. Baumert and S. J. Muller, Axisymmetric and non-axisymmetric elastic and inertio-elastic instabilities in Taylor-Couette flow, J. Non-Newtonian Fluid Mech. **83**, 33 (1999).

[102] A. Groisman and V. Steinberg, Couette-Taylor Flow in a Dilute Polymer Solution, Phys. Rev. Lett. **77**, 1480 (1996).

[103] A. Groisman and V. Steinberg, Solitary Vortex Pairs in Viscoelastic Couette Flow, Phys. Rev. Lett. **78**, 1460 (1997).

[104] A. Groisman and V. Steinberg, Mechanism of elastic instability in Couette flow of polymer solutions: Experiment, Phys. Fluids **10**, 2451 (1998).

[105] U. A. Al-Mubaiyedh, R. Sureshkumar, and B. Khomami, Linear stability of viscoelastic Taylor-Couette flow: Influence of fluid rheology and energetics, J. Rheol. **44**, 1121 (2000).

[106] J. M. White and S. J. Muller, Viscous Heating and the Stability of Newtonian and Viscoelastic Taylor-Couette Flows, Phys. Rev. Lett. **84**, 5130 (2000).

[107] J. M. White and S. J. Muller, Experimental studies on the stability of Newtonian Taylor-Couette flow in the presence of viscous heating, J. Fluid Mech. **462**, 133 (2002).

[108] J. M. White and S. J. Muller, Experimental studies on the effect of viscous heating on the hydrodynamic stability of viscoelastic Taylor-Couette flow, J. Rheol. **47**, 1467 (2003).

[109] C. Schäfer, A. Morozov, and C. Wagner, Geometric scaling of elastic instabilities in the Taylor-Couette geometry: A theoretical, experimental and numerical study, J. Non-Newton. Fluid Mech. **259**, 78 (2018).

[110] K. A. Kumar and M. D. Graham, Solitary Coherent Structures in Viscoelastic Shear Flow: Computation and Mechanism, Phys. Rev. Lett. **85**, 4056 (2000).

[111] K. A. Kumar and M. D. Graham, Finite-amplitude solitary states in viscoelastic shear flow: Computation and mechanism, J. Fluid Mech. **443**, 301 (2000).

[112] D. G. Thomas, R. Sureshkumar, and B. Khomami, Pattern Formation in Taylor-Couette Flow of Dilute Polymer Solutions: Dynamical Simulations and Mechanism, Phys. Rev. Lett. **97**, 054501 (2006).

[113] N. Liu and B. Khomami, Elastically induced turbulence in Taylor-Couette flow: Direct numerical simulation and mechanistic insight, J. Fluid Mech. **737**, R4 (2013).

[114] R. Ghanbari and B. Khomami, The onset of purely elastic and thermo-elastic instabilities in Taylor-Couette flow: Influence of gap ratio and fluid thermal sensitivity, J. Non-Newtonian Fluid Mech. **208–209**, 108 (2014).

[115] J. Song, H. Teng, N. Liu, H. Ding, X.-Y. Lu, and B. Khomami, The correspondence between drag enhancement and vortical structures in turbulent Taylor-Couette flows with polymer additives: A study of curvature dependence, J. Fluid Mech. **881**, 602 (2019).

[116] F. A. Cruz, R. J. Poole, A. M. Afonso, F. T. Pinho, P. J. Oliveira, and M. A. Alves, Influence of channel aspect ratio on the onset of purely-elastic flow instabilities in three-dimensional planar cross-slots, J. Non-Newtonian Fluid Mech. **227**, 65 (2016).

[117] R. I. Tanner, *Engineering Rheology*, 2nd ed. (Oxford University Press, Oxford, 2000).

[118] J. G. Oldroyd, On the formulation of rheological equations of state, Proc. R. Soc. London A **200**, 523 (1950).

[119] R. B. Bird, C. F. Curtiss, R. C. Armstrong, and O. Hassager, *Dynamics of Polymeric Liquids*, 2nd ed. (John Wiley & Sons, New York, 1987), Vol. 2.

[120] M. W. Johnson and D. Segalman, A model for viscoelastic fluid behavior which allows non-affine deformation, J. Non-Newtonian Fluid Mech. **2**, 255 (1977).

[121] R. J. Gordon and W. R. Schowalter, Anisotropic fluid theory: A different approach to the dumbbell theory of dilute polymer solutions, Trans. Soc. Rheol. **16**, 79 (1972).

[122] N. Phan-Thien and R. I. Tanner, A new constitutive equation derived from network theory, J. Non-Newtonian Fluid Mech. **2**, 353 (1977).

[123] A. I. Leonov and A. N. Prokunin, *Nonlinear Phenomena in Flows of Viscoelastic Polymer Fluids* (Chapman & Hall, London, 1994).

[124] C. Truesdell and W. Noll, The non-linear field theories of mechanics, in *Handbuch der Physik*, 3rd ed., edited by S. Flügge (Springer, Berlin, 2004), Vol. III/3.

[125] M. Grmela and P. J. Carreau, Conformation tensor rheological models, J. Non-Newtonian Fluid Mech. **23**, 271 (1987).

[126] A. N. Beris and B. J. Edwards, *Thermodynamics of Flowing Systems with Internal Microstructure* (Oxford University Press, New York, 1994).

[127] A. Souvaliotis and A. N. Beris, An extended White-Metzner viscoelastic fluid model based on an internal structural parameter, J. Rheol. **36**, 241 (1992).

[128] R. Sureshkumar, A. N. Beris, and R. A. Handler, Direct numerical simulation of polymer-induced drag reduction in turbulent channel flow, Phys. Fluids **9**, 743 (1997).

[129] K. D. Housiadas and A. N. Beris, Direct numerical simulations of viscoelastic turbulent channel flows at high drag reduction, Korea-Australia Rheol. J. **17**, 131 (2005).

[130] M. D. Graham and D. Floryan, Exact coherent states and the nonlinear dynamics of wall-bounded turbulent flows, Annu. Rev. Fluid Mech. **53**, 227 (2021).

[131] L. Zhu and L. Xi, Nonasymptotic elastoinertial turbulence for asymptotic drag reduction, Phys. Rev. Fluids **6**, 014601 (2021).

[132] R. Fattal and R. Kupferman, Constitutive laws for the matrix-logarithm of the conformation tensor, J. Non-Newtonian Fluid Mech. **123**, 281 (2004).

[133] R. Fattal and R. Kupferman, Time-dependent simulation of viscoelastic flows at high Weissenberg number using the log-conformation representation, J. Non-Newtonian Fluid Mech. **126**, 23 (2005).

[134] T. Vaithianathan and L. R. Collins, Numerical approach to simulating turbulent flow of a viscoelastic polymer solution, J. Comput. Phys. **187**, 1 (2003).

[135] M. A. Hulsen, R. Fattal, and R. Kupferman, Flow of viscoelastic fluids past a cylinder at high Weissenberg number: Stabilized simulations using matrix logarithms, J. Non-Newtonian Fluid Mech. **127**, 27 (2005).

[136] M. A. Alves, P. J. Oliveira, and F. T. Pinho, Numerical methods for viscoelastic fluid flows, Annu. Rev. Fluid Mech. **53**, 509 (2021).

[137] B. A. Toms, Some observations on the flow of linear polymer solutions through straight tubes at large Reynolds numbers, in *Proceedings of the International Rheological Congress* (North-Holland, Amsterdam, 1949), Vol. 2, pp. 135–141.

[138] A. Seyer and A. B. Metzner, Turbulence phenomena in drag-reducing systems, AIChE J. **15**, 426 (1969).

[139] J. L. Lumley, Drag reduction by additives, Annu. Rev. Fluid Mech. **1**, 367 (1969).

[140] P. S. Virk, Drag reduction fundamentals, AIChE J. **21**, 625 (1975).

[141] P. Garg, I. Chaudhary, M. Khalid, V. Shankar, and G. Subramanian, Viscoelastic Pipe Flow Is Linearly Unstable, Phys. Rev. Lett. **121**, 024502 (2018).

[142] I. Chaudhary, P. Garg, G. Subramanian, and V. Shankar, Linear instability of viscoelastic pipe flow, J. Fluid Mech. **908**, A11 (2021).

[143] J. Page, Y. Dubief, and R. R. Kerswell, Exact Traveling Wave Solutions in Viscoelastic Channel Flow, Phys. Rev. Lett. **125**, 154501 (2020).

[144] Y. Dubief, J. Page, R. R. Kerswell, V. E. Terrapon, and V. Steinberg, A first coherent structure in elasto-inertial turbulence, Phys. Rev. Fluids **7**, 073301 (2022).

[145] P. S. Doyle and E. S. G. Shaqfeh, Dynamic simulation of freely-draining, flexible bead-rod chains: Start-up of extensional and shear flow, J. Non-Newtonian Fluid Mech. **76**, 43 (1998).

[146] R. Radhakrishnan and P. T. Underhill, Models of flexible polymers in good solvents: Relaxation and coil-stretch transition, Soft Matter **8**, 6991 (2012).

[147] G. Lielens, R. Keunings, and V. Legat, The FENE-L and FENE-LS closure approximations to the kinetic theory of finitely extensible dumbbells, J. Non-Newtonian Fluid Mech. **87**, 179 (1999).

[148] C. M Schroeder, Single polymer dynamics for molecular rheology, J. Rheol. **62**, 371 (2018).

[149] M. H. N. Sefiddashti, B. J. Edwards, and B. Khomami, Elucidating the molecular rheology of entangled polymeric fluids *via* comparison of atomistic simulations and model predictions, Macromolecules **52**, 8124 (2019).

[150] S. M. Fielding, Complex dynamics of shear banded flows, Soft Matter **3**, 1262 (2007).

[151] N. Germann, L. P. Cook, and A. N. Beris, Nonequilibrium thermodynamic modeling of the structure and rheology of concentrated wormlike micellar solutions, J. Non-Newtonian Fluid Mech. **196**, 51 (2013).

[152] V. G. Mavrantzas and A. N. Beris, A hierarchical model for surface effects on chain conformation and rheology of polymer solutions. I. General formulation, J. Chem. Phys. **110**, 616; II. Application to a neutral surface, **110**, 628 (1999).

[153] A. Groisman and V. Steinberg, Elastic turbulence in curvilinear flows of polymer solutions, New J. Phys. **6**, 29 (2004).

[154] R. van Buel and H. Stark, Elastic turbulence in two-dimensional Taylor-Couette flows, Europhys. Lett. **124**, 14001 (2018).

[155] A. Fouxon and V. Lebedev, Spectra of turbulence in dilute polymer solutions, Phys. Fluids **15**, 2060 (2003).

[156] G. I. Taylor, The spectrum of turbulence, Proc. R. Soc. A **164**, 476 (1938).

[157] P. C. Sousa, F. T. Pinho, and M. A. Alves, Purely-elastic flow instabilities and elastic turbulence in microfluidic cross-slot devices, Soft Matter **14**, 1344 (2018).

[158] Y. Liu and V. Steinberg, Stretching of polymer in a random flow: Effect of a shear rate, Europhys. Lett. **90**, 44005 (2010).

[159] R. Neelamegam, V. Shankar, and D. Das, Suppression of purely elastic instabilities in the torsional flow of viscoelastic fluid past a soft solid, Phys. Fluids **25**, 124102 (2013).

[160] M. Davoodi, A. F. Domingues, and R. J. Poole, Control of a purely elastic symmetry-breaking flow instability in cross-slot geometries, J. Fluid Mech. **881**, 1123 (2019).

[161] D. M. Walkama, N. Waisbord, and J. S. Guasto, Disorder Suppresses Chaos in Viscoelastic Flows, Phys. Rev. Lett. **124**, 164501 (2020).

[162] R. van Buel and H. Stark, Active open-loop control of elastic turbulence, Sci. Rep. **10**, 15704 (2020).

[163] V. A. Gorodtsov and A. I. Leonov, On a linear instability of a plane parallel Couette flow of viscoelastic fluid, J. Appl. Math. Mech. **31**, 310 (1967).

[164] T. C. Ho and M. M. Denn, Stability of plane Poiseuille flow of a highly elastic liquid, J. Non-Newtonian Fluid Mech. **3**, 179 (1977).

[165] K.-C. Lee and B. A. Finlayson, Stability of plane Poiseuille and Couette flow of a Maxwell fluid, J. Non-Newtonian Fluid Mech. **21**, 65 (1986).

[166] M. Renardy and Y. Renardy, Linear stability of plane Couette flow of an upper convected Maxwell fluid, J. Non-Newtonian Fluid Mech. **22**, 23 (1986).

[167] M. Renardy, A rigorous stability proof for plane Couette flow of an upper convected Maxwell fluid at zero Reynolds number, Euro. J. Mech. Fluids B **11**, 511 (1992).

[168] R. G. Larson, Instabilities in viscoelastic flows, Rheol. Acta **31**, 213 (1992).

[169] H. J. Wilson and J. M. Rallison, Instability of channel flow of a shear-thinning White-Metzner fluid, J. Non-Newtonian Fluid Mech. **87**, 75 (1999).

[170] H. J. Wilson and V. Loridan, Linear instability of a highly shear-thinning fluid in channel flow, J. Non-Newtonian Fluid Mech. **223**, 200 (2015).

[171] M. Khalid, V. Shankar, and G. Subramanian, Continuous Pathway between the Elasto-Inertial and Elastic Turbulent States in Viscoelastic Channel Flow, Phys. Rev. Lett. **127**, 134502 (2021).

[172] G. Buza, J. Page, and R. R. Kerswell, Weakly nonlinear analysis of the viscoelastic instability in channel flow for finite and vanishing Reynolds numbers, J. Fluid Mech. **940**, A11 (2022).

[173] P. J. Schmid, Nonmodal stability theory, Annu. Rev. Fluid Mech. **39**, 129 (2007).

[174] S. Grossmann, The onset of shear flow turbulence, Rev. Mod. Phys. **72**, 603 (2000).

[175] L. N. Trefethen, A. E. Trefethen, S. C. Reddy, and T. A. Driscoll, Hydrodynamic stability without eigenvalues, Science **261**, 578 (1993).

[176] P. J. Schmid and D. S. Henningson, *Stability and Transition in Shear Flows*, Applied Mathematical Sciences (Springer, New York, NY, 2000).

[177] M. R. Jovanovic and S. Kumar, Transient growth without inertia, Phys. Fluids **22**, 023101 (2010).

[178] M. R. Jovanovic and S. Kumar, Nonmodal amplification of stochastic disturbances in strongly elastic channel flows, J. Non-Newtonian Fluid Mech. **166**, 755 (2011).

[179] J. E. Page and T. Zaki, Streak evolution in viscoelastic Couette flow, J. Fluid Mech. **742**, 520 (2014).

[180] J. E. Page and T. Zaki, The dynamics of spanwise vorticity perturbations in homogeneous viscoelastic shear flow, J. Fluid Mech. **777**, 327 (2015).

[181] G. Hariharan, M. R. Jovanovic, and S. Kumar, Localized stress amplification in inertialess channel flows of viscoelastic fluids, J. Non-Newtonian Fluid Mech. **291**, 104514 (2021).

[182] F. Waleffe, Transition in shear flows. Nonlinear normality versus non-normal linearity, Phys. Fluids **7**, 3060 (1995).

[183] B. Eckhardt, T. Schneider, B. Hof, and J. Westerweel, Turbulence transition in pipe flow, Annu. Rev. Fluid Mech. **39**, 447 (2007).

[184] B. Meulenbroek, C. Storm, V. Bertola, C. Wagner, D. Bonn, and W. van Saarloos, Intrinsic Route to Melt Fracture in Polymer Extrusion: A Weakly Nonlinear Subcritical Instability of Viscoelastic Poiseuille Flow, Phys. Rev. Lett. **90**, 024502 (2003).

[185] V. Bertola, B. Meulenbroek, C. Wagner, C. Storm, A. Morozov, W. van Saarloos, and D. Bonn, Experimental Evidence for an Intrinsic Route to Polymer Melt Fracture Phenomena: A Nonlinear Instability of Viscoelastic Poiseuille Flow, Phys. Rev. Lett. **90**, 114502 (2003).

[186] A. Morozov and W. van Saarloos, Subcritical Finite-Amplitude Solutions for Plane Couette Flow of Viscoelastic Fluids, Phys. Rev. Lett. **95**, 024501 (2005).

[187] A. N. Morozov and W. van Saarloos, An introductory essay on subcritical instabilities and the transition to turbulence in viscoelastic parallel shear flows, Phys. Rep. **447**, 112 (2007).

[188] L. S. Tuckerman, M. Chantry, and D. Barkley, Patterns in wall-bounded shear flows, Annu. Rev. Fluid Mech. **52**, 343 (2020).

[189] M. Nagata, Three-dimensional finite-amplitude solutions in plane Couette flow: Bifurcation from infinity, J. Fluid Mech. **217**, 519 (1990).

[190] F. Waleffe, On a self-sustaining process in shear flows, Phys. Fluids **9**, 883 (1997).

[191] B. Hof, C. W. H. van Doorne, J. Westerweel, F. T. M. Nieuwstadt, H. Faisst, B. Eckhardt, H. Wedin, R. R. Kerswell, and F. Waleffe, Experimental observation of nonlinear traveling waves in turbulent pipe flow, Science **305**, 1594 (2004).

[192] J. Hamilton, J. Kim, and F. Waleffe, Regeneration mechanisms of near-wall turbulence structures, J. Fluid Mech. **287**, 317 (1995).

[193] D. J. C. Dennis and F. M. Sogaro, Distinct Organizational States of Fully Developed Turbulent Pipe Flow, Phys. Rev. Lett. **113**, 234501 (2014).

[194] D. Bonn, F. Ingremeau, Y. Amarouchene, and H. Kellay, Large velocity fluctuations in small-Reynolds-number pipe flow of polymer solutions, Phys. Rev. E **84**, 045301(R) (2011).

[195] B. Qin and P. E. Arratia, Characterizing elastic turbulence in channel flows at low Reynolds number, Phys. Rev. Fluids **2**, 083302 (2017).

[196] B. Qin, P. F. Salipante, S. D. Hudson, and P. E. Arratia, Flow Resistance and Structures in Viscoelastic Channel Flows at Low Re, Phys. Rev. Lett. **123**, 194501 (2019).

[197] M. Kumar, S. Aramideh, C. A. Browne, S. S. Datta, and A. M. Ardekani, Numerical investigation of multistability in the unstable flow of a polymer solution through porous media, Phys. Rev. Fluids **6**, 033304 (2021).

[198] N. K. Jha and V. Steinberg, Coherent structures of elastic turbulence in straight channel with viscoelastic fluid flow, arXiv:2009.12258.

[199] N. K. Jha and V. Steinberg, Elastically driven Kelvin-Helmholtz-like instability in straight channel flow, Proc. Natl. Acad. Sci. USA **118**, e2105211118 (2021).

[200] R. Shnapp and V. Steinberg, Nonmodal elastic instability and elastic waves in weakly perturbed channel flow Ron Shnapp and Victor Steinberg, Phys. Rev. Fluids **7**, 063901 (2022).

[201] R. Shnapp and V. Steinberg, Splitting of localized disturbances in viscoelastic channel flow, J. Fluid Mech. **941**, R3 (2022).

[202] R. Zheng, N. Phan-Thien, and R. I. Tanner, The flow past a sphere in a cylindrical tube: Effects of intertia, shear-thinning and elasticity, Rheol. Acta **30**, 499 (1991).

[203] L. E. Becker, G. H. McKinley, H. Rasmussen, and O. Hassager, The unsteady motion of a sphere in a viscoelastic fluid, J. Rheol. **38**, 377 (1994).

[204] M. J. Solomon and S. J. Muller, Flow past a sphere in polystyrene-based Boger fluids: The effect on the drag coefficient of finite extensibility, solvent quality and polymer molecular weight, J. Non-Newtonian Fluid Mech. **62**, 81 (1996).

[205] G. H. McKinley, Steady and transient motion of spherical particles in viscoelastic liquids, in *Transport Processes in Bubble, Drops, and Particles*, edited by R. P. Chhabra and D. DeKee (Taylor & Francis, 2002), p. 338.

[206] A. Jayaraman and A. Belmonte, Oscillations of a solid sphere falling through a wormlike micellar fluid, Phys. Rev. E **67**, 065301(R) (2003).

[207] S. Chen and J. P. Rothstein, Flow of a wormlike micelle solution past a falling sphere, J. Non-Newtonian Fluid Mech. **116**, 205 (2004).

[208] K. D. Housiadas, G. C. Georgiou, and R. I. Tanner, A note on the unbounded creeping flow past a sphere for Newtonian fluids with pressure-dependent viscosity, Int. J. Eng. Sci. **86**, 1 (2015).

[209] H. Mohammadigoushki and S. J. Muller, Sedimentation of a sphere in wormlike micellar fluids, J. Rheol. **60**, 587 (2016).

[210] A. Anbari, H.-T. Chien, S. S. Datta, W. Deng, and D. A. Weitz, J. Fan. Microfluidic model porous media: Fabrication and applications, Small **14**, 1703575 (2018).

[211] M. Müller, J. Vorwerk, and P. O. Brunn, Optical studies of local flow behaviour of a non-Newtonian fluid inside a porous medium, Rheol. Acta **37**, 189 (1998).

[212] U. Eberhard, H. J. Seybold, E. Secchi, J. Jiménez-Martínez, P. A. Rühs, A. Ofner, J. S. Andrade, Jr., and M. Holzne, Mapping the local viscosity of non-Newtonian fluids flowing through disordered porous structures, Sci. Rep. **10**, 11733 (2020).

[213] D. Kawale, E. Marques, P. L. J. Zitha, M. T. Kreutzer, W. R. Rossen, and P. E. Boukany, Elastic instabilities during the flow of hydrolyzed polyacrylamide solution in porous media: Effect of pore-shape and salt, Soft Matter **13**, 765 (2017).

[214] A. Varshney and V. Steinberg, Elastic wake instabilities in a creeping flow between two obstacles, Phys. Rev. Fluids **2**, 051301(R) (2017).

[215] A. Varshney and V. Steinberg, Mixing layer instability and vorticity amplification in a creeping viscoelastic flow, Phys. Rev. Fluids **3**, 103303 (2018).

[216] A. Varshney and V. Steinberg, Drag enhancement and drag reduction in viscoelastic flow, Phys. Rev. Fluids **3**, 103302 (2018).

[217] A. A. Dey, Y. Modarres-Sadeghi, and J. P. Rothstein, Viscoelastic fluid-structure interactions between a flexible cylinder and wormlike micelle solution, Phys. Rev. Fluids **3**, 063301 (2018).

[218] C. C. Hopkins, S. J. Haward, and A. Q. Shen, Purely elastic fluid-structure interactions in microfluidics: Implications for mucociliary flows, Small **16**, 1903872 (2020).

[219] H. Rehage and H. Hoffmann, Rheological properties of viscoelastic surfactant systems, J. Phys. Chem. **92**, 4712 (1988).

[220] H. Rehage and H. Hoffmann, Viscoelastic surfactant solutions-model system for rheological research, Mol. Phys. **74**, 933 (1991).

[221] S. M. Fielding, Triggers and signatures of shear banding in steady and time-dependent flows, J. Rheol. **60**, 821 (2016).

[222] S. J. Haward, N. Kitajima, K. Toda-Peters, T. Takahashi, and A. Q. Shen, Flow of wormlike micellar solutions around microfluidic cylinders with high aspect ratio and low blockage ratio, Soft Matter **15**, 1927 (2019).

[223] C. C. Hopkins, S. J. Haward, and A. Q. Shen, Tristability in Viscoelastic Flow Past Side-by-Side Microcylinders, Phys. Rev. Lett. **126**, 054501 (2021).

[224] S. J. Haward, K. Toda-Peters, and A. Q. Shen, Steady viscoelastic flow around high-aspect-ratio, low-blockage-ratio microfluidic cylinders, J. Non-Newtonian Fluid Mech. **254**, 23 (2018).

[225] S. Varchanis, C. C. Hopkins, A. Q. Shen, J. Tsamopoulos, and S. J. Haward, Asymmetric flows of complex fluids past confined cylinders: A comprehensive numerical study with experimental validation, Phys. Fluids **32**, 053103 (2020).

[226] G. N. Rocha, R. J. Poole, M. A. Alves, and P. J. Oliveira, On extensibility effects in the cross-slot flow bifurcation, J. Non-Newtonian Fluid Mech. **156**, 58 (2009).

[227] A. Lanzaro and X. F. Yuan, Effects of contraction ratio on non-linear dynamics of semi-dilute, highly polydisperse PAAm solutions in microfluidics, J. Non-Newtonian Fluid Mech. **166**, 1064 (2011).

[228] L. E. Rodd, T. P. Scott, D. V. Boger, J. J. Cooper-White, and G. H. McKinley, The inertio-elastic planar entry flow of low-viscosity elastic fluids in micro-fabricated geometries, J. Non-Newtonian Fluid Mech. **129**, 1 (2005).

[229] S. Aramideh, P. P. Vlachos, and A. M. Ardekani, Pore-scale statistics of flow and transport through porous media, Phys. Rev. E **98**, 013104 (2018).

[230] S. S. Datta, H. Chiang, T. S. Ramakrishnan, and D. A. Weitz, Spatial Fluctuations of Fluid Velocities in Flow through a Three-Dimensional Porous Medium, Phys. Rev. Lett. **111**, 064501 (2013).

[231] C. A. Browne, A. A. Shih, and S. S. Datta. Pore-scale flow characterization of polymer solutions in microfluidic porous media, Small **16**, 1903944 (2019).

[232] K. S. Sorbie, *Polymer-Improved Oil Recovery* (Springer Science & Business Media, 2013).

[233] D. S. Roote, Technology status report: In situ flushing, Ground Water Remediation Technology Analysis Center, http://www.gwrtac.org (1998).

[234] M. M. Smith, J. A. K. Silva, J. Munakata-Marr, and J. E. McCray, Compatibility of polymers and chemical oxidants for enhanced groundwater remediation, Environ. Sci. Technol. **42**, 9296 (2008).

[235] P. Naik, P. Pandita, S. Aramideh, I. Bilionis, and A. M. Ardekani, Bayesian model calibration and optimization of surfactant-polymer flooding, Comput. Geosci. **23**, 981 (2019).

[236] P. Naik, S. Aramideh, and A. M. Ardekani, History matching of surfactant-polymer flooding using polynomial chaos expansion, J. Pet. Sci. Eng. **173**, 1438 (2019).

[237] S. Aramideh, R. Borgohain, P. K. Naik, C. T. Johnston, P. P. Vlachos, and A. M. Ardekani, Multi-objective history matching of surfactant-polymer flooding, Fuel **228**, 418 (2018).

[238] S. S. Datta, J.-B. Dupin, and D. A. Weitz, Fluid breakup during simultaneous two-phase flow through a three-dimensional porous medium, Phys. Fluids **26**, 062004 (2014).

[239] S. S. Datta, T. S. Ramakrishnan, and D. A. Weitz, Mobilization of a trapped non-wetting fluid from a three-dimensional porous medium, Phys. Fluids **26**, 022002 (2014).

[240] S. Aramideh, P. P. Vlachos, and A. M. Ardekani, Unstable displacement of non-aqueous phase liquids with surfactant and polymer, Transp. Porous Media **126**, 455 (2019).

[241] J. Mitchell, K. Lyons, A. M. Howe, and A. Clarke, Viscoelastic polymer flows and elastic turbulence in three-dimensional porous structures, Soft Matter **12**, 460 (2016).

[242] A. Clarke, A. M. Howe, J. Mitchell, J. Staniland, and L. A. Hawkes, How viscoelastic-polymer flooding enhances displacement efficiency, SPE J. **21**, 0675 (2016).

[243] S. Aramideh, P. P. Vlachos, and A. M. Ardekani, Nanoparticle dispersion in porous media in viscoelastic polymer solutions, J. Non-Newtonian Fluid Mech. **268**, 75 (2019).

[244] S. Parsa, E. Santanach-Carreras, L. Xiao, and D. A. Weitz, Origin of anomalous polymer-induced fluid displacement in porous media, Phys. Rev. Fluids **5**, 022001 (2020).

[245] S. Kenney, K. Poper, G. Chapagain, and G. F. Christopher, Large Deborah number flows around confined microfluidic cylinders, Rheol. Acta **52**, 485 (2013).

[246] X. Shi, S. Kenney, G. Chapagain, and G. F. Christopher, Mechanisms of onset for moderate Mach number instabilities of viscoelastic flows around confined cylinders, Rheol. Acta **54**, 805 (2015).

[247] X. Shi and G. F. Christopher, Growth of viscoelastic instabilities around linear cylinder arrays, Phys. Fluids **28**, 124102 (2016).

[248] D. Kawale, E. Marques, P. L. J. Zitha, M. T. Kreutzer, W. R. Rossen, and P. E. Boukany, Elastic instabilities during the flow of hydrolyzed polyacrylamide solution in porous media: Effect of pore-shape and salt, Soft Matter **13**, 765 (2017).

[249] D. Kawale, G. Bouwman, S. Sachdev, P. L. J. Zitha, M. T. Kreutzer, W. R. Rossen, and P. E. Boukany, Polymer conformation during flow in porous media, Soft Matter **13**, 8745 (2017).

[250] G. Astarita, Objective and generally applicable criteria for flow classification, J. Non-Newton. Fluid **6**, 69 (1979).

[251] D. E. Smith, H. P. Babcock, and S. Chu, Single-polymer dynamics in steady shear flow, Science **283**, 1724 (1999).

[252] G. G. Fuller and L. G. Leal, Flow birefringence of dilute polymer solutions in two-dimensional flows, Rheol. Acta **19**, 580 (1980).

[253] N. Burshtein, S. T. Chan, K. Toda-Peters, A. Q. Shen, and S. J. Haward, 3D-printed glass microfluidics for fluid dynamics and rheology, Curr. Opin. Colloid Interface Sci. **43**, 1 (2019).

[254] R. S. Maier, D. M. Kroll, R. S. Bernard, S. E. Howington, J. F. Peters, and H. T. Davis, Pore-scale simulation of dispersion, Phys. Fluids **12**, 2065 (2000).

[255] S. De, S. P. Koesen, R. V. Maitri, M. Golombok, J. T. Padding, and J. F. M. van Santvoort, Flow of viscoelastic surfactants through porous media, AIChE J. **64**, 773 (2018).

[256] E. Marafini, M. La Rocca, A. Fiori, I. Battiato, and P. Prestininzi, Suitability of 2D modelling to evaluate flow properties in 3D porous media, Transp. Porous Media **134**, 315 (2020).

[257] R. Marshall and A. Metzner, Flow of viscoelastic fluids through porous media, Ind. Eng. Chem. Fundam. **6**, 393 (1967).

[258] D. F. James and D. McLaren, The laminar flow of dilute polymer solutions through porous media, J. Fluid Mech. **70**, 733 (1975).

[259] F. Durst, R. Haas, and B. Kaczmar, Flows of dilute hydrolyzed polyacrylamide solutions in porous media under various solvent conditions, J. Appl. Polym. Sci. **26**, 3125 (1981).

[260] F. Durst and R. Haas, Dehnstromungen mit verdunnten Polymerlosungen: Ein theoretisches Modell und seine experimentelle Verifikations, Rheol. Acta **20**, 179 (1981).

[261] N. Kauser, L. D. Santos, M. Delgado, A. Muller, and A. Saez, Flow of mixtures of poly(ethylene oxide) and hydrolyzed polyacrylamide solutions through porous media, J. Appl. Polym. Sci. **72**, 783 (1999).

[262] C. A. Browne and S. S. Datta, Elastic turbulence generates anomalous flow resistance in porous media, Sci. Adv. **7**, eabj2619 (2021).

[263] P. De Gennes, Molecular individualism, Science **276**, 1999 (1997).

[264] S. De, J. A. M. Kuipers, E. A. J. F. Peters, and J. T. Padding, Viscoelastic flow simulations in random porous media, J. Non-Newtonian Fluid Mech. **248**, 50 (2017).

[265] D. F. do Nascimento, J. R. Vimieiro Junior, S. Paciornik, and M. S. Carvalho, Pore scale visualization of drainage in 3D porous media by confocal microscopy, Sci. Rep. **9**, 12333 (2019).

[266] T. Guo, A. M. Ardekani, and P. P. Vlachos, Microscale, scanning defocusing volumetric particle-tracking velocimetry, Exp. Fluids **60**, 89 (2019).

[267] B. Qin, R. Ran, P. F. Salipante, S. D. Hudson, and P. E. Arratia, Three-dimensional structures and symmetry breaking in viscoelastic cross-channel flow, Soft Matter **16**, 6969 (2020).

[268] S. Berg, H. Ott, S. A. Klapp, A. Schwing, R. Neiteler, N. Brussee, A. Makurat, L. Leu, F. Enzmann, J. O. Schwarz, M. Kersten, S. Irvine, and M. Stampanoni, Real-time 3D imaging of Haines jumps in porous media flow, Proc. Natl. Acad. Sci. USA **110**, 3755 (2013).

[269] T. Pak, I. B. Butler, S. Geiger, M. I. J. Van Dijke, and K. S. Sorbie, Droplet fragmentation: 3D imaging of a previously unidentified pore-scale process during multiphase flow in porous media, Proc. Natl. Acad. Sci. USA **112**, 1947 (2015).

[270] O. Reynolds, An experimental investigation of the circumstances which determine whether the motion of water shall be direct or sinuous and of the law of resistance in parallel channels, Philos. Trans. R. Soc. London A **174**, 935 (1883).

[271] W. Pfenniger, Transition in the inlet length of tubes at high Reynolds numbers, in *Boundary Layer and Flow Control*, edited by G. V. Lachman (Pergamon, New York, 1961), pp. 970–980.

[272] A. Meseguer and L. N. Trefethen, Linearized pipe flow to Reynolds number 10^7, J. Comput. Phys. **186**, 178 (2003).

[273] C. D. Andereck, S. S. Liu, and H. L. Swinney, Flow regimes in a circular Couette system with independently rotating cylinders, J. Fluid Mech. **164**, 155 (1986).

[274] K. Avila, D. Moxey, A. De Lozar, D. Barkley, and B. Hof, The onset of turbulence in pipe flow, Science **333**, 192 (2011).

[275] P. G. Drazin and W. H. Reid, *Hydrodynamic Stability* (Cambridge University Press, Cambridge, 1981).

[276] F. Waleffe, Three-Dimensional Coherent States in Plane Shear Flows, Phys. Rev. Lett. **81**, 4140 (1998).

[277] F. Waleffe, Exact coherent structures in channel flow, J. Fluid Mech. **435**, 93 (2001).

[278] H. Wedin and R. R. Kerswell, Exact coherent structures in pipe flow: Travelling wave solutions, J. Fluid Mech. **508**, 333 (2004).

[279] R. R. Kerswell, Recent progress in understanding the transition to turbulence in a pipe, Nonlinearity **18**, R17 (2005).

[280] D. Barkley, Theoretical perspective on the route to turbulence in a pipe, J. Fluid Mech. **803**, P1 (2016).

[281] N. B. Budanur, K. Y. Short, M. Farazmand, A. P. Willis, and P. Cvitanović, Relative periodic orbits form the backbone of turbulent pipe flow, J. Fluid Mech. **833**, 274 (2017).

[282] B. A. Toms, in *Proceedings of International Congress of Rheology* (North-Holland, Amsterdam, 1949).

[283] B. A. Toms, On the early experiments on drag reduction by polymers, Phys. Fluids **20**, S3 (1977).

[284] E. D. Burger, W. R. Munk, and H. A. Wahl, Flow increase in the trans Alaska pipeline through use of a polymeric drag-reducing additive, J. Petrol. Technol. **34**, 377 (1982).

[285] J. K. Fink, *Petroleum Engineer's Guide to Oil Field Chemicals and Fluids* (Gulf Professional Publishing, 2012).

[286] G. E. King, Hydraulic fracturing 101: What every representative, environmentalist, regulator, reporter, investor, university researcher, neighbor and engineer should know about estimating frac risk and im-

proving frac performance in unconventional gas and oil wells, in *SPE Hydraulic Fracturing Technology Conference* (Society of Petroleum Engineers, The Woodlands, TX, 2012).

[287] K. Kim, C.-F. Li, R. Sureshkumar, S. Balachandar, and R. J. Adrian, Effects of polymer stresses on eddy structures in drag-reduced turbulent channel flow, J. Fluid Mech. **584**, 281 (2007).

[288] C. M. White and M. G. Mungal, Mechanics and prediction of turbulent drag reduction with polymer additives, Annu. Rev. Fluid Mech. **40**, 235 (2008).

[289] P. A. Stone, F. Waleffe, and M. D. Graham, Toward a Structural Understanding of Turbulent Drag Reduction: Nonlinear Coherent States in Viscoelastic Shear Flows, Phys. Rev. Lett. **89**, 208301 (2002).

[290] P. A. Stone, A. Roy, R. G. Larson, F. Waleffe, and M. D. Graham, Polymer drag reduction in exact coherent structures of plane shear flow, Phys. Fluids **16**, 3470 (2004).

[291] W. Li and M. D. Graham, Polymer induced drag reduction in exact coherent structures of plane Poiseuille flow, Phys. Fluids **19**, 083101 (2007).

[292] W. Li, P. A. Stone, and M. D. Graham, Viscoelastic nonlinear traveling waves and drag reduction in plane Poiseuille flow, in Fluid Mechanics and Its Applications: Proceedings of the IUTAM Symposium on Laminar-Turbulent Transition and Finite Amplitude Solutions Vol. 77 (2005), p. 285.

[293] W. Li, L. Xi, and M. D. Graham, Nonlinear travelling waves as a framework for understanding turbulent drag reduction, J. Fluid Mech. **565**, 353 (2006).

[294] P. A. Stone and M. D. Graham, Polymer dynamics in a model of the turbulent buffer layer, Phys. Fluids **15**, 1247 (2003).

[295] A. Roy, A. Morozov, W. van Saarloos, and R. G. Larson, Mechanism of Polymer Drag Reduction Using a Low-Diemensional Model, Phys. Rev. Lett. **97**, 234501 (2006).

[296] D. Samanta, Y. Dubief, M. Holzner, C. Schäfer, A. N. Morozov, C. Wagner and B. Hof, Elasto-inertial turbulence, Proc. Nat. Acad. Sci. USA **110**, 10557 (2013).

[297] J. M. Lopez, G. H. Choueiri, and B. Hof, Dynamics of viscoelastic pipe flow at low Reynolds numbers in the maximum drag reduction limit, J. Fluid Mech. **874**, 699 (2019).

[298] V. E. Terrapon, Y. Dubief, and J. Soria, On the role of pressure in elasto-inertial turbulence, J. Turbul. **16**, 26 (2014).

[299] A. Shekar, R. M. McMullen, S.-N. Wang, B. J. McKeon, and M. D. Graham, Critical-Layer Structures and Mechanisms in Elastoinertial Turbulence, Phys. Rev. Lett. **122**, 124503 (2019).

[300] G. H. Choueiri, J. M. Lopez, and B. Hof, Exceeding the Asymptotic Limit of Polymer Drag Reduction, Phys. Rev. Lett. **120**, 124501 (2018).

[301] S. J. Haward, J. Page, T. A. Zaki, and A. Q. Shen, Inertioelastic Poiseuille flow over a wavy surface, Phys. Rev. Fluids **3**, 091302(R) (2018).

[302] J. Page and T. A. Zaki, Viscoelastic shear flow over a wavy surface, J. Fluid Mech. **801**, 392 (2016).

[303] S. J. Haward, J. Page, T. A. Zaki and A. Q. Shen, "Phase diagram" for viscoelastic Poiseuille flow over a wavy surface, Phys. Fluids **30**, 113101 (2018).

[304] A. Shekar, R. M. McMullen, B. J. McKeon, and M. D. Graham, Self-sustained elastoinertial Tollmien–Schlichting waves, J. Fluid Mech. **897**, A3 (2020).

[305] A. Shekar, R. M. McMullen, B. J. McKeon, and M. D. Graham, Tollmien-Schlichting route to elastoinertial turbulence in channel flow, Phys. Rev. Fluids **6**, 093301 (2021).

[306] A. Pereira, R. L. Thompson, and G. Mompean, Beyond the maximum drag reduction asymptote: The pseudo-laminar state, arXiv:1911.00439.

[307] P. G. Drazin and W. H. Reid, *Hydrodynamic Stability* (Cambridge University Press, Cambridge, 1981).

[308] M. Zhang, Energy growth in subcritical viscoelastic pipe flows, J. Non-Newton. Fluid Mech. **294**, 104581 (2021).

[309] M. Khalid, I. Chaudhary, P. Garg, V. Shankar, and G. Subramanian, The centre-mode instability of viscoelastic plane Poiseuille flow, J. Fluid Mech. **915**, A43 (2021).

[310] G. H. Choueiri, J. M. Lopez, A. Varshney, S. Sankar, and B. Hof, Experimental observation of the origin and structure of elasto-inertial turbulence, Proc National Acad Sci **118**, e2102350118 (2021).

[311] L. Xi and M. D. Graham, Dynamics on the Laminar-Turbulent Boundary and the Origin of the Maximum Drag Reduction Asymptote, Phys. Rev. Lett. **108**, 028301 (2012).

[312] I. Chaudhary, P. Garg, V. Shankar, and G. Subramanian, Elasto-inertial wall mode instabilities in viscoelastic plane Poiseuille flow, J. Fluid Mech. **881**, 119 (2019).

[313] S. Sid and V. E. Terrapon, and Y. Dubief, Two-dimensional dynamics of elasto-inertial turbulence and its role in polymer drag reduction, Phys. Rev. Fluids **3**, 011301(R) (2018).

[314] A. Shekar, Structures and Mechanisms in Elastoinertial Turbulence. Ph.D. thesis, University of Wisconsin–Madison (2021).

[315] H. J. Wilson, M. Renardy, and Y. Renardy, Structure of the spectrum in zero Reynolds number shear flow of the UCM and Oldroyd-B liquids, J. Non-Newtonian Fluid Mech. **80**, 251 (1999).

[316] M. Zhang, I. Lashgari, T. A. Zaki, and L. Brandt, Linear stability analysis of channel flow of viscoelastic Oldroyd-B and FENE-P fluids, J. Fluid Mech. **737**, 249 (2013).

[317] F. Snijkers and D. Vlassopoulos, Cone-partitioned-plate geometry for the ARES rheometer with temperature control, J. Rheol. **55**, 1167 (2011).

[318] E. A. Jensen and J. de C. Christiansen, Measurements of first and second normal stress differences in a polymer melt, J. Non-Newtonian Fluid Mech. **148**, 41 (2008).

[319] C.-S. Lee, B. C. Tripp, and J. J. Magda, Does N_1 or N_2 control the onset of edge fracture? Rheol. Acta **31**, 306 (1992).

[320] Y. W. Inn, K. F. Wissbrun, and M. M. Denn, Effect of edge fracture on constant torque rheometry of entangled polymer solutions, Macromolecules **38**, 9385 (2005).

[321] C. Sui and G. B. McKenna, Instability of entangled polymers in cone and plate rheometry, Rheol. Acta **46**, 877 (2007).

[322] T. Schweizer and M. Stöckli, Departure from linear velocity profile at the surface of polystyrene melts during shear in cone-plate geometry, J. Rheol. **52**, 713 (2008).

[323] K. M. Mattes, R. Vogt, and C. Friedrich, Analysis of the edge fracture process in oscillation for polystyrene melts, Rheol. Acta **47**, 929 (2008).

[324] S.-C. Dai, E. Bertevas, F. Qi, and R. I. Tanner, Viscometric functions for noncolloidal sphere suspensions with Newtonian matrices, J. Rheol. **57**, 493 (2013).

[325] S. E. Mall-Gleissle, W. Gleissle, G. H. McKinley, and H. Buggisch, The normal stress behaviour of suspensions with viscoelastic matrix fluids, Rheol. Acta **41**, 61 (2002).

[326] Th. Schweizer, Comparing cone-partitioned plate and cone-standard plate shear rheometry of a polystyrene melt, J. Rheol. **47**, 1071 (2003).

[327] T. Schweizer, J. van Meerveld, and H. Christian Öttinger, Nonlinear shear rheology of polystyrene melt with narrow molecular weight distribution—Experiment and theory, J. Rheol. **48**, 1345 (2004).

[328] J. Meissner, R. W. Garbella, and J. Hostettler, Measuring normal stress differences in polymer melt shear flow, J. Rheol. **33**, 843 (1989).

[329] T. Schweizer and W. Schmidheiny, A cone-partitioned plate rheometer cell with three partitions (CPP3) to determine shear stress and both normal stress differences for small quantities of polymeric fluids, J. Rheol. **57**, 841 (2013).

[330] S. Costanzo, G. Ianniruberto, G. Marrucci, and D. Vlassopoulos, Measuring and assessing first and second normal stress differences of polymeric fluids with a modular cone-partitioned plate geometry, Rheol. Acta **57**, 363 (2018).

[331] R. I. Tanner and M. Keentok, Shear fracture in cone-plate rheometry, J. Rheol. **27**, 47 (1983).

[332] M. Keentok and S.-C. Xue, Edge fracture in cone-plate and parallel plate flows, Rheol. Acta **38**, 321 (1999).

[333] E. J. Hemingway, H. Kusumaatmaja, and S. M. Fielding, Edge Fracture in Complex Fluids, Phys. Rev. Lett. **119**, 028006 (2017).

[334] E. J. Hemingway and S. M. Fielding, Edge fracture instability in sheared complex fluids: Onset criterion and possible mitigation strategy, J. Rheol. **63**, 735 (2019).

[335] E. J. Hemingway and S. M. Fielding, Edge-Induced Shear Banding in Entangled Polymeric Fluids, Phys. Rev. Lett. **120**, 138002 (2018).

[336] E. J. Hemingway and S. M. Fielding, Interplay of edge fracture and shear banding in complex fluids, J. Rheol. **64**, 1147 (2020).

[337] J. L. Goveas and P. D. Olmsted, A minimal model for vorticity and gradient banding in complex fluids, Eur. Phys. J. E **6**, 79 (2001).

[338] E. J. Hinch, O. J. Harris, and J. M. Rallison, The instability mechanism for two elastic liquids being co-extruded, J. Non-Newtonian Fluid Mech. **43**, 311 (1992).

[339] H. J. Wilson and J. M. Rallison, Short wave instability of co-extruded elastic liquids with matched viscosities, J. Non-Newtonian Fluid Mech. **72**, 237 (1997).

[340] P. Nghe, S. M. Fielding, P. Tabeling, and A. Ajdari, Interfacially Driven Instability in the Microchannel Flow of a Shear-Banding Fluid, Phys. Rev. Lett. **104**, 248303 (2010).

[341] S. Skorski and P. D. Olmsted, Loss of solutions in shear banding fluids driven by second normal stress differences, J. Rheol. **55**, 1219 (2011).

[342] Y. Li and G. B. McKenna, Startup shear of a highly entangled polystyrene solution deep into the nonlinear viscoelastic regime, Rheol. Acta **54**, 771 (2015).

[343] Y. Li, M. Hu, G. B. McKenna, C. J. Dimitriou, G. H. McKinley, R. M. Mick, D. C. Venerus, and L. A. Archer, Flow field visualization of entangled polybutadiene solutions under nonlinear viscoelastic flow conditions, J. Rheol. **57**, 1411 (2013).

[344] S.-Q. Wang, G. Liu, S. Cheng, P. E. Boukany, Y. Wang, and X. Li, Letter to the editor: Sufficiently entangled polymers do show shear strain localization at high enough Weissenberg numbers, J. Rheol. **58**, 1059 (2014).

[345] Y. Li, M. Hu, G. B. McKenna, C. J. Dimitriou, G. H. McKinley, R. M. Mick, D. C. Venerus, and L. A. Archer, Response to: Sufficiently entangled polymers do show shear strain localization at high enough Weissenberg numbers, J. Rheol. **58**, 1071 (2014).

[346] P. E. Boukany, S.-Q. Wang, S. Ravindranath, and L. J. Lee, Shear banding in entangled polymers in the micron scale gap: A confocal-rheoscopic study, Soft Matter **11**, 8058 (2015).

[347] M. M. Denn and J. F. Morris, Rheology of non-Brownian suspensions, Annu. Rev. Chem. Biomol. Eng. **5**, 203 (2014).

[348] G. H. McKinley and T. Sridhar, Filament-stretching rheometry of complex fluids, Annu. Rev. Fluid Mech. **34**, 375 (2002).

[349] T. Sridhar, V. Tirtaatmadja, D. A. Nguyen, R. K. Gupta, Measurement of extensional viscosity of polymer solutions, J. Non-Newtonian Fluid Mech. **40**, 271 (1991).

[350] H. Münstedt, Viscoelasticity of polystyrene melts in tensile creep experiments, Rheol. Acta **14**, 1077 (1975).

[351] H. Münstedt and Z. Starý, Steady states in extensional flow of strain hardening polymer melts and the uncertainties of their determination, J. Rheol. **57**, 1065 (2013).

[352] H. Münstedt, Rheological experiments at constant stress as efficient method to characterize polymeric materials, J. Rheol. **58**, 565 (2014).

[353] N. J. Alvarez, J. Marín, Q. Huang, M. Michelsen, and O. Hassager, Creep Measurements Confirm Steady Flow after Stress Maximum in Extension of Branched Polymer Melts, Phys. Rev. Lett. **110**, 168301 (2013).

[354] M. H. Wagner, H. Bastian, A. Bernnat, S. Kurzbeck, and C. K. Chai, Determination of elongational viscosity of polymer melts by RME and Rheotens experiments, Rheol. Acta **41**, 316 (2002).

[355] P. Szabo, G. H. McKinley, and C. Clasen, Constant force extensional rheometry of polymer solutions, J. Non-Newtonian Fluid Mech. **169–170**, 26 (2012).

[356] V. C. Barroso and J. M. Maia, Influence of long-chain branching on the rheological behavior of polyethylene in shear and extensional flow, Polym. Eng. Sci. **45**, 984 (2005).

[357] G. Liu, H. Ma, H. Lee, H. Xu, S. Cheng, H. Sun, T. Chang, R. P. Quirk, and S.-Q. Wang, Long-chain branched polymers to prolong homogeneous stretching and to resist melt breakup, Polymer **54**, 6608 (2013).

[358] T. I. Burghelea, Z. Starý, and H. Münstedt, On the viscosity overshoot during the uniaxial extension of a low density polyethylene, J. Non-Newtonian Fluid Mech. **166**, 1198 (2011).

[359] A. Tripathi, K. C. Tam, and G. H. McKinley, Rheology and Dynamics of Associative Polymer Solutions in Shear and Extension: Theory and Experiments, Macromolecules **39**, 1981 (2006).

[360] A. Bhardwaj, E. Miller, and J. P. Rothstein, Filament stretching and capillary breakup extensional

rheometry measurements of viscoelastic wormlike micelle solutions, Journal of Rheology **51**, 693 (2007).

[361] M. Arciniaga, C.-C. Kuo, and M. Dennin, Size dependent brittle to ductile transition in bubble rafts, Colloids Surf. A **382**, 36 (2011).

[362] M. I. Smith, R. Besseling, M. E. Cates, and V. Bertola, Dilatancy in the flow and fracture of stretched colloidal suspensions, Nat. Commun. **1**, 114 (2010).

[363] R. J. Andrade and J. M. Maia, A study on the flow, failure, and rupture mechanisms of low-density polyethylene in controlled-stress uniaxial extensional flow, J. Rheol. **55**, 925 (2011).

[364] A. Ya. Malkin, A. Arinstein, and V. G. Kulichikhin, Polymer extension flows and instabilities, Prog. Polym. Sci. **39**, 959 (2014).

[365] Y. Wang, P. Boukany, S.-Q. Wang, and X. Wang, Elastic Breakup in Uniaxial Extension of Entangled Polymer Melts, Phys. Rev. Lett. **99**, 237801 (2007).

[366] S. M. Fielding, Criterion for Extensional Necking Instability in Polymeric Fluids, Phys. Rev. Lett. **107**, 258301 (2011).

[367] D. M. Hoyle and S. M. Fielding, Age-Dependent Modes of Extensional Necking Instability in Soft Glassy Materials, Phys. Rev. Lett. **114**, 158301 (2015).

[368] D. M. Hoyle and S. M. Fielding, Criteria for extensional necking in complex fluids: Strain-imposed protocols, J. Rheol. **60**, 1347 (2016).

[369] D. M. Hoyle and S. M. Fielding, Criteria for extensional necking in complex fluids: Stress- and force-imposed protocols, J. Rheol. **60**, 1377 (2016).

[370] D. M. Hoyle and S. M. Fielding, Necking after extensional filament stretching of complex fluids and soft solids, J. Non-Newtonian Fluid Mech. **247**, 132 (2017).

[371] R. Larson, *Constitutive Equations for Polymer Melts and Solutions* (Butterworth Publishers, Stoneham, MA, 1988).

[372] A. E. Likhtman and R. S. Graham, Simple constitutive equation for linear polymer melts derived from molecular theory: Rolie-poly equation, J. Non-Newtonian Fluid Mech. **114**, 1 (2003).

[373] T. C. B. McLeish and R. G. Larson, Molecular constitutive equations for a class of branched polymers: The pom-pom polymer, J. Rheol. **42**, 81 (1998).

[374] G. H. McKinley, Visco-elasto-capillary thinning and break-up of complex fluids, in *Rheology Reviews* (British Society of Rheology, Aberystwyth, 2005), pp. 1–49.

[375] A. V. Bazilevskii, S. I. Voronkov, V. M. Entov, and A. N. Rozhkov, Orientational effects in the decomposition of streams and strands of diluted polymer solutions, Sov. Phys. Dokl. **26**, 333 (1981).

[376] J. Eggers, Nonlinear dynamics and breakup of free-surface flows, Rev. Mod. Phys. **69**, 865 (1997).

[377] J. Li and M. A. Fontelos, Drop dynamics on the beads-on-string structure of viscoelastic jets: A numerical study, Phys. Fluids **15**, 922 (2003).

[378] C. Wagner, Y. Amarouchene, D. Bonn, and J. Eggers, Droplet Detachment and Satellite Bead Formation in Visco-Elastic Fluids, Phys. Rev. Lett. **95**, 164504 (2005).

[379] R. B. Bird, R. C. Armstrong, and O. Hassager, *Dynamics of Polymeric Liquids, Volume I: Fluid Mechanics; Volume II: Kinetic Theory* (Wiley, New York, 1987).

[380] A. V. Bazilevskii, V. M. Entov, and A. N. Rozhkov, Liquid filament microrheometer and some of its applications, in *Proceedings of the Third European Rheology Conference*, edited by D. R. Oliver (Elsevier Applied Science, New York, 1990), p. 41.

[381] M. Doi and S. F. Edwards, *The Theory of Polymer Dynamics* (Clarendon Press, Oxford, 1986).

[382] V. M. Entov and E. J. Hinch, Effect of a spectrum of relaxation times on the capillary thinning of a filament of elastic liquids, J. Non-Newtonian Fluid Mech. **72**, 31 (1997).

[383] S. L. Anna and G. H. McKinley, Elasto-capillary thinning and breakup of model elastic liquids, J. Rheol. **45**, 115 (2001).

[384] C. Clasen, J. P. Plog, W. M. Kulicke, M. Owens, C. Macisko, L. E. Seriven, V. Verani, and G. H. McKinley, How dilute are dilute solutions in extensional flows? J. Rheol. **50**, 849 (2006).

[385] A. Deblais, K. P. Velikov, and D. Bonn, Pearling Instabilities of a Viscoelastic Thread, Phys. Rev. Lett. **120**, 194501 (2018).

[386] A. Deblais, M. A. Herrada, J. Eggers, and D. Bonn, Self-similarity in the breakup of very dilute viscoelastic solutions, J. Fluid Mech. **904**, R2 (2020).

[387] C. Clasen, J. Eggers, M. A. Fontelos, J. Li, and G. H. McKinley, The beads-on-string structure of viscoelastic jets, J. Fluid Mech. **556**, 283 (2006).

[388] J. Eggers, M. A. Herrada, and J. H. Snoeijer, Self-similar breakup of polymeric threads as described by the Oldroyd-B model, J. Fluid Mech. **887**, A19 (2020).

[389] J. Dinic and V. Sharma, Macromolecular relaxation, strain, and extensibility determine elastocapillary thinning and extensional viscosity of polymer solutions, Proc. Natl. Acad. Sci. USA **116**, 8766 (2019).

[390] J. Dinic and V. Sharma, Flexibility, extensibility, and ratio of Kuhn length to packing length govern the pinching dynamics, coil-stretch transition, and rheology of polymer solutions, Macromolecules **53**, 4821 (2020).

[391] M. Renardy, Similarity solutions for jet break-up for various models of viscoelastic fluids, J. Non-Newtonian Fluid Mech. **104**, 65 (2002).

[392] M. A. Fontelos and J. Li, On the evolution and rupture of filaments in Giesekus and FENE models, J. Non-Newtonian Fluid Mech. **118**, 1 (2004).

[393] J. Eggers and E. Villermaux, Physics of liquid jets, Rep. Prog. Phys. **71**, 036601 (2008).

[394] M. S. N. Oliveira and G. H. McKinley, Iterated stretching and multiple beads-on-a-string phenomena in dilute solutions of high extensible flexible polymers, Phys. Fluids **17**, 071704 (2005).

[395] H.-C. Chang, E. A. Demekhin, and E. Kalaidin, Iterated stretching of viscoelastic jets, Phys. Fluids **11**, 1717 (1999).

[396] R. Sattler, C. Wagner, and J. Eggers, Blistering Pattern and Formation of Nanofibers in Capillary Thinning of Polymer Solutions, Phys. Rev. Lett. **100**, 164502 (2008).

[397] R. Sattler, S. Gier, J. Eggers, and C. Wagner, The final stages of capillary break-up of polymer solutions, Phys. Fluids **24**, 023101 (2012).

[398] J. Eggers, Instability of a polymeric thread, Phys. Fluids **26**, 033106 (2014).

[399] E. Helfand and G. H. Fredrickson, Large Fluctuations in Polymer Solutions under Shear, Phys. Rev. Lett. **62**, 2468 (1989).

[400] M. Cromer, M. C. Villet, G. H. Fredrickson, and L. G. Leal, Shear banding in polymer solutions, Phys. Fluids **25**, 051703 (2013).

[401] A. N. Beris and V. G. Mavrantzas, On the compatibility between various macroscopic formalisms for the concentration and flow of dilute polymer solutions, J. Rheol. **38**, 1235 (1994).

[402] S. Ya. Frenkel', V. G. Baranov, N. G. Belanikevich, and Yu. N. Panov, Orientation mechanism of solid phase formation in polymer solutions subjected to a longitudinal hydrodynamic field, Polym. Sci. USSR **6**, 2124 (1964).

[403] A. V. Semakov, V. G. Kulichikhin, A. K. Tereshin, S. V. Antonov, and A. Ya. Malkin, On the nature of phase separation of polymer solutions at high extension rates, J. Polym. Sci. B **53**, 559 (2015).

[404] N. J. Balmforth, I. A. Frigaard, and G. Ovarlez, Yielding to stress: Recent developments in viscoplastic fluid mechanics, Annu. Rev. Fluid Mech. **46**, 121 (2014).

[405] G. Ovarlez and S. Hormozi, *Lectures on Visco-Plastic Fluid Mechanics*, edited by G. Ovarlez and S. Hormozi, CISM International Centre for Mechanical Sciences (Springer, Cham, 2019).

[406] Y. Holenberg, O. M. Lavrenteva, U. Shavit, and A. Nir, Particle tracking velocimetry and particle image velocimetry study of the slow motion of rough and smooth solid spheres in a yield-stress fluid, Phys. Rev. E **86**, 066301 (2012).

[407] F. Ahonguio, L. Jossic, and A. Magnin, Influence of surface properties on the flow of a yield stress fluid around spheres, J. Non-Newtonian Fluid Mech. **206**, 57 (2014).

[408] M. Firouznia, B. Metzger, G. Ovarlez, and S. Hormozi, The interaction of two spherical particles in simple-shear flows of yield stress fluids, J. Non-Newtonian Fluid Mech. **255**, 19 (2018).

[409] D. Fraggedakis, Y. Dimakopoulos, and J. Tsamopoulos, Yielding the yield-stress analysis: A study focused on the effects of elasticity on the settling of a single spherical particle in simple yield-stress fluids, Soft Matter **12**, 5378 (2016).

[410] M. Sarabian, M. Rosti, L. Brandt, and S. Hormozi, Numerical simulations of a sphere settling in simple shear flows of yield stress fluids, J. Fluid Mech. **896**, A17-1 (2020).

[411] C. J. Dimitriou, R. H. Ewoldt and G. H. McKinley, Describing and prescribing the constitutive response of yield stress fluids using large amplitude oscillatory shear stress (LAOStress), J. Rheol. **57**, 27 (2013).

[412] C. J. Dimitriou and G. H. McKinley, A comprehensive constitutive law for waxy crude oil: A thixotropic yield stress fluid, Soft Matter **10**, 6619 (2014).

[413] C. Nouar *et al.*, Modal and non-modal linear stability of the plane Bingham-Poiseuille flow, J. Fluid Mech. **577**, 211 (2007).

[414] C. Metivier, C. Nouar, and J. P. Brancher, Linear stability involving the Bingham model when the yield stress approaches zero, Phys. Fluids **17**, 104106 (2005).

[415] S. Hormozi and I. A. Frigaard, Nonlinear stability of a visco-plastically lubricated viscoelastic fluid flow, J. Non-Newtonian Fluid Mech. **169-170**, 61 (2012).

[416] C. Metivier, C. Nouar and J. P. Brancher, Weakly nonlinear dynamics of thermoconvective instability involving viscoplastic fluids, J. Fluid Mech. **660**, 316 (2010).

[417] M. A. Moyers-Gonzalez *et al.*, Transient effects in oilfield cementing flows: Qualitative behaviour, Eur. J. Appl. Math. **18**, 477 (2007).

[418] C. Nouar and I. A. Frigaard, Nonlinear stability of Poiseuille flow of a Bingham fluid: Theoretical results and comparison with phenomenological criteria, J. Non-Newtonian Fluid Mech. **100**, 127 (2001).

[419] J. P. Rothstein and H. Mohammadigoushki, Complex flows of viscoelastic wormlike micelle solutions, J. Non-Newtonian Fluid Mech. **285**, 104382 (2020).

[420] C. A. Dreiss, Wormlike micelles: Where do we stand? Recent developments, linear rheology and scattering techniques, Soft Matter **3**, 956 (2007).

[421] J. Yang, Viscoelastic wormlike micelles and their applications, Curr. Opin. Colloid Interface Sci. **7**, 276 (2002).

[422] P. D. Olmsted, Perspectives on shear banding in complex fluids, Rheol. Acta **47**, 283 (2008).

[423] M.-A. Fardin and S. Lerouge, Flows of living polymer fluids, Soft Matter **10**, 8789 (2014).

[424] N. Kumar, S. Majumdar, A. Sood, R. Govindarajan, S. Ramaswamy, and A. K. Sood, Oscillatory settling in wormlike-micelle solutions: Bursts and a long time scale, Soft Matter **8**, 4310 (2012).

[425] M. Kostrzewa, A. Delgado, and A. Wierschem, Particle settling in micellar solutions of varying concentration and salt content, Acta Mech. **227**, 677 (2016).

[426] S. Wu and H. Mohammadigoushki, Sphere sedimentation in wormlike micelles: Effect of micellar relaxation spectrum and gradients in micellar extensions, J. Rheol. **62**, 1061 (2018).

[427] H. Mohammadigoushki and S. J. Muller, Creeping flow of a wormlike micelle solution past a falling sphere: Role of boundary conditions, J. Non-Newtonian Fluid Mech. **257**, 44 (2018).

[428] Y. Zhang and S. J. Muller, Unsteady sedimentation of a sphere in wormlike micellar fluids, Phys. Rev. Fluids **3**, 043301 (2018).

[429] Z. Wang, S. Wang, L. Xu, Y. Dou, and X. Su, Extremely slow settling behavior of particles in dilute wormlike micellar fluid with broad spectrum of relaxation times, J. Disp. Sci. Tech. **41**, 639 (2020).

[430] C. Sasmal, Unsteady motion past a sphere translating steadily in wormlike micellar solutions: A numerical analysis, J. Fluid Mech. **912**, A52 (2021).

[431] P. A. Vasquez, G. H. McKinley, and L. P. Cook, A network scission model for wormlike micellar solutions I. Model formulation and viscometric flow predictions, J. Non-Newtonian Fluid Mech. **144**, 122 (2007).

[432] C. J. Pipe, N. J. Kim, P. A. Vasquez, L. P. Cook, and G. H. McKinley, Wormlike micellar solutions: II. Comparison between experimental data and scission model predictions, J. Rheol. **54**, 881 (2010).

[433] L. Zhou, G. H. McKinley, and L. P. Cook, Wormlike micellar solutions: III. VCM model predictions in steady and transient shearing flows, J. Non-Newtonian Fluid Mech. **211**, 70 (2014).

[434] J. E. López-Aguilar, M. F. Webster, H. R. Tamaddon-Jahromi, and O. Manero, Predictions for circular contraction-expansion flows with viscoelastoplastic & thixotropic fluids, J. Non-Newtonian Fluid Mech. **261**, 188 (2018).

[435] J. Gladden and A. Belmonte, Motion of a Viscoelastic Micellar Fluid Around a Cylinder: Flow and Fracture, Phys. Rev. Lett. **98**, 224501 (2007).

[436] G. R. Moss and J. P. Rothstein, Flow of wormlike micelle solutions past a confined circular cylinder, J. Non-Newtonian Fluid Mech. **165**, 1505 (2010).

[437] M. B. Khan and C. Sasmal, Effect of chain scission on flow characteristics of wormlike micellar solutions past a confined microfluidic cylinder: A numerical, Soft Matter **16**, 5261 (2020).

[438] T. Hashimoto, K. Kido, S. Kaki, T. Yamamoto, and N. Mori, Effects of surfactant and salt concentrations on capillary flow and its entry flow for wormlike micelle solutions, Rheol. Acta **45**, 841 (2006).

[439] V. Lutz-Bueno, J. Kohlbrecher, and P. Fischer, Micellar solutions in contraction slit-flow: Alignment mapped by SANS, J. Non-Newtonian Fluid Mech. **215**, 8 (2015).

[440] P. F. Salipante, S. E. Meek, and S. D. Hudson, Flow fluctuations in wormlike micelle fluids, Soft Matter **14**, 9020 (2018).

[441] R. M. Matos, M. A. Alves, and F. T. Pinho, Instabilities in micro-contraction flows of semi-dilute CTAB and CPyCl solutions: Rheology and flow instabilities, Exp. Fluids **60**, 145 (2019).

[442] C. Sasmal, Flow of wormlike micellar solutions through a long micropore with step expansion and contraction, Phys. Fluids **32**, 013103 (2020).

[443] J. E. López-Aguilar, M. F. Webster, H. R. Tamaddon-Jahromi, and O. Manero, A new constitutive model for worm-like micellar systems—Numerical simulation of confined contraction-expansion flows, J. Non-Newtonian Fluid Mech. **204**, 7 (2014).

[444] J. E. López-Aguilar, M. F. Webster, H. R. Tamaddon-Jahromi, and O. Manero, High-Weissenberg predictions for micellar fluids in contraction-expansion flows, J. Non-Newtonian Fluid Mech. **222**, 190 (2015).

[445] J. E. López-Aguilar, M. F. Webster, H. R. Tamaddon-Jahromi, and O. Manero, Numerical modelling of thixotropic and viscoelastoplastic materials in complex flows, Rheol. Acta **54**, 307 (2015).

[446] S. Tabatabaei, J. E. López-Aguilar, H. R. Tamaddon-Jahromi, M. F. Webster, and R. Williams, Modified Bautista-Manero (MBM) modelling for hyperbolic contraction-expansion flows, Rheol. Acta **54**, 869 (2015).

[447] J. E. López-Aguilar, M. F. Webster, H. R. Tamaddon-Jahromi, and O. Manero, Convoluted models and high-Weissenberg predictions for micellar thixotropic fluids in contraction-expansion flows, J. Non-Newtonian Fluid Mech. **232**, 55 (2016).

[448] J. E. López-Aguilar, M. F. Webster, H. R. Tamaddon-Jahromi, and O. Manero, A comparative numerical study of time-dependent structured fluids in complex flows, Rheol. Acta **55**, 197 (2016).

[449] J. A. Pathak and S. D. Hudson, Rheo-optics of equilibrium polymer solutions: Wormlike micelles in elongational flow in a microfluidic cross-slot, Macromolecules **39**, 8782 (2006).

[450] N. Dubash, P. Cheung, and A. Q. Shen, Elastic instabilities in a microfluidic cross-slot flow of wormlike micellar solutions, Soft Matter **8**, 5847 (2012).

[451] A. Kalb, L. A. Villasmil-Urdaneta, and M. Cromer, Role of chain scission in cross-slot flow of wormlike micellar solutions, Phys. Rev. Fluids **2**, 071301(R) (2017).

[452] A. Kalb, L. A. Villasmil-Urdaneta, and M. Cromer, Elastic instability and secondary flow in cross-slot flow of wormlike micellar solutions, J. Non-Newtonian Fluid Mech. **262**, 79 (2018).

[453] J. P. Rothstein, Transient extensional rheology of wormlike micelle solutions,, J. Rheol. **47**, 1227 (2003).

[454] E. Miller, C. Clasen, and J. P. Rothstein, The effect of step-stretch parameters on capillary breakup extensional rheology (CaBER) measurements, Rheol. Acta **48**, 625 (2009).

[455] B. Yesilata, C. Clasen, and G. H. McKinley, Nonlinear shear and extensional flow dynamics of wormlike surfactant solutions, J. Non-Newtonian Fluid Mech. **133**, 73 (2006).

[456] N. J. Kim, C. J. Pipe, K. H. Ahn, S. J. Lee, and G. H. McKinley, Capillary breakup extensional rheometry of a wormlike micellar solution, Korea-Australia Rheol. J. **22**, 31 (2010).

[457] D. Sachsenheimer, C. Oelschlaeger, S. Müller, J. Küstner, S. Bindgen, and N. Willenbacher, Elongational deformation of wormlike micellar solutions, J. Rheol. **58**, 2017 (2017).

[458] R. Omidvar, A. Dalili, A. Mir, and H. Mohammadigoushki, Exploring sensitivity of the extensional flow to wormlike micellar structure, J. Non-Newtonian Fluid Mech. **252**, 48 (2018).

[459] R. Omidvar, S. Wu, and H. Mohammadigoushki, Detecting wormlike micellar microstructure using extensional rheology, J. Rheol. **63**, 33 (2019).

[460] M. Cromer, L. P. Cook, and G. H. McKinley, Extensional flow of wormlike micellar solutions, Chem. Eng. Sci. **64**, 4588 (2009).

[461] A. A. Dey, Y. Modarres-Sadeghi, and J. P. Rothstein, Viscoelastic flow-induced oscillations of a

cantilevered beam in the crossflow of a wormlike micelle solution, J. Non-Newtonian Fluid Mech. **286**, 104433 (2020).

[462] S. Lerouge and J. F. Berret, Shear-induced transitions and instabilities in surfactant wormlike micelles, in K. Dusek, J. F. Joanny (eds.) Adv. Polym. Sci.: Polym. Charact. **230**, 1 (2009).

[463] S. Lerouge, M. Argentina, and J. P. Decruppe, Interface Instability in Shear-Banding Flow, Phys. Rev. Lett. **96**, 088301 (2006).

[464] S. Lerouge, M. A. Fardin, M. Argentina, G. Grégoire, and O. Cardoso, Interface dynamics in shear-banding flow of giant micelles, Soft Matter **4**, 1808 (2008).

[465] M. A. Fardin, B. Lasne, O. Cardoso, G. Grégoire, M. Argentina, J. P. Decruppe, and S. Lerouge, Taylor-Like Vortices in Shear-Banding Flow of Giant Micelles, Phys. Rev. Lett. **103**, 028302 (2009).

[466] M. A. Fardin, D. Lopez, J. Croso, G. Grégoire, O. Cardoso, G. H. McKinley, and S. Lerouge, Elastic Turbulence in Shear Banding Wormlike Micelles, Phys. Rev. Lett. **104**, 178303 (2010).

[467] S. Fielding, Viscoelastic Taylor-Couette Instability of Shear Banded Flow, Phys. Rev. Lett. **104**, 198303 (2010).

[468] A. Nicolas and A. Morozov, Nonaxisymmetric Instability of Shear-Banded Taylor-Couette Flow, Phys. Rev. Lett. **108**, 088302 (2012).

[469] M. A. Fardin, T. J. Ober, C. Gay, G. Grégoire, G. H. McKinley, and S. Lerouge, Criterion for purely elastic Taylor-Couette instability in the flows of shear-banding fluids, Europhys. Lett. **96**, 44004 (2011).

[470] M. A. Fardin, T. J. Ober, V. Grenard, T. Divoux, S. Manneville, G. H. McKinley, and S. Lerouge, Interplay between elastic instabilities and shear-banding: Three categories of Taylor-Couette flows and beyond, Soft Matter **8**, 10072 (2012).

[471] M. A. Fardin, C. Perge, N. Taberlet, and S. Manneville, Flow-induced structures versus flow instabilities, Phys. Rev. E **89**, 011001(R) (2014).

[472] C. Perge, M. A. Fardin, and S. Manneville, Inertio-elastic instability of non shear-banding wormlike micelles, Soft Matter **10**, 1450 (2013).

[473] M. A. Fardin, L. Casanellas, B. Saint-Michel, S. Manneville, and S. Lerouge, Shear-banding in wormlike micelles: Beware of elastic instabilities, J. Rheol. **60**, 917 (2016).

[474] M. S. Turner and M. E. Cates, Flow-induced phase transitions in rod-like micelles, J. Phys.: Condens. Matter **4**, 3719 (1992).

[475] S. Dutta and M. D. Graham, Mechanistic constitutive model for wormlike micelle solutions with flow-induced structure formation, J. Non-Newtonian Fluid Mech. **251**, 97 (2018).

[476] R. J. Hommel and M. D. Graham, Constitutive modeling of dilute wormlike micelle solutions: Shear-induced structure and transient dynamics, J. Non-Newtonian Fluid Mech. **295**, 104606 (2021).

[477] J. E. López-Aguilar, M. F. Webster, H. R. Tamaddon-Jahromi, and O. Manero, On shear-banding and wormlike micellar system response under complex flow, Ann. Trans. Nord. Soc. Rheol. **25**, 197 (2017).

[478] F. Bautista, J. H. Pérez-López, J. P. García, J. E. Puig, and O. Manero, Stability analysis of shear banding flow with the BMP model, J. Non-Newton. Fluid Mech. **144**, 160 (2007).

[479] J. P. García-Sandoval, O. Manero, F. Bautista, and J. E. Puig, Inhomogeneous flows and shear banding formation in micellar solutions: Predictions of the BMP model, J. Non-Newton. Fluid Mech. **179–180**, 43 (2012).

[480] S. Hooshyar and N. Germann, Shear banding of semidilute polymer solutions in pressure-driven channel flow, J. Non-Newton. Fluid Mech. **242**, 1 (2017).

[481] S. Hooshyar and N. Germann, Shear banding in 4:1 planar contraction, Polymers **11**, 417 (2019).

[482] P. D. Olmsted, O. Radulescu, and C. Y. F. Lu, Johnson-Segalman model with a diffusion term in a cylindrical Couette flow, J. Rheol. **44**, 257 (2000).

[483] A. K. Gurnon and N. J. Wagner, Large amplitude oscillatory shear (LAOS) measurements to obtain constitutive equation model parameters: Giesekus model of banding and nonbanding wormlike micelles, J. Rheol. **56**, 333 (2012).

[484] N. Germann, A. K. Gurnon, L. Zhou, L. P. Cook, A. N. Beris, and N. J. Wagner, Validation of constitutive modeling of shear banding, threadlike wormlike micellar fluids, J. Rheol. **60**, 983 (2016).

[485] R. Radhakrishnan, T. Divoux, S. Manneville, and S. M. Fielding, Understanding rheological hysteresis in soft glassy materials, Soft Matter **13**, 1834 (2017).

[486] R. Radhakrishnan and S. M. Fielding, Shear banding in large amplitude oscillatory shear (LAOStrain and LAOStress) of soft glassy materials, J. Rheol. **62**, 559 (2018)\.

[487] M. F. Webster, H. R. Tamaddon-Jahromi, J. E. López-Aguilar, and D. M. Binding, Enhanced pressure drop, planar contraction flows and continuous-spectrum models, J. Non-Newtonian Fluid Mech. **273**, 104184 (2019).

[488] M. T. Arigo and G. H. McKinley, An experimental investigation of negative wakes behind spheres settling in a shear-thinning viscoelastic fluid, Rheol. Acta **37**, 307 (1998).

[489] A. N. Beris, B. J. Edwards *et al.*, *Thermodynamics of Flowing Systems: With Internal Microstructure*, no. 36 (Oxford University Press, Oxford, 1994).

[490] P. Oswald and P. Pieranski, *Nematic and Cholesteric Liquid Crystals: Concepts and Physical Properties Illustrated by Experiments* (CRC Press, Boca Raton, FL, 2005).

[491] P. Mather, D. Pearson, and R. Larson, Flow patterns and disclination-density measurements in sheared nematic liquid crystals II: Tumbling 8CB, Liq. Cryst. **20**, 539 (1996).

[492] R. Larson and D. Mead, Development of orientation and texture during shearing of liquid-crystalline polymers, Liq. Cryst. **12**, 751 (1992).

[493] G. Duclos, R. Adkins, D. Banerjee, M. S. Peterson, M. Varghese, I. Kolvin, A. Baskaran, R. A. Pelcovits, T. R. Powers, A. Baskaran *et al.*, Topological structure and dynamics of three-dimensional active nematics, Science **367**, 1120 (2020).

[494] P. J. Collings, J. N. Goldstein, E. J. Hamilton, B. R. Mercado, K. J. Nieser, and M. H. Regan, The nature of the assembly process in chromonic liquid crystals, Liq. Cryst. Rev. **3**, 1 (2015).

[495] S. Zhou, A. Sokolov, O. D. Lavrentovich, and I. S. Aranson, Living liquid crystals, Proc. Natl. Acad. Sci. USA **111**, 1265 (2014).

[496] C. Peng, T. Turiv, Y. Guo, Q.-H. Wei, and O. D. Lavrentovich, Command of active matter by topological defects and patterns, Science **354**, 882 (2016).

[497] S. Zhou, Y. A. Nastishin, M. Omelchenko, L. Tortora, V. Nazarenko, O. Boiko, T. Ostapenko, T. Hu, C. Almasan, S. Sprunt *et al.*, Elasticity of Lyotropic Chromonic Liquid Crystals Probed by Director Reorientation in a Magnetic Field, Phys. Rev. Lett. **109**, 037801 (2012).

[498] L. Tortora and O. D. Lavrentovich, Chiral symmetry breaking by spatial confinement in tactoidal droplets of lyotropic chromonic liquid crystals, Proc. Natl. Acad. Sci. USA **108**, 5163 (2011).

[499] G. Park, S. Copar, A. Suh, M. Yang, U. Tkalec, and D. K. Yoon, Periodic arrays of chiral domains generated from the self-assembly of micropatterned achiral lyotropic chromonic liquid crystal, ACS Cent. Sci. **6**, 1964 (2020).

[500] H. Baza, T. Turiv, B.-X. Li, R. Li, B. M. Yavitt, M. Fukuto, and O. D. Lavrentovich, Shear-induced polydomain structures of nematic lyotropic chromonic liquid crystal disodium cromoglycate, Soft Matter **16**, 8565 (2020).

[501] Q. Zhang, B. Ge, R. Zhang, Z. Yaqoob, P. T. C. So, and I. Bischofberger, Structures and topological defects in pressure-driven lyotropic chromonic liquid crystals, Proc. Natl. Acad. Sci. USA **118**, e2108361118 (2021).

[502] E. Balkovsky, A. Fouxon, and V. Lebedev, Turbulence of polymer solutions, Phys. Rev. E **64**, 056301 (2001).

[503] E. Afik and V. Steinberg, On the role of initial velocities in pair dispersion in a microfluidic chaotic flow, Nat. Commun. **8**, 468 (2017).

[504] V. Kumar, A. Varshney, D. Li, and V. Steinberg, Relaminarization of elastic turbulence, Phys. Rev. Fluids **7**, L081301 (2022).

[505] A. Groisman and V. Steinberg, Efficient mixing at low Reynolds numbers using polymer additives, Nature (London) **410**, 905 (2001).

[506] T. Burghelea, E. Segre, and V. Steinberg, Mixing by Polymers: Experimental Test of Decay Regime of Mixing, Phys. Rev. Lett. **92**, 164501 (2004).

[507] B. Traore, C. Castelain, and T. Burghelea, Efficient heat transfer in a regime of elastic turbulence, J. Non-Newtonian Fluid Mech. **223**, 62 (2015).

[508] W. M. Abed, R. D. Whalley, D. J. Dennis, and R. J. Poole, Experimental investigation of the impact of elastic turbulence on heat transfer in a serpentine channel, J. Non-Newtonian Fluid Mech. **231**, 68 (2016).

[509] D. Y. Li, H. Zhang, J. P. Cheng, X. B. Li, F. C. Li, S. Qian, and S. W. Joo, Numerical simulation of heat transfer enhancement by elastic turbulence in a curvy channel, Microfluid. Nanofluid. **21**, 25 (2017).

[510] H. Yang, G. Yao, and D. Wen, Experimental investigation on convective heat transfer of Shear-thinning fluids by elastic turbulence in a serpentine channel, Exp. Therm. Fluid Sci. **112**, 109997 (2020).

[511] R. J. Poole, B. Budhiraja, A. R. Cain, and P. A. Scott, Emulsification using elastic turbulence, J. Non-Newtonian Fluid Mech. **177-178**, 15 (2012).